

AD-A243 654



AFIT/GSO/ENS/91D-09

DTIC

1991

DEC 3 1991

C 4  
C 4

ANALYSIS OF ORBITAL ELEMENTS  
AND ATMOSPHERIC ACTIVITY TO ASCERTAIN  
POSSIBLE PRESENCE OF AN ION PROPULSION  
CAPABILITY ABOARD SALYUT 7/COSMOS 1686

THESIS

Kris R. Howard, Captain, USAF

AFIT/GSO/ENS/91D-09

Approved for public release; distribution unlimited

91-19079



91 12 24 062

# REPORT DOCUMENTATION PAGE

*Form Approved  
OMB No. 0704-0188*

Public reporting burden for this collection of information is estimated to average 1 hour per response, including the time for reviewing instructions, searching existing data sources, gathering and maintaining the data needed, and completing and reviewing the collection of information. Send comments regarding this burden estimate or any other aspect of this collection of information, including suggestions for reducing this burden, to Washington Headquarters Services, Directorate for Information Operations and Reports, 1215 Jefferson Davis Highway, Suite 1204, Arlington, VA 22202-4302, and to the Office of Management and Budget's Paperwork Reduction Project (0704-0188), Washington, DC 20503.

1. AGENCY USE ONLY (Leave blank)	2. REPORT DATE	3. REPORT TYPE AND DATES COVERED
	December 1991	Master's Thesis
4. TITLE AND SUBTITLE		5. FUNDING NUMBERS
<b>ANALYSIS OF ORBITAL ELEMENTS AND ATMOSPHERIC ACTIVITY TO ASCERTAIN POSSIBLE PRESENCE OF AN ION PROPULSION CAPABILITY ABOARD SALYUT 7/COSMOS 1686</b>		
6. AUTHOR(S)		
Kris R. Howard, Captain, USAF		
7. PERFORMING ORGANIZATION NAME(S) AND ADDRESS(ES)		8. PERFORMING ORGANIZATION REPORT NUMBER
Air Force Institute of Technology, WPAFB, OH 45433-6583		AFIT/GSO/ENS/91D-09
9. SPONSORING / MONITORING AGENCY NAME(S) AND ADDRESS(ES)		10. SPONSORING / MONITORING AGENCY REPORT NUMBER
11. SUPPLEMENTARY NOTES		
12a. DISTRIBUTION / AVAILABILITY STATEMENT		12b. DISTRIBUTION CODE
Approved for public release; distribution unlimited		<i>Set 1 Set 1</i>
13. ABSTRACT (Maximum 200 words) The purpose of this study was to analyze solar and geomagnetic activity in concert with orbital element data for the Soviet space station Salyut 7 as a means toward a determination of the possible use of an ion propulsion source aboard Salyut 7 and the Cosmos 1686 module to which it was docked. Solar activity was represented by sunspot number and 10.7-cm solar radio flux, and geomagnetic activity was represented by the general activity indices Ap and Kp. The effects of atmospheric activity were examined both by direct comparison with orbital data, and by using solar and geomagnetic data as inputs to an atmospheric density model. For cases where neither atmospheric activity nor known maneuvers could explain changes in an orbital parameter, the feasibility of an ion propulsion source being the cause was examined. Because the orbital element data sets were taken at inconsistent time intervals, direct comparison with the atmospheric data was difficult. However, despite this limitation, the analysis suggests that the use of ion propulsion was possible during the period 6 May to 25 June 1986.		
14. SUBJECT TERMS		15. NUMBER OF PAGES
Atmospheric density, solar activity, orbits, artificial satellites, perturbations, ion propulsion		125
		16. PRICE CODE
17. SECURITY CLASSIFICATION OF REPORT	18. SECURITY CLASSIFICATION OF THIS PAGE	19. SECURITY CLASSIFICATION OF ABSTRACT
Unclassified	Unclassified	Unclassified
20. LIMITATION OF ABSTRACT		
		UL

ANALYSIS OF ORBITAL ELEMENTS AND ATMOSPHERIC ACTIVITY TO ASCERTAIN  
POSSIBLE PRESENCE OF AN ION PROPULSION CAPABILITY ABOARD

SALYUT 7/COSMOS 1686

THESIS

Presented to the Faculty of the School of Engineering

of the Air Force Institute of Technology

Air University

In Partial Fulfillment of the  
Requirements for the Degree of  
Master of Science in Space Operations

Kris R. Howard, B.S.

Captain, USAF

December 1991

Approved for public release; distribution unlimited	<input checked="" type="checkbox"/>
Dist	Specified
A-1	

Approved for public release; distribution unlimited

THEESIS APPROVAL

STUDENT: Kris R. Howard  
Captain, USAF

CLASS: GSO-91D

THEESIS TITLE: Analysis of Orbital Elements and Atmospheric Activity to  
Ascertain Possible Presence of an Ion Propulsion  
Capability Aboard Salyut 7/Cosmos 1686

DEFENSE DATE: 25 November 1991

COMMITTEE:	NAME/TITLE	SIGNATURE
Advisor	Maj Thomas S. Kelso Assistant Professor of Space Operations	_____
Reader	Dr William E. Wiesel Professor of Astronautical Engineering	_____

## PREFACE

The purpose of this study was to analyze solar and geomagnetic activity in concert with orbital element data for the Soviet space station Salyut 7 as a means toward a determination of the possible presence of an ion propulsion source aboard Salyut 7 and the Cosmos 1686 module to which it was docked. Solar and geomagnetic data were compared with orbital data to determine the extent to which they could be deemed causes for any unusual changes in orbital parameters.

Some difficulty was experienced in attempts to directly compare solar and geomagnetic data with orbital data given that the orbital element data sets were taken at inconsistent time intervals. This limited the extent to which direct comparisons could be done, and was a primary reason for the inconclusiveness of the results. There is a need for further work to enable accurate transformation of orbital element data to consistent time scales; if that could be done, the procedures outlined in this study could be used to get more conclusive results.

I owe many thanks to my faculty advisor, Maj T. S. Kelso, for his invaluable assistance and guidance throughout the course of this research. I also wish to thank Dr W. E. Wiesel for his thorough review of this project to ensure its accuracy and completeness. Additional thanks go to Capt Hart at ETAC for her quick response to my request for data. Finally, I must express my gratitude for the unending patience and moral support provided by my wife, Elizabeth; her support was invaluable in helping to sustain my sanity level.

Kris R. Howard

## TABLE OF CONTENTS

Preface . . . . .	iii
List of Figures . . . . .	vii
List of Tables . . . . .	xi
List of Notation . . . . .	xii
Abstract . . . . .	xv
I. Introduction . . . . .	1
Background . . . . .	1
Salyut 7/Cosmos 1686 . . . . .	1
Long Duration Exposure Facility (LDEF) . . . . .	3
Problem Statement . . . . .	4
Scope of Research . . . . .	5
Assumptions . . . . .	6
General Approach . . . . .	7
Sequence of Presentation . . . . .	7
II. Theory . . . . .	8
The Earth's Atmosphere . . . . .	8
Reference Atmospheres . . . . .	8
Solar Activity . . . . .	10
Geomagnetic Activity . . . . .	13
Sources of Orbital Perturbations . . . . .	16
Earth's Magnetic Field . . . . .	17
Charged/Uncharged Particles . . . . .	17
Gravity . . . . .	17

Solar Radiation . . . . .	18
Atmospheric Drag . . . . .	18
Propulsion . . . . .	20
Ion Propulsion . . . . .	21
Basic Theory . . . . .	22
Existing Ion Propulsion Systems . . . . .	22
Applications of Ion Propulsion . . . . .	23
III. Methodology . . . . .	26
Introduction . . . . .	26
Examination of Orbital Data . . . . .	26
Comparing Solar Data With Orbital Data . . . . .	30
Comparing Geomagnetic Data With Orbital Data . . . . .	31
Atmospheric Density Model . . . . .	32
Determine Possible Use of Ion Propulsion . . . . .	33
IV. Analysis and Findings . . . . .	34
Discussion of Data Analyzed . . . . .	34
Orbital Data . . . . .	35
Solar/Geomagnetic Data . . . . .	38
Examination of Orbital Data . . . . .	39
LDEF . . . . .	39
Salyut 7/Cosmos 1686 . . . . .	42
Combined Analysis of LDEF and Salyut 7/Cosmos 1686	48
Comparing Solar Data With Orbital Data . . . . .	58
LDEF . . . . .	61
Salyut 7/Cosmos 1686 . . . . .	63

Comparing Geomagnetic Data With Orbital Data . . . . .	73
LDEF . . . . .	75
Salyut 7/Cosmos 1686 . . . . .	76
Atmospheric Density Model . . . . .	79
Determining Possible Use of Ion Propulsion . . . . .	85
V. Conclusions and Recommendations . . . . .	87
Summary of Results . . . . .	87
Potential Applications . . . . .	88
APPENDIX: Plots of Orbital Elements for Salyut 7/Cosmos 1686 .	89
Bibliography . . . . .	107
Vita . . . . .	109

List of Figures

<u>Figure</u>	<u>Page</u>
1. Space Shuttle, Salyut 7, and Mir . . . . .	2
2. LDEF . . . . .	4
3. Ellipse Geometry . . . . .	27
4. Orbital Elements . . . . .	28
5. Eccentric Anomaly . . . . .	28
6. ECI Radius for Salyut 7 and Cosmos 1686 . . . . .	38
7. Semi-major Axis vs. Time for LDEF . . . . .	40
8. Eccentricity vs. Time for LDEF . . . . .	41
9. Inclination vs. Time for LDEF . . . . .	42
10. Semi-major Axis vs. Time for Salyut 7 . . . . .	43
11. Semi-major Axis vs. Time for Salyut 7 . . . . .	45
12. Eccentricity vs. Time for Salyut 7 . . . . .	46
13. Inclination vs. Time for Salyut 7 . . . . .	48
14. Semi-major Axis (Fitted) for LDEF . . . . .	52
15. Semi-major Axis (Fitted, Subset 1) for Salyut 7 . . . . .	55
16. Semi-major Axis (Fitted, Subset 2) for Salyut 7 . . . . .	55
17. Semi-major Axis (Fitted, Subset 3) for Salyut 7 . . . . .	56
18. Semi-major Axis (Fitted, Subset 4) for Salyut 7 . . . . .	56
19. Semi-major Axis (Fitted, Total) for Salyut 7 . . . . .	57
20. Semi-major Axis for LDEF and Salyut 7/Cosmos 1686 . . . . .	58
21. Sunspot Number vs. Time . . . . .	59

<u>Figure</u>	<u>Page</u>
22. 10.7-cm Solar Radio Flux vs. Time . . . . .	60
23. Semi-major Axis and R for LDEF . . . . .	61
24. Semi-major Axis and Flux for LDEF . . . . .	62
25. Eccentricity and Inclination for LDEF . . . . .	64
26. Sunspot Number and Flux . . . . .	64
27. Semi-major Axis and R for Salyut 7/Cosmos 1686 . . . . .	65
28. Semi-major Axis and Flux for Salyut 7/Cosmos 1686 . . . . .	66
29. Inclination and Eccentricity for Salyut 7/Cosmos 1686 . . . . .	67
30. Sunspot Number and Solar Flux . . . . .	67
31. Semi-major Axis and R for Salyut 7/Cosmos 1686 (Pre-Boost) . . . . .	68
32. $i$ and $e$ for Salyut 7/Cosmos 1686 (Pre-Boost) . . . . .	70
33. $R$ and $F_{10.7}$ (Pre-Boost) . . . . .	70
34. $w$ and $\Omega$ for Salyut 7/Cosmos 1686 (Pre-Boost) . . . . .	72
35. $R$ and $F_{10.7}$ (Pre-Boost) . . . . .	72
36. $A_p$ vs. Time . . . . .	74
37. $K_p$ vs. Time . . . . .	74
38. Semi-major Axis and $A_p$ for LDEF . . . . .	75
39. Semi-major Axis and $K_p$ for LDEF . . . . .	76
40. Inclination and Eccentricity for LDEF . . . . .	77
41. $A_p$ and $K_p$ . . . . .	77
42. Semi-major Axis and $A_p$ for Salyut 7/Cosmos 1686 . . . . .	78
43. Semi-major Axis and $K_p$ for Salyut 7/Cosmos 1686 . . . . .	78
44. $i$ and $e$ for Salyut 7/Cosmos 1686 (Pre-Boost) . . . . .	80

<u>Figure</u>	<u>Page</u>
45. $A_p$ and $K_p$ (Pre-Boost) . . . . .	80
46. $w$ and $\Omega$ for Salyut 7/Cosmos 1686 (Pre-Boost) . . . . .	81
47. $A_p$ and $K_p$ (Pre-Boost) . . . . .	81
48. $a$ and Density for Salyut 7/Cosmos 1686 . . . . .	83
49. $a$ and Density for Salyut 7/Cosmos 1686 (Pre-Boost) . . . . .	84
50. Argument of Perigee for Salyut 7, 1983 . . . . .	89
51. Right Ascension of the Ascending Node for Salyut 7, 1983 . .	89
52. Mean Anomaly for Salyut 7, 1983 . . . . .	90
53. Mean Motion for Salyut 7, 1983 . . . . .	90
54. Argument of Perigee for Salyut 7, 1984 . . . . .	91
55. Right Ascension of the Ascending Node for Salyut 7, 1984 . .	91
56. Mean Anomaly for Salyut 7, 1984 . . . . .	92
57. Mean Motion for Salyut 7, 1984 . . . . .	92
58. Argument of Perigee for Salyut 7, 1985 . . . . .	93
59. Right Ascension of the Ascending Node for Salyut 7, 1985 . .	93
60. Mean Anomaly for Salyut 7, 1985 . . . . .	94
61. Mean Motion for Salyut 7, 1985 . . . . .	94
62. Argument of Perigee for Salyut 7, 1986 . . . . .	95
63. Right Ascension of the Ascending Node for Salyut 7, 1986 . .	95
64. Mean Anomaly for Salyut 7, 1986 . . . . .	96
65. Mean Motion for Salyut 7, 1986 . . . . .	96
66. Argument of Perigee for Salyut 7, 1987 . . . . .	97
67. Right Ascension of the Ascending Node for Salyut 7, 1987 . .	97

<u>Figure</u>	<u>Page</u>
68. Mean Anomaly for Salyut 7, 1987 . . . . .	98
69. Mean Motion for Salyut 7, 1987 . . . . .	98
70. Argument of Perigee for Salyut 7, 1988 . . . . .	99
71. Right Ascension of the Ascending Node for Salyut 7, 1988 . .	99
72. Mean Anomaly for Salyut 7, 1988 . . . . .	100
73. Mean Motion for Salyut 7, 1988 . . . . .	100
74. Argument of Perigee for Salyut 7, 1989 . . . . .	101
75. Right Ascension of the Ascending Node for Salyut 7, 1989 . .	101
76. Mean Anomaly for Salyut 7, 1989 . . . . .	102
77. Mean Motion for Salyut 7, 1989 . . . . .	102
78. Argument of Perigee for Salyut 7, 1990 . . . . .	103
79. Right Ascension of the Ascending Node for Salyut 7, 1990 . .	103
80. Mean Anomaly for Salyut 7, 1990 . . . . .	104
81. Mean Motion for Salyut 7, 1990 . . . . .	104
82. Argument of Perigee for Salyut 7, 1991 . . . . .	105
83. Right Ascension of the Ascending Node for Salyut 7, 1991 . .	105
84. Mean Anomaly for Salyut 7, 1991 . . . . .	106
85. Mean Motion for Salyut 7, 1991 . . . . .	106

List of Tables

<u>Table</u>	<u>Page</u>
1. Sources of Orbital Perturbations . . . . .	20
2. XIPS Ion Propulsion Thruster . . . . .	24
3. RIT-10 Ion Propulsion Thruster . . . . .	24
4. Salyut 7 Activity . . . . .	45
5. Polynomial Curves for Salyut 7/Cosmos 1686 Semi-major Axis .	54

List of Notation

<u>Symbol</u>	<u>Definition</u>
a	Semi-major Axis
A	Cross-sectional area
$A_p$	Geomagnetic general activity index
$C_D$	Drag coefficient
cm	Centimeter
$d, d_0$	Density ( $o$ subscript: base density, sea level)
e	Eccentricity
E	Eccentric anomaly
f	True anomaly
$F_{10.7}$	10.7-cm solar radio flux
$F'_{10.7}$	Mean reference value of $F_{10.7} = 145 \times 10^{-22}$ watts/m <sup>2</sup> /Hz
h	Scale height
Hz	Hertz
i	Inclination
kHz	Kilohertz
kg	Kilogram
km	Kilometer
$K_p$	Geomagnetic general activity index
kw	Kilowatts
MPa	Megapascals = $10^6$ N/m <sup>2</sup>
mN	Millinewton
m	Mass, meters

<u>Symbol</u>	<u>Definition</u>
M	Mean anomaly
N	Newton's
R <sup>2</sup>	Statistical measure for goodness of fit
r <sub>a</sub>	Radius of apogee
r <sub>p</sub>	Radius of perigee
R <sub>e</sub>	Radius of earth = 6378.135 km
R	Sunspot number
V	Volts
t	Time
T <sub>c</sub>	Exospheric temperature
x	Polynomial coefficient
W	Watts
δT <sub>c</sub>	Change in exospheric temperature
w	Argument of perigee
Ω	Right ascension of ascending node

<u>Acronym</u>	<u>Definition</u>
ECI	Earth-Centered Inertial
ETAC	Environmental Technical Applications Center
GPS	Global Positioning System
IR	Infrared
LDEF	Long Duration Exposure Facility

<u>Acronym</u>	<u>Definition</u>
NSSK	North-South Station Keeping
RF	Radio Frequency
RIT	RF Ion Thruster
UV	Ultraviolet

Abstract

The purpose of this study was to analyze solar and geomagnetic activity in concert with orbital element data for the Soviet space station Salyut 7 as a means toward a determination of the possible presence of an ion propulsion source aboard Salyut 7 and the Cosmos 1686 module to which it was docked. Orbital elements examined include semi-major axis, eccentricity, inclination, right ascension of the ascending node, and argument of perigee. Solar activity was represented by sunspot number and 10.7-cm solar radio flux, and geomagnetic activity was represented by the general activity indices  $A_p$  and  $K_p$ .

The effects of atmospheric activity were examined both by direct comparison with orbital data, and by using solar and geomagnetic data as inputs to an atmospheric density model. For cases where neither atmospheric activity nor known maneuvers could explain changes in an orbital parameter(s), the feasibility of an ion propulsion source being the cause was examined. General perturbation theory was used to assist in the determination of possible causes for anomalies seen in the orbital data.

Because the orbital element data sets were taken at inconsistent time intervals, direct point-to-point comparison with the atmospheric data was not possible. This limitation was influential in the overall outcome of the study being inconclusive. However, the analysis suggests that the use of ion propulsion was possible during the period from 6 May 1986 to 25 June 1986, which represents the time spent on Salyut 7/Cosmos 1686 by the Soyuz T-15 crew.

## I. Introduction

### Background

Salyut 7/Cosmos 1686. According to a detailed report published by the British Interplanetary Society, the Soviets launched the Salyut 7 space station on 19 April 1982 to replace the Salyut 6 space station. Figure 1 illustrates the relative size of Salyut 7 (middle) compared to the space shuttle and the Soviet's new Mir space station. In addition to being a valuable research bed, the new Salyut 7 station allowed many cosmonauts to break space endurance records. In fact, the very first cosmonaut crew to inhabit Salyut 7 broke the manned space duration record when they remained in space for over 211 days (10:112). The station's own longevity, however, fell short of most expectations.

In December 1984, the station failed to respond to ground controller commands. Following numerous unsuccessful attempts to regain control of the space station from the ground, a cosmonaut crew was dispatched in June 1985 (Soyuz T-13) in an effort to rescue the Salyut 7. The cosmonauts successfully returned the station to operational status and were joined by a relief crew aboard Soyuz T-14 in September 1985 (10:114). The revived space station and its new crew were now ready to continue long-duration experimentation.

A separate report by the same group indicates that the Soviets launched the Cosmos 1686 spacecraft on 27 September 1985, and docking occurred with Salyut 7 on 2 October 1985 (6:206). The 20,000 kg

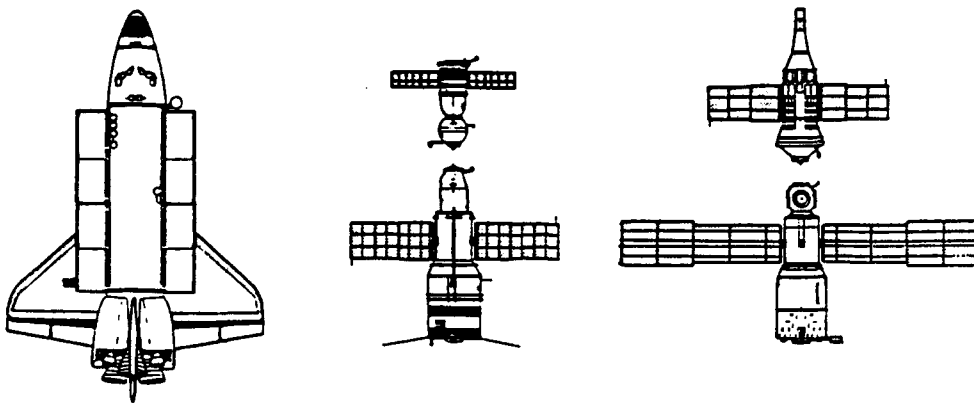


Figure 1. Space Shuttle, Salyut 7, and Mir (Reprinted from (14:53))

Cosmos 1686 reportedly "carried food, water, propellants, and scientific instruments for use by Soyuz T-13/14 cosmonauts" and also "augmented Salyut 7 power generation capability" (13:169). The crew that was aboard the station at the time the Cosmos 1686 docked (Soyuz T-14) remained until 21 November 1985, at which time they undocked and left the Salyut 7/Cosmos 1686 complex (6:206-207). Unmanned and still unable to respond to ground controllers, the complex again began to slowly fall towards earth. Except for a small maneuver in February 1986 and a brief visit by the Soyuz T-15 crew from 6 May 1986 through 25 June 1986, the complex's orbit continued to decay naturally until a series of maneuvers in August 1986 boosted it to a significantly higher orbit (6:207,209).

Based on the scenario outlined above, it would appear reasonable that the Cosmos 1686 module, while attached to the Salyut 7, was a necessary source of propulsion. Furthermore, there has been speculation

that one of the purposes of the Cosmos 1686 mission was to test an advanced ion propulsion system. This assertion, however, has been neither confirmed nor denied by the Soviets. Nevertheless, it may be possible to determine the presence of an ion propulsion source aboard the Salyut 7/Cosmos 1686 orbital complex through the use of existing orbital and atmospheric data. If the analysis of this data does enable such a deduction, the associated methodology may lend itself to the successful analysis of other Soviet missions and further insight into Soviet advanced technology efforts in space.

In the area of advanced propulsion techniques, the potential payoff is significant. Nonchemical propulsion techniques (such as ion propulsion) are often much more feasible than chemical systems for things like orbital transfers and stationkeeping maneuvers since they are very small and operate at low thrust levels.

Long Duration Exposure Facility (LDEF). LDEF, shown in Figure 2, was launched in April 1984 with many experiments aboard to study the long-term effects of the space environment. The 12-sided satellite, which was 9.14 m long, 4.26 m in diameter and weighed 9980 kg, was not capable of maneuvering itself as it had no propulsion system (13:59). It thus decayed naturally over time until its rescue in January 1990 by the space shuttle (16:23).

Because of the free-flying nature of LDEF and because it was at a similar altitude as Salyut 7/Cosmos 1686 for a good portion of its orbit, it was seen as a natural baseline to assist in this research. Specifically, perturbations of the LDEF orbit could conceivably be more

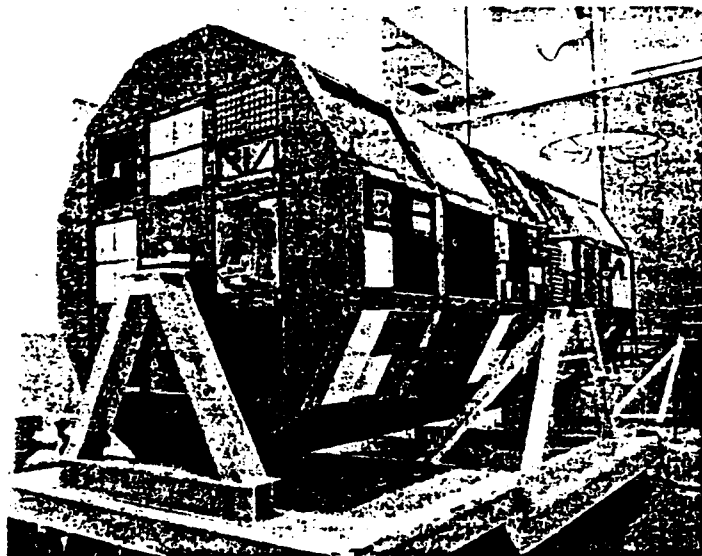


Figure 2. LDEF (Reprinted from (13:59))

easily traced to natural causes such as solar and geomagnetic activity without having to subtract out various maneuvers.

#### Problem Statement

The Soviet Union announced in March 1985 that the Salyut 7 mission was completed. However, subsequent visits by several cosmonaut crews and resupply vessels, as well as movement of the Salyut 7/Cosmos 1686 complex into a high orbit in August 1986 to postpone its reentry, make a strong case for the argument that the Soviets still valued its research potential. There has been speculation that the Cosmos 1686 carried an ion propulsion device and that it was tested while in orbit with Salyut 7. This study will incorporate the effects of solar and geomagnetic activity to allow a detailed analysis of the orbital decay of Salyut 7/Cosmos 1686 as a means to determine the possible existence and operation of an ion propulsion thruster.

### Scope of Research

The scope of this research encompassed study in a wide variety of topics, including orbital mechanics, solar and geomagnetic activity, ion propulsion, and time series analysis. The research also involved three different systems (Salyut 7, Cosmos 1686, and LDEF), although two of them (Salyut 7 and Cosmos 1686) were assumed to act as one as far as orbital behavior. The study covered the time period January 1983 through March 1991.

The orbital mechanics portion of the study included a venture into perturbation theory to determine the causes of orbital perturbations. General perturbation theory regarding effects on all of the orbital elements was studied. Trends and first-order approximations were used primarily to gain insight into the relative effects of individual phenomena as opposed to the application of higher-order equations.

The influences of solar and geomagnetic activity on the satellite orbits were strongly considered as perturbation causes. Two indices each for solar and geomagnetic activity were chosen to represent overall behavior. These included sunspot number, R, 10.7-cm solar radio flux,  $F_{10.7}$ , and the geomagnetic general activity indices  $A_p$  and  $K_p$ .

Ion propulsion was researched to a considerable level of detail to gain an understanding of the underlying principles involved. However, the determination as to whether or not ion propulsion was used was done more qualitatively than analytically.

Time series analysis was not used to the extent initially envisioned, but the basic concepts of univariate and multivariate time series analysis were studied in the early phases of the research. It

was found that the problem of dealing with data sets taken at different time intervals was more significant than originally anticipated, thus moving time series analysis outside the scope of this project.

#### Assumptions

Most of the assumptions made throughout the course of this research are highlighted within the text. Some worth noting involve the accuracy of the data, standard atmosphere assumptions, and the density profile.

It is noted in Chapter IV that the orbital element data should only be considered accurate to about 12 km. However, a 12-km error band was not included in any of the graphs, so therefore the orbital data was treated as if it were accurate for the purpose of the analysis. It was also assumed that the solar and geomagnetic data received from the Air Force Environmental Technical Applications Center (ETAC) was accurate.

Reference atmospheres such as the 1976 U.S. Standard Atmosphere were built around various assumptions about the earth's atmosphere. These assumptions were assumed to hold for this research as well. For example, it was assumed that the earth's atmosphere rotates with the earth.

The density model used in this study was taken from the 1985 Handbook of Geophysics and the Space Environment. However, the model given in the handbook was actually taken from research published in 1971. One possible limitation of the model is that it uses exospheric temperature extensively, and as noted in Chapter II, the mean exospheric temperatures used in reference atmospheres have been decreasing over the

last twenty to thirty years. The extent to which this would limit the applicability of the model to current data is not known, although the fact that it was presented in the above handbook suggests that it is still a valid model.

#### General Approach

The overall approach used to complete the research for this study can be summarized as follows: 1) review theoretical causes of orbital perturbations; 2) examine capabilities of various ion propulsion systems; 3) compare existing orbital data between LDEF and Salyut 7; 4) compare orbital data with solar and geomagnetic data; 5) develop density profile and compare with orbital data; and 6) determine extent to which ion propulsion might have been used.

#### Sequence of Presentation

This report will be presented in the following order. First, Chapter II will address the theory behind the earth's atmosphere, sources of orbital perturbations, and ion propulsion. Next, Chapter III will provide a more detailed overview of the methodology used. The analysis done throughout the research is discussed in Chapter IV, and conclusions are summarized in Chapter V.

## II. Theory

### The Earth's Atmosphere

The purpose of this section is to briefly discuss those characteristics of the earth's atmosphere that are important with respect to this research effort. Specifically, reference atmospheres, solar activity and geomagnetic activity will be discussed.

Reference Atmospheres. According to the 1985 Handbook of Geophysics and the Space Environment, the World Meteorological Organization defines the Standard Atmosphere as "a hypothetical vertical distribution of atmospheric temperature, pressure and density which by international agreement and for historic reasons, is roughly representative of year-round, midlatitude conditions" (11:14-1). It goes on to say that "the air is assumed to obey the perfect gas law and the hydrostatic equation" and that "only one standard atmosphere should be specified at a particular time and this standard atmosphere must not be subjected to amendment except at intervals of many years" (11:14-1). In essence, what this says is that a standard, or reference atmosphere is one based largely on idealized, theoretical calculations. Nevertheless, it is one that is widely accepted as representative of average conditions.

The U.S. Standard Atmosphere, 1976, perfectly fits the above description. It is based on theoretical relations such as the perfect gas law and it has not been significantly altered for many years. In fact, the 1976 U.S. Standard Atmosphere is still widely used as a

reference atmosphere. One of the reasons it continues to be used is that there was an addition made for the 1976 version that was not included in previous versions. The addition, which particularly increased its usefulness for applications at higher altitudes, was as follows:

The atmosphere shall also be considered to rotate with the earth, and be an average over the diurnal cycle, semiannual variation and the range of conditions from active to quiet geomagnetic, and active to quiet sunspot conditions. Above the turbopause (about 110 km) generalized forms of the hydrostatic equations apply. (11:14-1)

The handbook also outlines specific details and assumptions of the 1976 U.S. Standard Atmosphere. For example, it states that the atmosphere is useful up to 1000 km, represents conditions at midlatitude (45°), and utilizes temperature-height profiles based on sea-level temperature and pressure (11:14-1). It is also noted that the U.S. Standard Atmosphere is similar to other reference atmospheres in that it defines the various atmospheric layers in terms of temperature (11:14-6). The layer of most interest in terms of the majority of artificial satellite operations is the thermosphere. The thermosphere lies between the mesopause, which is a small region at about 80-90 km characterized as being the coldest region of the atmosphere, and the exosphere--the outermost layer of the atmosphere (11:14-7). Temperature within the thermosphere rises rapidly from the mesopause to about 200 km, and then becomes nearly isothermal between 300-500 km, with the temperature above 200 km being strongly influenced by solar activity (11:14-7).

An interesting trend is also highlighted in the handbook involving mean atmospheric temperatures. It is shown that the mean exospheric temperature used in various reference atmospheres over time has steadily decreased; it was 1500°K in 1962, 1200°K in 1965, and 1000°K in 1972 and 1978 (11:14-26). The reason for this, it is explained, is that the early atmospheres used satellite orbital drag measurements taken during periods of uncharacteristically low solar activity, and subsequent measurements have reflected more and more realistic conditions (11:14-26). In fact, a study was done which looked back over 12 11-year solar cycles and the result was a prediction of mean exospheric temperature of 882°K (11:14-27). It also recommends that the next reference atmosphere use a mean exospheric temperature of 900°K (11:14-27).

Exospheric temperature was used in the analysis to build atmospheric density profiles for both LDEF and Salyut 7. It will be shown in the next section, and later in the analysis, that atmospheric density is a major contributor to the drag force acting upon the vehicle. Further, the extent to which drag influences various orbital parameters will be discussed as well.

Solar Activity. As mentioned above, solar activity has a strong influence on the characteristics of the thermosphere. It follows, then, that solar activity could potentially have a strong influence on satellite operation since the majority of satellites operate within the thermosphere at altitudes of 100-500 km.

The sun consists of several layers, all of which heavily influence the characteristics of the sun's radiation. Starting from the inside and proceeding outward, these layers are: 1) the core, 2) an

intermediate interior, 3) the convection zone, 4) the photosphere, 5) the chromosphere, 6) a transition region, and 7) the corona (11:1-5). The extent to which each of these contribute to the overall solar radiation pattern is very difficult, if not impossible, to quantify completely. Fortunately, extensive detail on the workings of the sun is not within the scope of this study. However, it is helpful to keep the above structure in mind as certain solar radiation features are addressed.

Total solar irradiance is defined as the "amount of radiant energy at all wavelengths received per unit time and area at the top of the earth's atmosphere, corrected to the mean earth-sun distance, and is customarily expressed in units of Watts per square meter ( $\text{W/m}^2$ )" (11:1-4). The breakdown of this irradiance into conventional wavelength bands provides a good feel for the composition of the radiation. It is estimated that more than 70 percent is in the near ultraviolet (UV), visible, and near infrared (IR) regions, with most of this energy reaching the earth's surface (11:1-5). Another 2 percent is in the UV and X-ray regions; most of this is absorbed in the upper atmosphere (11:1-5). The remaining energy lies in the IR and radio regions with wavelengths greater than 1  $\mu\text{m}$  ( $10^{-6}$  m), and most of the IR portion of this is absorbed in the atmosphere by water vapor and  $\text{CO}_2$ .

One of the two indices used in the analysis is the 10.7-cm solar radio flux index,  $F_{10.7}$ , which is commonly used as a "reliable indicator of the general level of solar activity" (11:2-18). The origin of the 10.7-cm flux is in the upper chromosphere and lower corona (11:2-18). It is received on earth as energy at a wavelength of 10.7 cm, which

falls within the category of radio waves. This inherently makes data collection easier since energy at radio wave wavelengths is not absorbed by the atmosphere and collection can be done by ground stations. However, it must be emphasized that  $F_{10.7}$  is limited in its ability to accurately represent the many aspects of overall solar activity. This could be said about any single solar activity index which is limited in bandwidth, since solar energy is radiated across a wide spectrum of wavelengths and behavior at different wavelengths varies greatly.

As an example,  $F_{10.7}$  does not necessarily depict activity in the ultraviolet (UV) region. To illustrate the significance of this limitation, it has been noted that "although this UV region accounts for less than 2 percent of the total solar irradiance, it is the principal source of energy in the upper atmosphere" (11:2-16). Unfortunately, it is difficult to measure UV irradiance because the energy at those wavelengths is totally absorbed in the upper atmosphere. Therefore, we have to rely on indices which can be more readily measured such as 10.7-cm solar flux. Fortunately, it is believed that there is a fairly good correlation between 10.7-cm flux and UV activity.

The other index used in the analysis to represent solar activity is the sunspot number, R. Based on records dating back to the mid-17th century, it has been determined that sunspots, and thus sunspot numbers, follow a predictable 11.4-year cycle (11:2-18). Sunspot number is defined as follows (11:1-14):

$$R = k(n + 10g) \quad (1)$$

where

R = sunspot number

k = station constant for a particular observatory

n = number of spots visible on the solar disk

g = number of sunspot groups

Geomagnetic Activity. While solar activity has several direct effects on the earth's atmosphere, it has some marked indirect effects as well. Although the particular relationships are complex, it has been shown that variations in the earth's magnetic field are closely tied to solar activity. Specifically, it has been shown that there is both an 11-year and a 27-day cycle correlation between solar and geomagnetic activity; the 11-year cycle corresponds to the sunspot cycle discussed above and the 27-day cycle represents phenomena associated with the rotation of the sun, such as solar flares (11:4-1). Solar activity, however, is not the only factor influencing the geomagnetic field.

To better understand the catalysts which influence the earth's magnetic field, it is helpful to first briefly address the general characteristics of a magnetic field. Scientists such as Oersted and Ampère postulated in the early 19th century that magnetic fields are set up solely by the movement of electric charges (21:834). This is the basis for present theory, although modifications have been made to include the concept of permanent magnetism associated with a given material (11:4-5; 21:834). With this in mind, the discussion of the geomagnetic field can be continued.

The effects of solar radiation on the geomagnetic field can actually be broken down into two separate effects. One is due to the insertion of charged particles into the earth's atmosphere by the solar wind, and the other is due to the interaction between the magnetic field inherent in the solar wind itself and the earth's magnetic field (11:4-5).

Additional sources which contribute to the overall composition of the earth's magnetic field include motion of the core, magnetization of the earth's crust, and gravitational effects (11:4-5). First, motion of the earth's fluid core contributes to the field as it involves the movement of charged particles; second, the crust has its own permanent magnetization; and third, the tidal effects of the sun and moon gravitational fields create particle movement similar to that created by the solar wind (11:4-5).

The geomagnetic field is contained within an area confined by the magnetopause, which is a boundary layer formed by the interaction of the solar wind and the earth's magnetic field. The area within the magnetopause is called the magnetosphere, and the field that makes up the magnetosphere can be considered as a main field subject to various time-varying perturbations.

The main field is also termed the steady field, based on the convention that it is that component of the magnetic field that varies with periodicities of greater than about one year (11:4-5). The perturbation component can be broken down into "quiet variation fields" and "disturbance fields," where the former is characterized by daily or

seasonal variations and the latter by all of the remaining variations (11:4-5).

Measurement of these variations is done at ground stations positioned throughout the world, and the resulting data is often put into usable form via calculation of a general activity index, K (11:4-12). Several other related indices have also been developed. These include  $K_p$  and  $A_p$ , both of which were used in this study to represent geomagnetic activity. The  $K_p$  index in particular was chosen for the purposes of this study because it is a good indicator of global geomagnetic activity. This choice is underscored by the statement "the  $K_p$  index ("p" for "planetary") is probably the most widely used of all the indices" (11:4-28).  $A_p$  was also chosen as it is directly related to  $K_p$ , but lends itself more to calculation of a daily average due to its linear nature.

The specific procedure used to derive the  $K_p$  index from the K index, as outlined in the 1985 Handbook of Geophysics and the Space Environment, is basically done in two steps (11:4-28 - 4-29). First, seasonal variations are taken into account through the use of tables which transform the K index into a  $K_s$  index (the subscript s meaning standardized). Values of  $K_s$  are then taken from 12 different stations around the world and averaged to give the  $K_p$  index. The result is an index which gives an indication of overall global geomagnetic activity. However, arguments similar to those made earlier with respect to the limitations of  $F_{10.7}$  can also be made in this case.

For example, it is argued that the use of  $K_p$  for the purpose of calculating density is deficient in that  $K_p$  does not have a short enough

time resolution to accurately represent actual atmospheric changes (5:46). The alternative offered is that the auroral electrojet (AE) index, which is taken at intervals of one hour (or less), would produce a more accurate density model due to its shorter time resolution (5:46; 11:4-31). It is noted, however, that AE values are typically not available (5:46). This realization bears a striking resemblance to the solar flux situation. In short, it says that while these indices may have some limitations, they are probably the best currently available.

While  $K_p$  is useful, it does have some limitations. For instance,  $K_p$  is logarithmic in nature, and thus does not lend itself to a straightforward computation of a daily average. To get around this, a daily sum of the eight 3-hour  $K_p$  values is often plotted to represent day-to-day changes. Another way to represent daily activity is by using the  $A_p$  index.  $A_p$  is simply a linearized transformation of  $K_p$  which represents the daily average of geomagnetic activity (11:4-29).

#### Sources of Orbital Perturbations

The idealized elliptical orbit for 2-body motion was clearly described by Kepler and others early in the 17th century (2:141-142). The associated relationships are still used widely today to analyze satellite orbits about the earth, but are modified to the extent necessary using perturbation techniques to account for non-idealized motion.

Forces acting on a satellite which could cause deviations from a Keplerian orbit can be attributed to the following causes: the earth's magnetic field, charged and uncharged particles, gravitational fields of

the earth and other bodies, solar radiation, and the atmosphere (19:282). Another obvious force would be that due to a propulsion source aboard the satellite.

Earth's Magnetic Field. First, the effect that the earth's magnetic field has on any given satellite is dependent on the construction of the satellite. For example, if the satellite is constructed of metal, the magnetic field will induce current flow in the satellite. The result is a slight retardation force, which has a minimal overall effect on the orbit (19:283).

Charged/Uncharged Particles. The type of effect due to charged particles is similar to the electromagnetic interaction described above. The effect of uncharged particles is more mechanical in nature and is similar to atmospheric drag. The combined effects of charged and uncharged particles are found to negligible (19:283).

Gravity. Satellites are also subject to gravitational forces from the earth, moon, sun, and other bodies. It has been estimated that for orbits less than about 1600 km in altitude, the effects of the earth's gravitational field dominate and gravitational forces from other bodies can be neglected (19:282). Current models suggest that this altitude limit may be even higher. In either case, the earth's gravitational field is the dominant force for satellites in near-earth orbits. Although this would seem to simplify the analysis in that only the earth's gravitational effects need be considered, the fact is that the earth is not symmetrical and thus its gravitational field is not uniform.

The earth is actually an oblate spheroid (larger around the equator), and the resulting unsymmetrical gravitational field gives rise to orbital perturbations. The magnitude of these perturbations is significant. In fact, it is noted that "besides air drag, the most pronounced departure from two-body motion for a low earth satellite is caused by the fact that the earth is not perfectly spherical" (23:86).

The earth's oblateness causes notable perturbations to most of orbital elements. Most significant are the "regression of nodes" and "advance of the perigee," which represent a secular (steady) increase in the right ascension of the ascending node,  $\Omega$  (for  $i < 90^\circ$ ), and a secular decrease in the argument of perigee,  $w$ , respectively (23:86-87; 19:290). Actually, perigee advances only if inclination,  $i$ , is less than  $63^\circ 26'$  (which holds in this study for both satellites) (19:290). The result is a change in both  $\Omega$  and  $w$  of about  $4^\circ/\text{day}$  (19:290). Additional perturbations include small periodic changes in eccentricity,  $e$ , and inclination,  $i$  (19:290; 23:87).

Solar Radiation. The fourth potential cause of orbital perturbations is solar radiation. The direct influence of solar radiation is most pronounced for satellites with a low mean density (such as balloon satellites) as a result of particles impacting the satellite (19:283). Indirectly, solar radiation increases atmospheric density, which increases with decreasing altitude for any satellite. Density, in turn, influences atmospheric drag.

Atmospheric Drag. Drag is an aerodynamic phenomenon which by definition opposes the motion of a vehicle, and it can have a signif-

icant adverse affect on a satellite's orbit. The drag force per unit mass exerted on a satellite can be expressed as:

$$F = C_D d V^2 A / (2m) \quad (2)$$

where

$C_D$  = drag coefficient

$d$  = atmospheric density,  $\text{kg/m}^3$

$V$  = vehicle velocity,  $\text{m/s}$

$A$  = cross-sectional area,  $\text{m}^2$

$m$  = satellite mass,  $\text{kg}$

Based on this expression, the direct effect of density on atmospheric drag is obvious. The factors in Equation (2) that will undergo the largest changes during the reentry of a satellite will be velocity and density.

Most theoretical developments of atmospheric drag effects assume an exponential density profile (15; 19:298; 23:83-86). A typical expression for an exponential density profile is (23:84):

$$d = d_0 e^{-(r-R_e)/h} \quad (3)$$

where

$d$  = density at some altitude ( $\text{kg/m}^3$ )

$d_0$  = base density of the atmosphere ( $\text{kg/m}^3$ )

$r$  = distance to earth center (km)

$R_e$  = earth radius (km)

$h$  = scale height (km)

The scale height,  $h$ , is defined as "that vertical distance in which the density changes by a factor  $e$  and depends upon the altitude" (19:298). This treatment of density, while useful for many applications, obviously is not one which takes into account changes in the atmosphere due to day-to-day fluctuations in solar and/or geomagnetic activity. It was thus determined that for the purposes of this research, a density profile would be used which was more able to represent these changes. The details of the density model used are presented in Chapter IV. The effects of drag, as well as oblateness and solar-lunar forces, are given in Table 1.

Table 1  
Sources of Orbital Perturbations (Compiled from (15:8))

Perturbation Source	Effect			
	Secular		Periodic	
	Large	Small	Moderate	Small
Earth's Gravity	$\Omega, w$	--	$e$	$i, \Omega, w$
Atmosphere	$a, e$	$i$	--	$\Omega, w$
Luni-Solar Forces	--	--	--	$a, e, i, \Omega, w$

Propulsion. The contention that use of a propulsion system can cause orbital perturbations is an obvious one, but it is considered separately here for two reasons. First, it differs from all others considered to this point in that all other phenomena were naturally occurring. Second, it is necessary to keep this possible cause in mind for the purposes of this research since the goal is to determine the

extent to which the use of ion propulsion can be postulated once the other causes have been considered.

### Ion Propulsion

Spacecraft propulsion in general can be broken into two broad categories: chemical and nonchemical. Chemical propulsion is by far the most common, and remains the only proven choice for launching vehicles from earth. Nonchemical propulsion systems, however, have unique attributes which make them desirable for other mission phases which do not have the inherent thrust requirements of launch.

Nonchemical propulsion can be broken down into four separate areas: electric, solar, nuclear, and exotic. Electric propulsion can be further broken down into electrothermal, electromagnetic, and electrostatic propulsion. Ion propulsion falls under the electrostatic category.

Ion thrusters are by nature low thrust devices, with thrust levels generally smaller than 1 N. They are also much lighter than their chemical counterparts and offer high specific impulse. These qualities make them good candidates for things such as stationkeeping maneuvers. However, these attributes come with a cost. High specific impulse implies significant (heavy) power generating equipment which may negate the advantages mentioned above (12:322). As power generation capabilities increase, this drawback will become less and less of a factor. The following subsections will provide some basic information about the theory behind ion propulsion, some existing systems, and potential applications.

Basic Theory. There are several types of ion thrusters that have been or are currently under development, and some models are even seeing some limited operation. However, the underlying theory behind the operation of an ion thruster is essentially the same for all types. For the purpose of explaining the basic principles of an ion propulsion device, it is convenient to break the thruster down into four parts: electron production, ion production, accelerating system, and neutralization.

In the case of an electron bombardment system, electron production is accomplished by heating a cathode made of a material that readily releases electrons when heated. The released electrons are then mixed with a neutral propellant stream in a discharge chamber to create ions. The ions are then accelerated through the chamber by means of an electric field set up across a set of screen grids. Finally, electrons are injected back into the exhaust flow to create a neutral particle stream so that the possibility of spacecraft charging is minimized. This scenario represents a typical ion thruster setup. Although other types of ion thrusters may utilize different methods of ion production, the principle of accelerating ions through a screen grid to produce thrust is the same.

Existing Ion Propulsion Systems. There are many ion propulsion systems currently in existence. Most are of the same basic design described earlier, but some use minor variations. Three such systems are the xenon ion propulsion system (XIPS), the radio-frequency ion thruster (RIT-10), and the United Kingdom ion thruster (UK-10).

According to a paper published last year in the Journal of Propulsion and Power, the XIPS ion thruster is a 25-cm device designed by Hughes Research Laboratories for north-south stationkeeping (NSSK) for 2500-kg-class geosynchronous communications satellites (4:145). At the time the paper was written, the thruster was still a laboratory model. Some operational characteristics of this thruster as tested in the laboratory are given in Table 2.

The design of the RIT-10 is notably different than the more conventional XIPS thruster. The primary difference is that ionization of the propellant gas occurs as a result of an RF field produced by an RF generator in the range of 900-1100 KHz at 15-55 V (8:406). Therefore, the available thrust is adjustable as it varies directly with the voltage output of the generator (8:407). Some operational characteristics of the RIT-10 ion propulsion device are given in Table 3. The UK-10 thruster is similar in concept to the electron bombardment design discussed earlier, with the only significant difference being in the discharge chamber. The addition of solenoids in the chamber has the effect of lengthening the path of electrons from cathode to anode so as to increase the probability for collision/ionization (9:3). At the UK-10's maximum thrust of 25 mN, it has a specific impulse of 3486 sec and exhaust velocity of 40.2 km/sec (9:6).

Applications of Ion Propulsion. Several efforts are underway to examine specific applications for ion propulsion systems. Potential applications will be discussed for each of the systems described above, as well as one additional mission.

Table 2  
XIPS Ion Propulsion Thruster (Compiled from (4:145-149))

---

<u>Characteristic</u>	<u>Value</u>
Thrust	63.3 mN
Input Power	1.3 kW
Specific Impulse	2900 sec
Propellant Storage Pressure	7.6-29 MPa
Acceleration Voltage	750 V
Exhaust Velocity	28.4 km/sec *

---

\* Calculated from given data

---

Table 3  
RIT-10 Ion Propulsion Thruster (Compiled from (1:3,6))

---

<u>Characteristic</u>	<u>Value</u>
Thrust	5-10 mN
Input Power	270-440 W
Specific Impulse	4791 sec *
Propellant Storage Pressure	5-6 MPa
Acceleration Voltage	1500 V
Exhaust Velocity	47 km/sec

---

\* Calculated from given data

---

The XIPS thruster was designed specifically with the newer Intelsat satellites in mind, and to that end several calculations have been made regarding the benefits of using the ion propulsion device. For example, it is claimed that the XIPS can operate adequately using available onboard battery power for 1 hour/day, thus negating the mass penalty associated with a separate power source (4:145). Further, the paper referenced earlier states that if 200 kg of chemical propellant on an Intelsat VI satellite is replaced with a XIPS system of equal mass,

the satellite's NSSK capability could be extended from 14 years to 23 years (4:145).

A paper presented at the 25th Joint Propulsion Conference in 1989 highlighted the future plans for MBB's RIT-10 ion thruster. At that time, plans called for a 1991 space shuttle mission on the European Retrievable Carrier (EURECA) which would have put it into a 500-km orbit for 6 months (1:1). Plans also call for use of the RIT-10 for NSSK on the European SAT-2 satellite, which is scheduled for launch in 1993 (1:1).

The UK-10 is being looked at for possible use for NSSK on the new Intelsat VII satellites (9:1). It is projected that useful lifetimes for the Intelsat VII satellites could be as long as 19.6 years, so there is considerable interest in ion propulsion given that savings over chemical propulsion increases linearly with mission duration (9:1-2).

In addition to the potential applications just mentioned, the Global Positioning System (GPS) Program Office has looked into the feasibility of using a xenon ion propulsion device for transferring GPS satellites from a parking orbit to their mission orbit (20:445). If this were feasible, it could offer potentially significant savings in required initial launch mass as compared to conventional chemical propellants. It was found that current generation ion thrusters could offer life cycle cost reductions of up to 61 percent relative to the baseline GPS upper stage (20:451).

### III. Methodology

#### Introduction

This chapter will outline the details of each phase of the research conducted for this project. These phases, and the order in which they will be presented, are: 1) the examination of orbital data, 2) comparison of solar data with orbital data, 3) comparison of geomagnetic data with orbital data, 4) calculation of an atmospheric density model and its comparison with orbital data, and 5) determination of the possible use of ion propulsion. These phases will be presented in the above order to assure continuity and to reflect the order in which the research was actually accomplished. In a more practical sense, this sequence of presentation might best be described in the context of a cause-and-effect scenario. The purpose of the initial phase of the research was to examine the effects (i.e., the orbital parameters), and work in subsequent phases sought to examine possible causes. Finally, the last phase of the research attempts to infer the extent to which ion propulsion could have been an additional cause.

#### Examination of Orbital Data

The overall emphasis of this research project was to examine the effects of solar and geomagnetic activity on the orbital parameters of the Salyut 7/Cosmos 1686 complex. However, the orbit of the LDEF satellite was also studied as it provided a baseline against which solar and geomagnetic effects could be compared. This comparison was possible

because LDEF was a free-flying satellite, meaning that it was not capable of maneuvering itself and thus effects due to atmospheric activity were more easily discernible.

Specific parameters evaluated for both Salyut 7 and LDEF include semi-major axis,  $a$ , eccentricity,  $e$ , inclination,  $i$ , argument of perigee,  $w$ , right ascension of the ascending node,  $\Omega$ , and mean anomaly,  $M$ . Figure 3 illustrates the geometric significance of  $a$  and  $e$ , and Figure 4 shows how  $i$ ,  $w$ , and  $\Omega$  relate to a satellite orbit. Mean anomaly is defined as  $M = n(t-t_0) + M_0$ , where the "0" subscripts represent values at some epoch time. Mean anomaly can also be expressed as  $M = E - esinE$ , where  $E$  is eccentric anomaly as shown in Figure 5. Figure 5 illustrates the geometric relationship between  $E$  and true anomaly,  $f$ , which is the angular displacement of the satellite along its elliptical path. Eccentric anomaly is simply the vertical projection of the point on the ellipse used to define  $f$  onto an auxiliary circle.

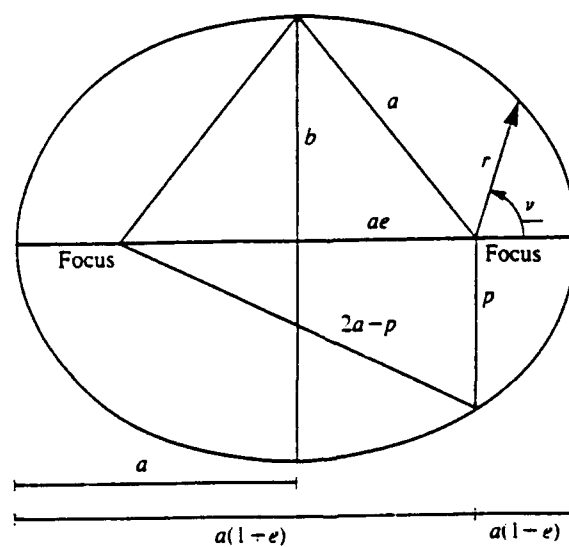


Figure 3. Ellipse Geometry (Reprinted from (22:52))

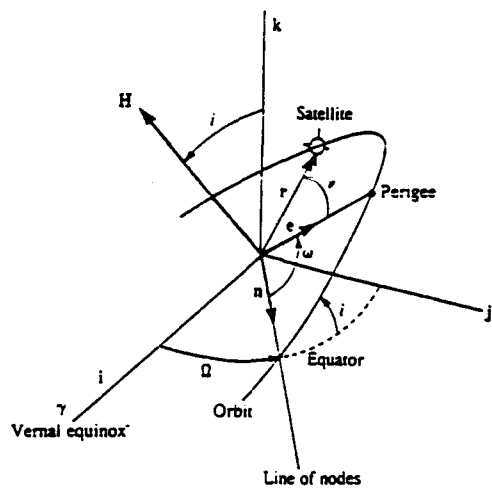


Figure 4. Orbital Elements (Reprinted from (22:58))

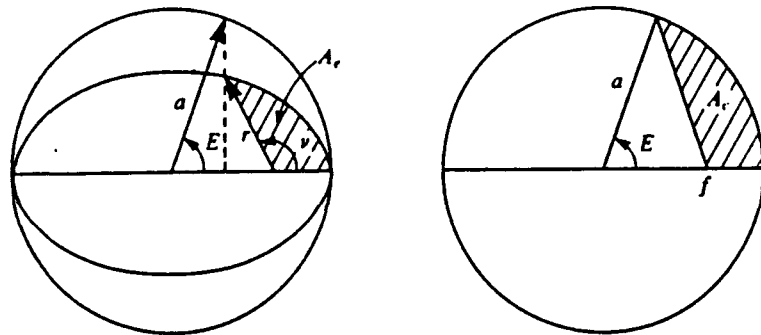


Figure 5. Eccentric Anomaly (Reprinted from (22:55))

The level of emphasis or importance placed on any of these individual parameters was based on the perturbation theory outlined in Chapter II. For example, emphasis was placed on  $a$ ,  $e$ , and  $i$  when considering secular perturbations due to atmospheric drag (see Table 1).

The orbital parameters of Salyut 7 and LDEF were first studied independently. For each system, the parameters mentioned above were

plotted individually as time series (functions of time) for each year (Appendices A and B). Each orbital element was also plotted as a continuous function over time using 0 Jan 83 as the standard epoch. Whereas the yearly plots highlighted short-term variations, the multi-year plots allowed visualization of changes over a much longer period of time and provided some initial insight into potential areas (time periods) of interest.

Once the orbital data had been plotted for each system, the data were manipulated where possible so that direct comparisons could be made of individual parameters between Salyut 7 and LDEF. Data manipulation was necessary since the time series data for each of the two systems was recorded at different time intervals. While cumbersome to overcome, this problem is unfortunately inherent with two-line element sets.

To get the time series on consistent time scales, two methods were used. For cases where the data was relatively smooth (gradual changes over time), a polynomial curve was fit through the data which allowed prediction of the value at any desired time interval. This was accomplished with the help of a commercially available software program called SPLOT, which will fit up to a tenth-order polynomial through a data set and provides statistical information regarding goodness of fit. In general, polynomials were fitted so as to produce no more than a 5-km difference between the fitted curve and the actual data at any given point. For cases where the data did not lend itself to this approach, linear interpolation was used to obtain values at consistent time intervals.

In this study, semi-major axis for LDEF and Salyut 7/Cosmos 1686 were the only data sets transformed to another time scale. Other parameters fluctuated too much to allow curve fits which would not lose the fidelity of the original data. Once the semi-major axis data was transformed to a consistent time scale (one-day time interval), both LDEF and Salyut 7/Cosmos 1686 were plotted simultaneously to compare relative behavior.

#### Comparing Solar Data with Orbital Data

Given that the orbital elements had now been analyzed, some knowledge had been gained regarding the effects of some unknown combination of inputs, or causes. The first potential cause to be examined was solar activity.

Two measures of solar activity were used in this research: sunspot number, R, and 10.7-cm solar radio flux,  $F_{10.7}$ . Data was obtained for these indices for the period Jan 1983 through Mar 1991 from the USAF Environmental Technical Applications Center (ETAC). These indices were selected for use in this study because they are two of the most widely used and accepted indicators of overall solar activity (11:1-14,2-16).

Plots were first made of R and  $F_{10.7}$  independently on a yearly basis. Values over multiple years were then plotted using the 0 Jan 83 epoch to facilitate direct comparison with the orbital plots already completed.

Fortunately, sunspot and solar flux data (and geomagnetic data, which will be discussed in the next section) are collected at regular intervals. Specifically, the data obtained from ETAC provided values of

both R and  $F_{10.7}$  for each day of the period stated. This enabled the data to be compared in a straightforward manner with the revised orbital data sets which reflected values at one-day intervals. Accordingly, plots of solar data and orbital data versus time were developed to enable further examination into possible correlations. For example, a plot of a and R for Salyut 7 suggest a correlation between increased solar activity and increased decay rate during the last couple of years of orbit. Plots for LDEF allowed a check as to possible direct effects of solar activity on the Salyut 7/Cosmos 1686 complex via comparison of responses of both systems to changes in R and/or  $F_{10.7}$ . Detailed plots and analysis can be found in Chapter IV.

#### Comparing Geomagnetic Data with Orbital Data

The next phase of the research was to determine the extent to which geomagnetic activity played a part in influencing the orbital elements of Salyut 7 and LDEF. Several different geomagnetic indices were obtained from ETAC for the 1983-1991 time period. Of these, two were used in this study:  $A_p$  and  $K_p$ .

As was done with the solar data, plots were first made of the indices independently on a yearly basis. Values over multiple years were then plotted using the 0 Jan 83 epoch to facilitate direct comparison with the orbital data. Again, this direct comparison was made easier by the fact that data was collected at regular intervals. Geomagnetic data and orbital data versus time were then plotted together for both Salyut 7 and LDEF to permit further examination into possible correlations.

### Atmospheric Density Model

As was discussed in Chapter II, atmospheric drag is a large contributor to orbital perturbations. Most notably, it is the primary cause of long-term secular perturbations of the semi-major axis and eccentricity. Therefore it was deemed appropriate that the direct effects of atmospheric density be studied in this project. It was mentioned in Chapter II that most theoretical developments of atmospheric drag assume an exponential density profile, and that, while useful for many applications, does not take into account changes in the atmosphere due to day-to-day fluctuations in solar and/or geomagnetic activity. It was thus determined that a density profile should be developed which would be more able to represent these changes.

The model used in this study is based on work done by L.G. Jacchia as outlined in the 1985 Handbook of Geophysics and the Space Environment (11:14-36 - 14-42). It enables calculation of atmospheric density as a function of exospheric temperature and altitude, where exospheric temperature is determined as a function of  $K_p$  and  $F_{10.7}$ . Thus, whereas the only variable in the exponential model is altitude, the model used in this study incorporates geomagnetic and solar activity as well as altitude. Details of the model are addressed in Chapter IV.

The above model was then applied to both Salyut 7 and LDEF to give values of atmospheric density at actual satellite altitudes over time. As before, use of the standardized orbital data sets at one-day intervals permitted density and semi-major axis to be plotted simultaneously.

Analysis of density with respect to certain orbital parameters, namely  $a$  and  $e$ , was done in light of the knowledge that density directly affects these parameters in a secular way as previously discussed. LDEF was again used as a verification tool to increase confidence with respect to any possible correlation between density changes and Salyut 7/Cosmos 1686.

#### Determine Possible Use of Ion Propulsion

In this final phase of the research, an attempt was made to make an inference regarding the possible use of ion propulsion. Conceptually, such an inference could only be made with the understanding that ion propulsion might be one of several variables causing orbital perturbations which could not be explained using the other effects.

To summarize, the first phase was to examine the orbital parameters of Salyut 7 and LDEF to determine areas where a specific parameter did not behave as expected. Next, solar and geomagnetic data were analyzed and compared with the orbital data to determine any possible correlation. Using certain orbital, solar and geomagnetic data, a density profile was then constructed and compared with the orbital data. Finally, for any orbital effects not able to be explained via the other causes, a judgment was made as to the Salyut 7/Cosmos 1686 complex's possible use of ion propulsion.

#### IV. Analysis and Findings

##### Discussion of Data Analyzed

The nature of this project dictated the need for a significant amount of data. In fact, analysis of existing data was the primary thrust of the entire project. Therefore, it is useful at the outset of this chapter to discuss the type of data collected for analysis before progressing to the actual analysis.

The data collected for use in this study can be broken down into two general categories: orbital data and solar/geomagnetic data. These will be discussed separately in the following subsections before moving into the results of the data analysis.

It should also be reiterated that all graphs presented are based on a 0 January 1983 epoch. This provides consistency and allows direct comparisons between multiple plots. More specifically, most graphs are multi-year time series plots, with data given from Day 0 (0 January 1983) to Day 3000 (19 March 1991). These multi-year plots are used to illustrate the long-term behavior of the satellite; however, this is accomplished at the expense of detail over shorter time periods. Accordingly, some graphs provide data over shorter time periods to focus on particular areas of interest not sufficiently portrayed via the multi-year plots. Such plots presented in the text retain the standard time scale discussed above. Plots are also provided on a yearly basis of some parameters for Salyut 7 in the Appendix, but are given in terms of day-of-the-year for the particular year of interest.

Orbital Data. Orbital data for Salyut 7, Cosmos 1686, and LDEF was obtained from NORAD to cover time periods appropriate for this study. At the very minimum, data was needed to allow analysis of orbital elements throughout the life of the combined Salyut 7/Cosmos 1686 complex. Therefore, this minimum requirement was from docking (2 October 1985) through reentry (7 February 1991). Data was actually acquired for the time period 1 January 1983 through reentry. This extra data allowed possible analysis of pre-docking behavior of Salyut 7, if deemed necessary. Additionally, LDEF data was obtained which covered its entire life from launch in April 1984 to its retrieval by the space shuttle in January 1990.

The data was provided separately for each of the three systems via the standard two-line element sets. Many parameters were extracted from these element sets initially and examined so as to ensure that nothing was overlooked in the early stages. These included eccentricity,  $e$ , inclination,  $i$ , mean motion,  $n$ , mean anomaly,  $M$ , right ascension of the ascending node,  $\Omega$ , and argument of perigee,  $w$ . Semi-major axis,  $a$ , was also used in this study, for reasons that will be discussed momentarily. It was calculated from the mean motion using Kepler's Third Law:

$$\mu = n^2 a^3 \quad (3)$$

where

$\mu$  = gravitational parameter =  $3.986012 \times 10^5 \text{ km}^3/\text{sec}^2$

$n$  = mean motion (revs/day)

$a$  = semi-major axis (km)

The semi-major axis is typically used in conjunction with the above parameters to describe a standard Keplerian elliptical orbit. It was used extensively in this study to portray orbital behavior for several reasons. First, it is easily derived from the other parameters in the two-line element sets. Second, it gives a general feel for satellite altitude, especially for orbits with low eccentricities such as LDEF and Salyut 7. This can be seen from the expressions  $r_a = a(1 + e)$  and  $r_p = a(1 - e)$  which represent radius of apogee and radius of perigee, respectively (see Figure 3). For small eccentricity, the orbit is nearly circular since  $r_a \approx r_p$ . If the orbit is assumed to be circular, letting  $r = r_a = r_p$ , then altitude at any point would simply be  $r - R_e \approx a - R_e$ , where  $R_e$  is the radius of the earth.

This, of course, is only a rough illustration of the relationship between semi-major axis and altitude, as it assumes a spherical earth. In reality, the distinction would have to be made between geocentric and geodetic altitude, which are equal only if the earth is a sphere. Geocentric altitude is based on the premise that the radius vector goes through the earth's center; geodetic altitude is measured perpendicular to the earth's surface, such as would be done from a ground station. While this difference can be significant, the above development for orbits with small eccentricities suggests that a conceptual feel for altitude can be gained from examination of semi-major axis behavior.

It is interesting to note that Salyut 7 and Cosmos 1686 data were collected and provided separately, since the two spacecraft were essentially one body once docked in October 1985. Conceptually, orbital data for two satellites docked together should be identical, excluding

perhaps some mechanical errors introduced during data collection and/or computational errors associated with data reduction. An additional problem related to the latter case is that data for two systems is typically collected at different times, or epochs. Thus, when direct comparisons are desired between two systems, conversion of the data is necessary to enable comparison based on a standard epoch. This obviously creates another possible way for errors to be introduced.

Figure 6, which is a plot of satellite radius in the earth centered inertial (ECI) reference frame, illustrates that such errors were also present in this study. Note that this is "geocentric radius," per the above discussion. The errors appear to be on the order of 10 km or less, which suggests that any analysis using the orbital data should be done in consideration of this error band. In light of these limitations, it was decided that the Salyut 7 orbital data would be used exclusively to represent the Salyut 7/Cosmos 1686 complex. This allowed continuity throughout the entire 1983-1991 timeframe, but did not limit the accuracy of the data beyond the limits described above.

The parameters used to the greatest extent in this study were  $a$ ,  $e$ ,  $i$ ,  $\Omega$ , and  $w$ . Although mean motion and mean anomaly were graphed and examined in the early stages of the research, it was determined that any changes in these parameters would show up in one or more of the others. In the case of mean motion, for example, changes would be reflected in semi-major axis, since semi-major axis was determined from mean motion using Kepler's Third Law.

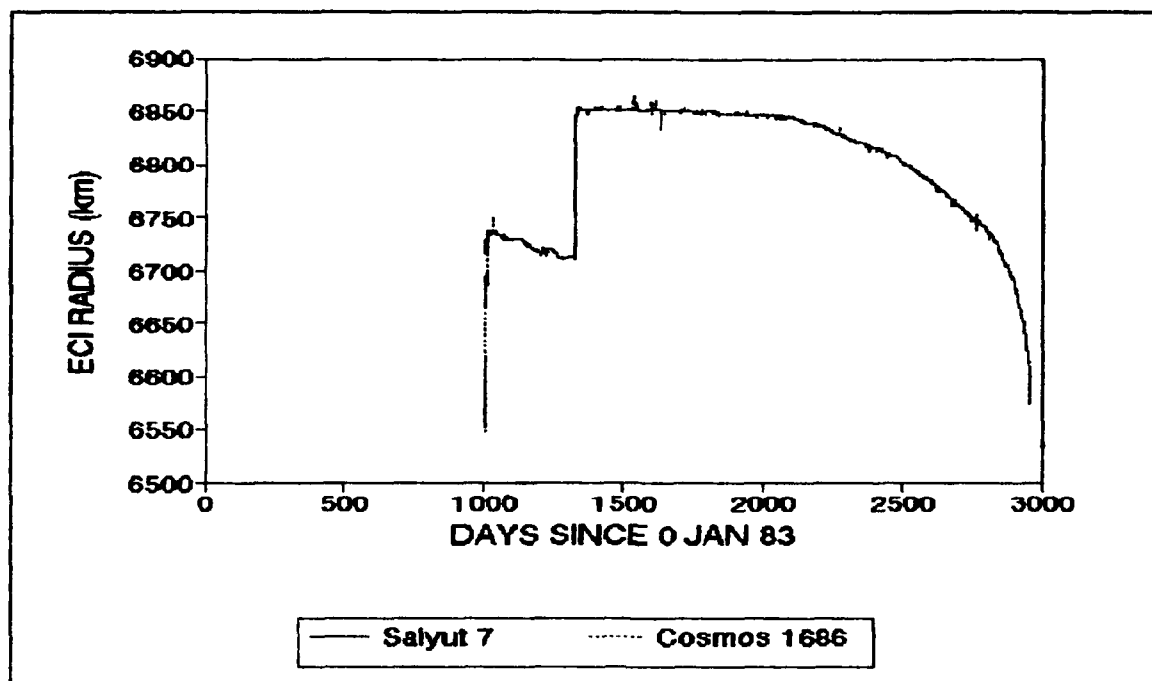


Figure 6. ECI Radius for Salyut 7 and Cosmos 1686

Solar/Geomagnetic Data. In addition to the orbital data described above, solar and geomagnetic indices were also used extensively throughout the course of this work. As discussed briefly in Chapters II and III, two solar indices and two geomagnetic indices were used to indicate general levels of solar and geomagnetic activity, respectively, over time. The sunspot number,  $R$ , and 10.7-cm solar radio flux,  $F_{10.7}$ , were used to reflect solar activity, and the general activity indices  $A_p$  and  $K_p$  were used to reflect geomagnetic activity.

ETAC was the source for all four of these indices, and they were able to provide data for the period 1 January 1983 through 31 March 1991. This allowed full overlap with the orbital data already obtained.

The sunspot number,  $R$ , is relatively self-explanatory in that it represents the number of sunspots on the sun at any given time. To be

precise, it is a function of visible sunspots and sunspot groups as given by Equation (1) in Chapter II. Its use in this analysis is based on the fact that it "remains the single most important index for the general level of solar activity" (11:1-14). The other solar index used is 10.7-cm solar radio flux,  $F_{10.7}$ , which was also outlined in Chapter II.

Geomagnetic activity was introduced into the analysis via the indices  $A_p$  and  $K_p$ . As indicated in Chapter II,  $K_p$  is derived from the basic K activity index, which represents readings at a particular location.  $A_p$ , which represents an average daily value of geomagnetic activity, is derived from  $K_p$  using tables to remove the logarithmic nature of  $K_p$ .

#### Examination of Orbital Data

LDEF. As mentioned earlier, the LDEF satellite was utilized in this study to provide a baseline for investigating the effects of various atmospheric perturbations. Accordingly, it was evaluated before Salyut 7/Cosmos 1686.

Figure 7 is a plot of semi-major axis for LDEF using the 0 January 1983 epoch. For example, it can be seen from Figure 7 that there are noticeable slope changes near Days 1700, 2100, and 2400; at these points the LDEF satellite decay rate is increased. As mentioned earlier, LDEF was not capable of maneuvering itself, so these slope changes must be due to natural perturbations. The most likely explanation is that the changes at those points were due to increased atmospheric drag. Further analysis must be done, however, to show

whether or not an increase in drag was actually the cause of these slope changes.

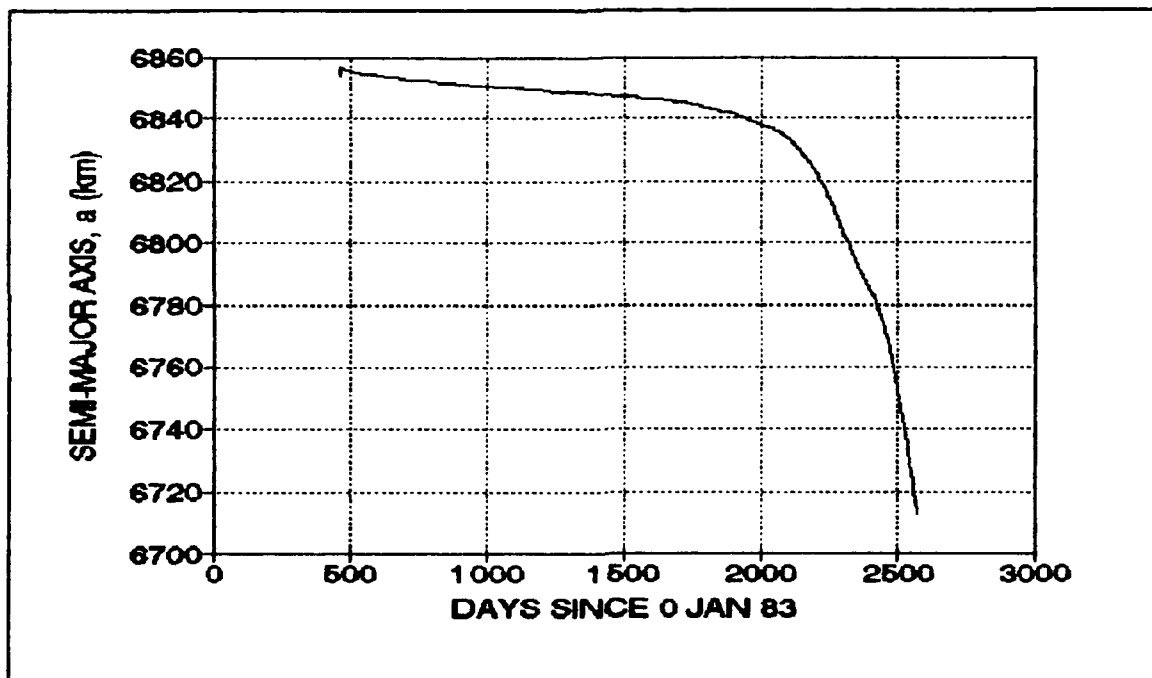


Figure 7. Semi-major Axis vs. Time for LDEF

Eccentricity for LDEF is plotted in Figure 8. Based on the theoretical effects of atmospheric drag, which was discussed in Chapter II, it was expected that the orbit would be affected secularly by decreasing the eccentricity. Interestingly, this trend is not as clearly shown in Figure 8 as might be expected, although there appears to be a slight downward trend between days 2000 and 2400 corresponding to the slope change noted above for semi-major axis. The large fluctuations toward the end of the orbit make this determination difficult, and they themselves are an interesting aspect of the eccentricity curve. It is possible that they are due to oblateness

effects, as outlined in Chapter II. Per Table 1, the earth's gravitational field has a moderate periodic effect on eccentricity, so it follows that as the satellite altitude decreases the effects of the gravitational field should increase, thus making the periodic pattern more pronounced. These issues will be studied in more detail when comparisons are made with solar and geomagnetic activity and density.

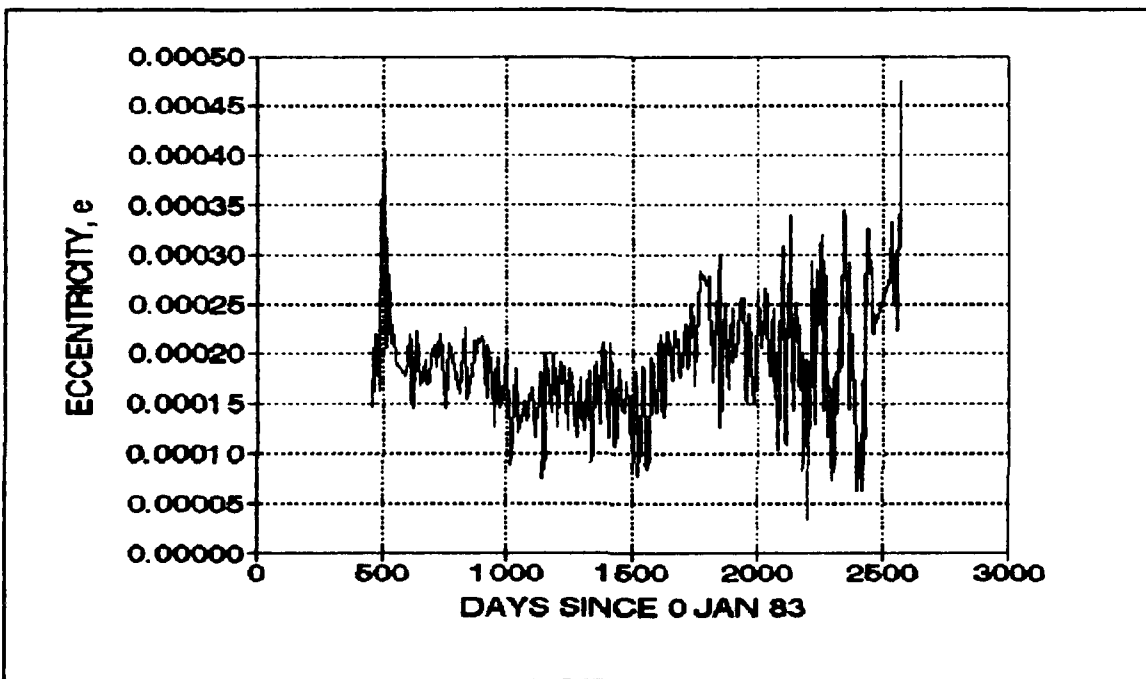


Figure 8. Eccentricity vs. Time for LDEF

The third orbital parameter to be presented for LDEF is inclination, which is shown in Figure 9. A slight decrease in inclination can be seen over time, as well as some large fluctuations toward the latter part of the orbit, especially around day 2200. A small secular decrease is expected due to drag, and the periodicity can possibly be attributed to oblateness effects and solar radiation

pressure. However, no cause can be predicted at this point for the large changes around day 2200. Potential causes for each of these phenomena will be examined later in the analysis.

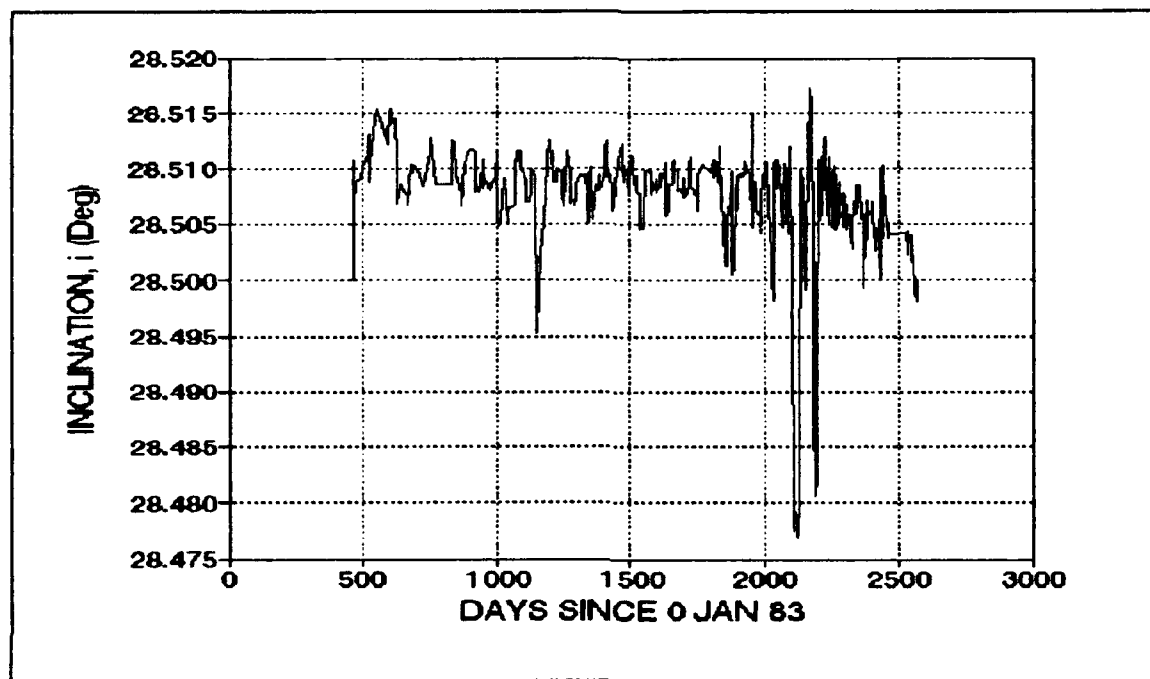


Figure 9. Inclination vs. Time for LDEF

Salyut 7/Cosmos 1686. The above plots for LDEF illustrate the general behavior of that satellite over its lifetime. The same insight should thus be possible with similar plots for the Salyut 7/Cosmos 1686 complex. These plots are provided as Figures 10-13, and discussion of each follows.

Figure 10 depicts the time series behavior of semi-major axis for Salyut 7 over the same time period. An initial look at this graph indicates many areas of interest. The most noticeable is the large increase in semi-major axis between Days 1325 and 1330. This corresponds

to the series of maneuvers made in August 1986 which put the then-unmanned Salyut 7/Cosmos 1686 complex into a much higher orbit. At that point in time, the Soviet's new Mir space station had already been launched (19 February 1986), so the troubled Salyut 7 station was no longer necessary to continue their manned space program (6:207). In fact, this series of maneuvers in August 1986 strongly suggested that at that time, there were "no plans to visit Salyut again" (6:209). For the purposes of this study, this boost phase of the orbit also formed a natural dividing line about which the orbit of Salyut 7 could be analyzed.

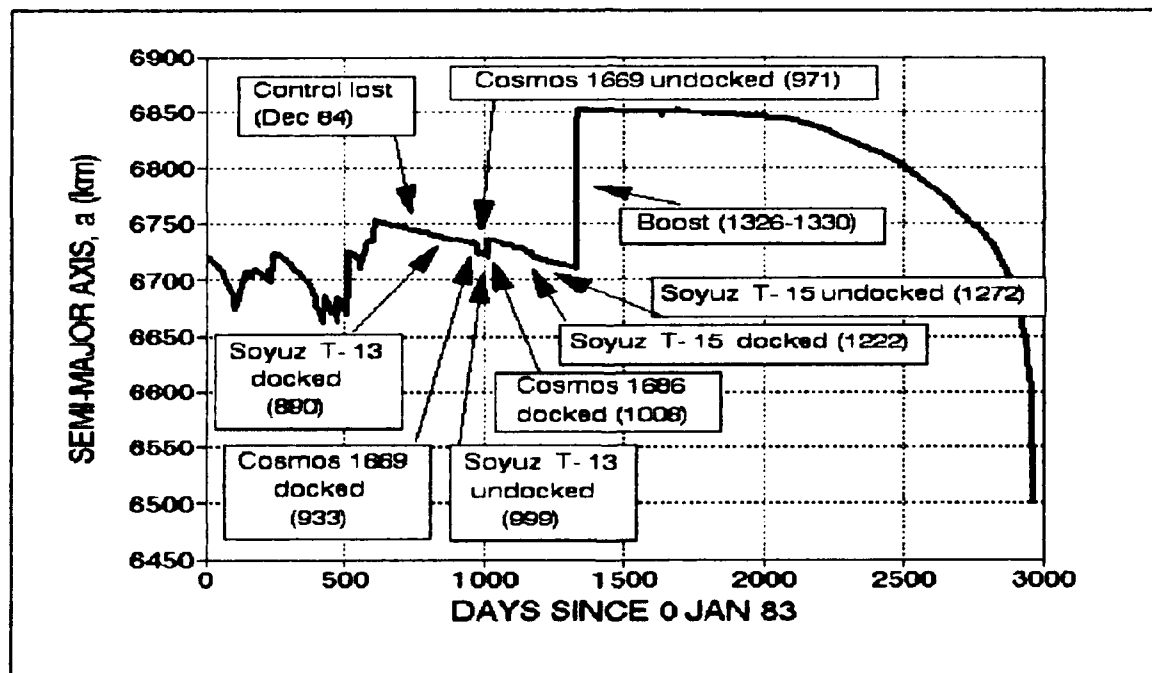


Figure 10. Semi-major Axis vs. Time for Salyut 7

Prior to the boost, it can be seen that the station was the hub for much activity, which of course is expected for an operational space station. However, missions to Salyut 7 after December 1984, when control was lost, were missions aimed primarily at trying to rescue the spacecraft. All of this activity makes for a more difficult analysis within the context of this research since the effects of these maneuvers would have to be accounted for in addition to other effects. However, since this study was aimed at determining the possibility of an ion propulsion source aboard Cosmos 1686, analysis of the orbital data was focused on the time period after it was docked with Salyut 7. Accordingly, the time period between Days 1006 and 1325 was the primary window of interest for activity prior to the large boost phase. Figure 11 provides an exploded view of this region, and highlights detailed station activity during that period. All of the activity prior to and including the boost is summarized in Table 4.

Following the boost to the higher orbit, a much more gradual decay is evident, which is representative of a satellite not being maneuvered. An absence of maneuvers is obviously one explanation, but there are other possible explanations for the decreased activity. The most obvious is that at the higher altitudes the atmospheric density experienced by the satellite would have been considerably lower, thus tending to slow the decay rate of the Salyut 7/Cosmos 1686 system relative to what it was at a lower altitude.

Other highlights of Figure 10 include apparent changes in slope (increases in decay rate) near Days 2100, 2500, and 2800. As hypothesized for LDEF, these changes may have been due to increases in

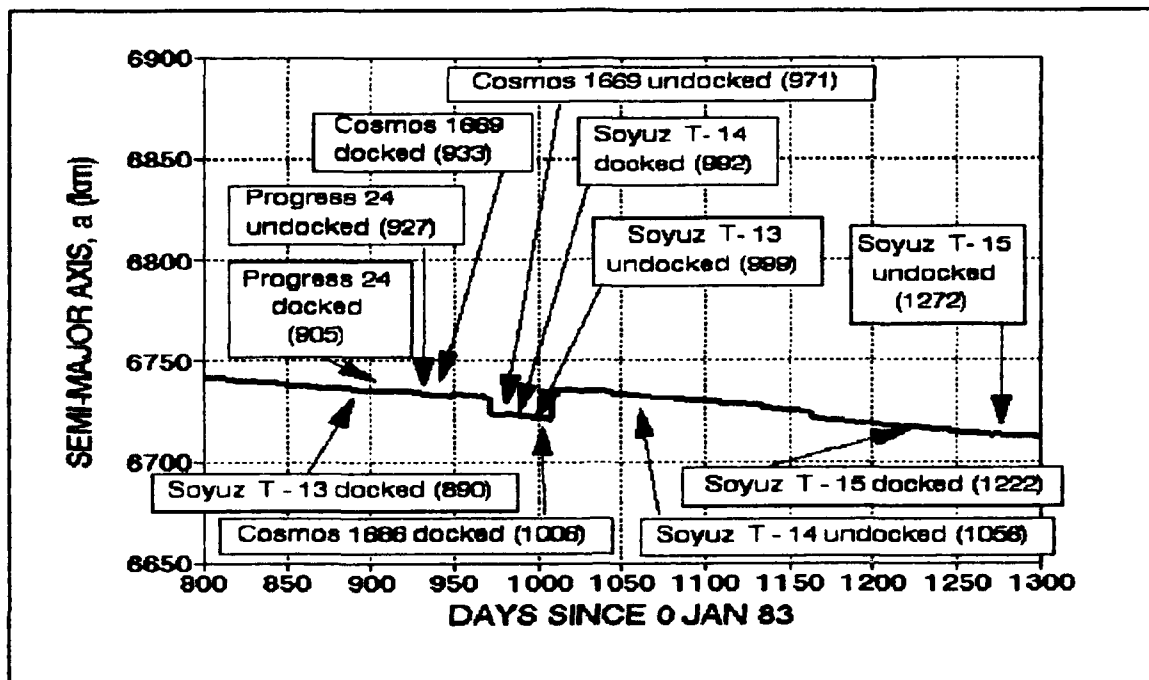


Figure 11. Semi-major Axis vs. Time for Salyut 7

Table 4  
Salyut 7 Activity (Compiled from (6:206))

<u>Maneuver/Activity</u>	<u>Date(s)</u>	<u>Std Day (83 Epoch)</u>	<u>a (Before)</u> <u>(km)</u>	<u>a (After)</u> <u>(km)</u>
Soyuz T-13 docked	3 Jun 85	890	6736.2	6735.7
Progress 24 docked	23 Jun 85	905	6735.6	6735.3
Progress 24 undocked	15 Jul 85	927	6735.0	6734.5
Cosmos 1669 docked	21 Jul 85	933	6734.0	6733.8
Maneuver	5 Aug 85	948	6732.5	6733.9
Cosmos 1669 undocked	28 Aug 85	971	6731.8	6724.2
Soyuz T-14 docked	18 Sep 85	992	6722.7	6723.1
Soyuz T-13 undocked	25 Sep 85	999	6722.6	6722.4
Cosmos 1686 docked	2 Oct 85	1006	6722.0	6720.9
Maneuvers	3-4 Oct 85	1007-1008	6720.9	6736.0
Soyuz T-14 undocked	21 Nov 85	1056	6733.8	6732.4
Maneuver	6 Feb 86	1133	6728.2	6727.0
Soyuz T-15 docked	6 May 86	1222	6717.0	6717.0
Soyuz T-15 undocked	25 Jun 86	1272	6713.7	6713.7
Maneuvers	18-22 Aug 86	1326-1330	6710.0	6852.6

atmospheric drag, but further analysis must be done to make that determination. The results of that portion of the analysis are presented later in this chapter.

Figure 12 illustrates the changes in eccentricity over time for Salyut 7/Cosmos 1686. As with the semi-major axis plots in Figures 10-11, there are also some obvious areas of interest in the eccentricity profile of the orbit. The most obvious occurs near Day 1325 which coincides with the major boost just discussed. It is also possible to see a sharp rise and fall coinciding with the Cosmos 1669 undocking and Cosmos 1686 docking, respectively.

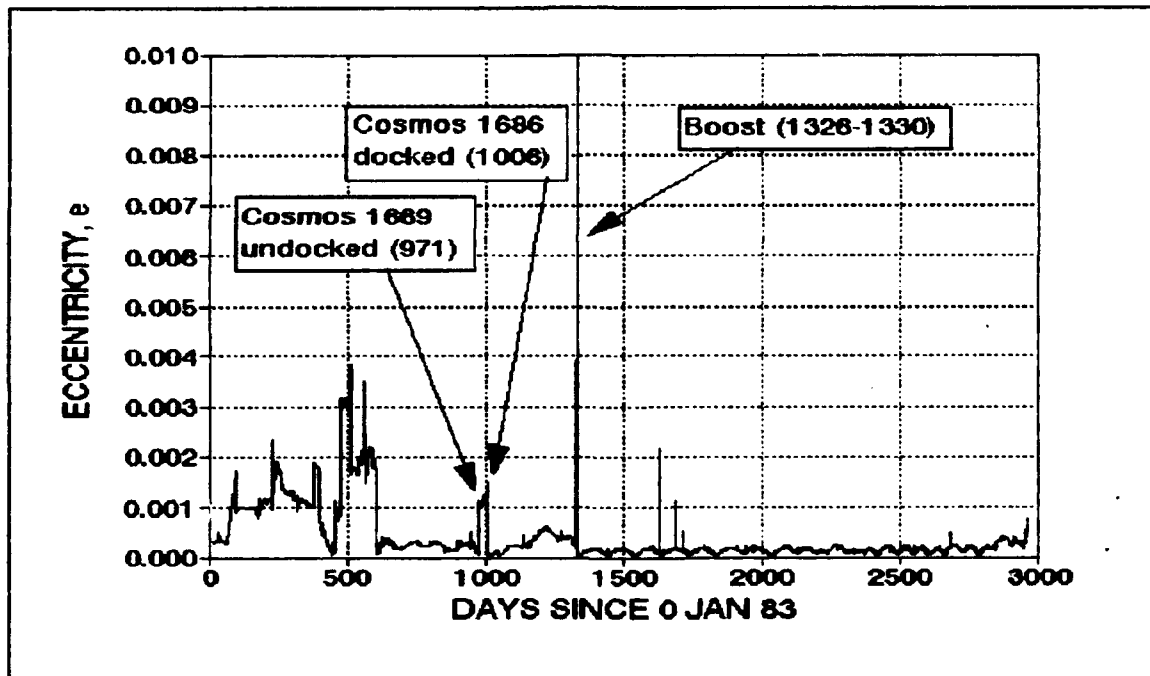


Figure 12. Eccentricity vs. Time for Salyut 7

The increase in eccentricity associated with the undocking of Cosmos 1669 is actually due to a maneuver just prior to the actual

release, most likely so that Cosmos 1669 could be released at as low an altitude as possible. Specifically, the perigee height was reduced from 352 km to 339 km; apogee height remained the same at 353 km (6:206).

As a check of the data used in this study as compared to the data given in the literature, the observed values of  $a$  and  $e$  from the two-line element set just prior to and just after the reported maneuver were used to calculate the change in perigee height. The result was a calculated change of 13.9 km, as compared to the 13-km difference noted above. Considering round-off errors and times of observation, this gives a reasonably good check.

The eccentricity change at Day 1006 also appears plausible when compared with the change in semi-major axis at that time. Also, the sudden decrease in eccentricity just after docking would be consistent with a maneuver to increase perigee height to recircularize the orbit. This is in fact what was done via maneuvers 3-4 October 1985 which increased perigee height from 336 km to 358 km; apogee height was also increased slightly from 353 km to 359 km (6:206).

Another characteristic of the eccentricity plot worth noting is that periodic changes are quite noticeable, especially after the station was boosted to its higher orbit. As discussed in Chapter II and above for LDEF, this is probably due to oblateness effects.

One final aspect of Figure 12 is of interest. There appears to be an increase in eccentricity between Days 1000 and 1250. No direct explanation can be offered at this point for this unusual behavior, but this area will be examined in further detail later in the analysis.

Inclination versus time is plotted in Figure 13. The same major breakpoints as previously noted can again be seen, as can the periodic behavior after the boost. Again, the periodicity is probably due to gravitational field irregularities. Plots of other orbital parameters for Salyut 7/Cosmos 1686 can be found in Appendix B.

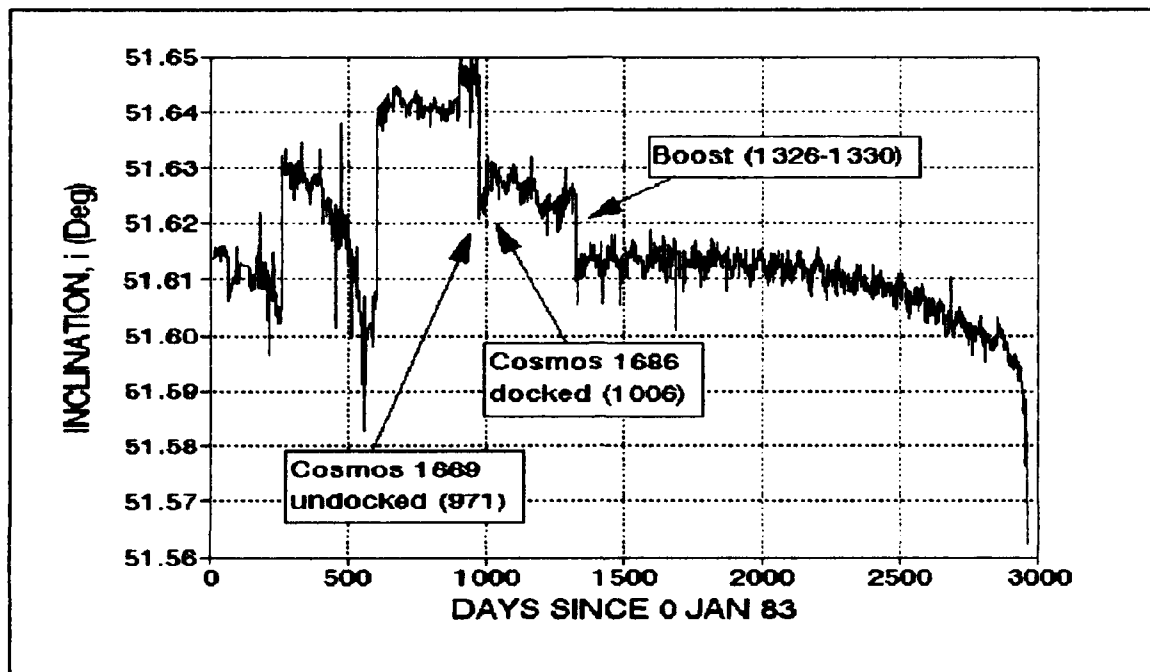


Figure 13. Inclination vs. Time for Salyut 7

Combined Analysis of LDEF and Salyut 7/Cosmos 1686. To this point, orbital elements for both LDEF and Salyut 7/Cosmos 1686 have been examined independently over the 1983-1991 time period. This approach has proven useful in illustrating certain significant events in the orbits of both systems (especially Salyut 7), but makes it difficult to do a direct comparison. Accordingly, it was deemed desirable to plot curves for both systems simultaneously on the same graph. This proved

to be more of a challenge than initially anticipated, with the main difficulty stemming from the fact that the two-line element sets from which the data was taken give values at different time intervals.

It was decided that any manipulation of the data to transform it to a standardized time scale should be done in such a way that the remaining data to be analyzed (i.e., the solar and geomagnetic data) could also be related to the new time scale in a straightforward manner. More importantly, any time scale transformation had to be able to preserve to the maximum extent possible the actual behavior of the data. These conditions were considered in each case, and it was determined that the new temporal standard would be a time scale at one-day intervals, with 0 January 1983 as the epoch date.

The transformation to a consistent time scale can be done in many different ways. In this project, one of the primary methods used was simply to fit a polynomial curve through the data. While this approach may not be as elegant or as accurate as more modern techniques used in statistical or time series analysis circles, it proved useful in this analysis to examine general trends. In addition, many of the classic time series analysis approaches such as autoregression, differencing, and moving averages assume that the data is given at constant time intervals. That was not the case for the orbital data used here, so its application seemed somewhat limited. Time series analysis techniques could conceivably be used, however, on the solar and geomagnetic data since they are at standard time intervals. While this might have proven useful, it was not within the scope of this project.

The usefulness of a polynomial fit is that the data can be transformed to any other time standard desired. Simply put, the conversion to another time scale is accomplished by inputting values of time as the independent variable and letting the equation produce the resulting curve in the new time scale. This type of conversion obviously requires that the time inputs are within the domain of the fitted polynomial.

The only data actually transformed to another time scale in this study was the semi-major axis for both systems. This was primarily due to the fact that these curves were relatively smooth, so there was less chance of oversimplifying the data and losing any specific fluctuations that might prove meaningful. Curves were also fit through the solar and geomagnetic data, but that was done only to help illustrate trends.

The curve fitting procedure was accomplished with the help of a commercially available software program called SPLOT. It will fit up to a tenth-order polynomial using the least-squares technique and gives statistical information for each polynomial to indicate goodness of fit. In particular, it uses two parameters: residual variance and coefficient of determination. The first of these, residual variance, is related to the conventional  $R^2$  statistic which estimates the "proportion of variance in one of the variables that can be explained by variation in the other variable" (7:73). For a univariate model such as the one considered here where there is only one independent variable (time) and one dependent variable (a),  $R^2$  would represent the ability of changes in time to explain changes in semi-major axis. Residual variance represents a similar correlation; it indicates the variance of the

residuals, which are the differences between the actual values and the fitted (estimated) values. The practical difference between  $R^2$  and residual variance is that higher is better with  $R^2$ , while lower is better with residual variance.

To fit a curve using SPLIT, successively higher order polynomials were examined until the change in residual variance became small, thus indicating the minimal benefit of going to higher order functions. To borrow a term from the time series analysis discipline, this represents the concept of "parsimony" (17:20).

Curves were also evaluated on the basis of the magnitude of the residuals themselves. This was done as an added assurance that the fitted curve was not misrepresenting the data. A maximum deviation of approximately 5 km was used for this purpose as a rough criteria for accepting or rejecting potential polynomial fits. This criterion was deemed appropriate, and perhaps overly restrictive, in light of the fact that NORAD states that their orbital data gives position to within 12 km at a 90 percent confidence interval.

The curve fitting procedure for LDEF semi-major axis resulted in a sixth-order polynomial of the following form:

$$a = x_6 t^6 + x_5 t^5 + x_4 t^4 + x_3 t^3 + x_2 t^2 + x_1 t + x_0 \quad (4)$$

where

$$\begin{array}{lll} x_6 = -2.284566 \times 10^{-17} & x_3 = 8.112119 \times 10^{-7} & x_0 = 6812.815 \\ x_5 = 1.697687 \times 10^{-13} & x_2 = -6.822717 \times 10^{-4} & \\ x_4 = -5.16397 \times 10^{-10} & x_1 = 0.2780805 & \end{array}$$

Figure 14 illustrates the results of plotting predicted values of semi-major axis using this polynomial with original time values against the original semi-major axis data. Residual values are also plotted to show absolute deviation from the actual data. It can be seen that the curve does an extremely good job of matching the data until around Day 2000, at which point the residuals begin to grow and reach a maximum of just over 5 km at about Day 2500. Still, this is a good fit given the accuracy of the data as discussed earlier. It is worth noting that the

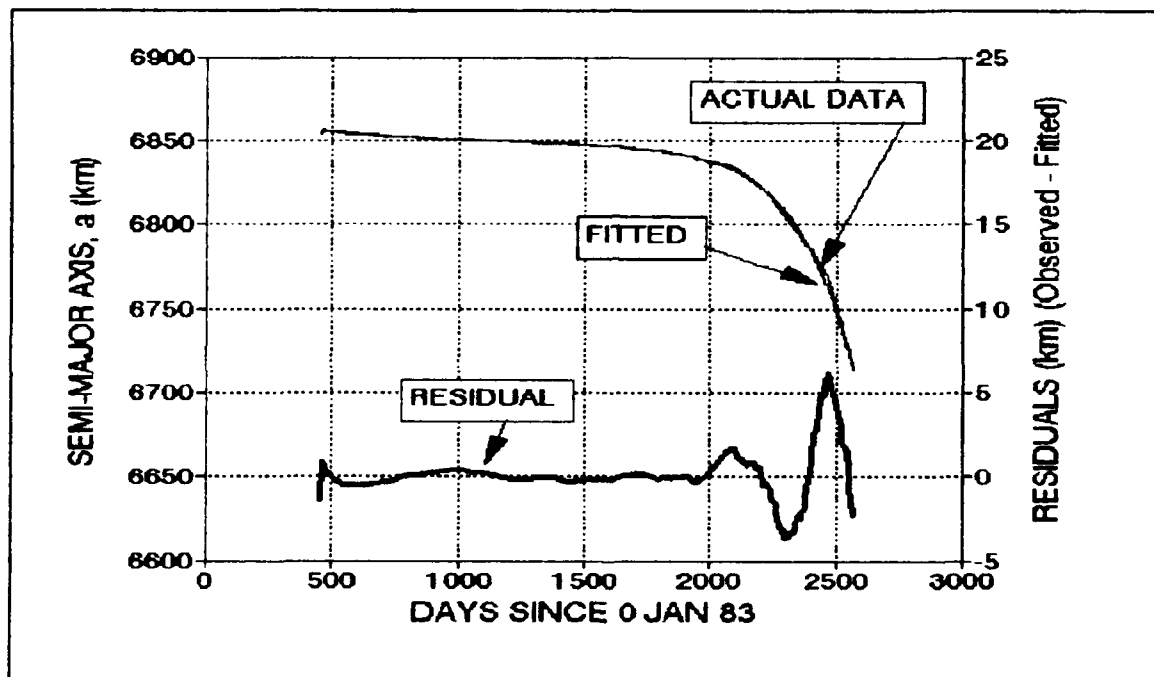


Figure 14. Semi-major Axis (Fitted) for LDEF

large residuals occur toward the end of the curve where the slope is much steeper. This highlights an inherent limitation of curve fitting: as the slope gets steeper, changes in the dependent variable are getting larger for a given step size in the independent variable, so a

univariate model is less likely to be able to match the changes. This same limitation was also brought out during curve fitting for the Salyut 7/Cosmos 1686 semi-major axis data.

Overall, the same concept of curve fitting was applied to the Salyut 7/Cosmos 1686 semi-major axis data, although the procedure was not quite as straightforward. As was shown earlier, the semi-major axis curve for Salyut 7/Cosmos 1686 has many variations in it, which limits the extent to which any single curve could accurately model the actual data. To get around this limitation, the data was split up so that curves could be fit to smaller subsets, with the hope that they could be pieced back together for a complete model. Accordingly, subsets were defined on the intervals between Days 1008-1326, 1330-1999, 2000-2699, 2700-2799, and 2800-2960. A satisfactory polynomial fit was not possible for the last subset due to the large slope of the curve, as noted above. For that subset, linear interpolation was used to get values at the standard one-day intervals.

The results of the curve fits for Subsets 1-4 for Salyut 7/Cosmos 1686 are shown in Figures 15-18, respectively. As was done with the LDEF curve fit (Figure 14), the curves are plotted along with the original data to show goodness of fit and the residuals. The coefficients of the curves fitted through the data are presented in Table 5.

One feature of Figure 16 worth noting is the existence of two outliers. Examination of the actual data confirmed that these were bad data points, and they were not included in the data for the curve fitting procedure.

Table 5  
Polynomial Curves for Salyut 7/Cosmos 1686 Semi-major Axis

<u>Subset</u>	<u>Coefficient</u>	<u>Value</u>
1 (1008-1326)	$x_5$	$-9.844355 \times 10^{-11}$
	$x_4$	$5.723031 \times 10^{-7}$
	$x_3$	$-0.001326839$
	$x_2$	$1.533437$
	$x_1$	$-883.507$
	$x_0$	$2.097877 \times 10^5$
2 (1330-1999)	$x_4$	$3.785978 \times 10^{-11}$
	$x_3$	$-2.834992 \times 10^{-7}$
	$x_2$	$7.687336 \times 10^{-4}$
	$x_1$	$-0.9085962$
	$x_0$	7249.688
3 (2000-2699)	$x_5$	$1.67916 \times 10^{-12}$
	$x_4$	$-2.027495 \times 10^{-8}$
	$x_3$	$9.753569 \times 10^{-5}$
	$x_2$	$-0.2338183$
	$x_1$	279.3643
	$x_0$	$-1.26231 \times 10^5$
4 (2700-2799)	$x_3$	$-1.708335 \times 10^{-5}$
	$x_2$	0.1405543
	$x_1$	-385.6566
	$x_0$	$3.596429 \times 10^5$

Overall, examination of the residuals in each case reveals that the curve fits did a good job of accurately matching the actual data, as all residuals were under 2 km. This is more than adequate given the accuracy of the data.

When all of the subset curves were pieced together, there were some slight mismatches between the endpoints of the curves. In those cases, linear interpolation using the actual data was done to smooth the transitions. Figure 19 shows the combined Salyut 7/Cosmos 1686 semi-

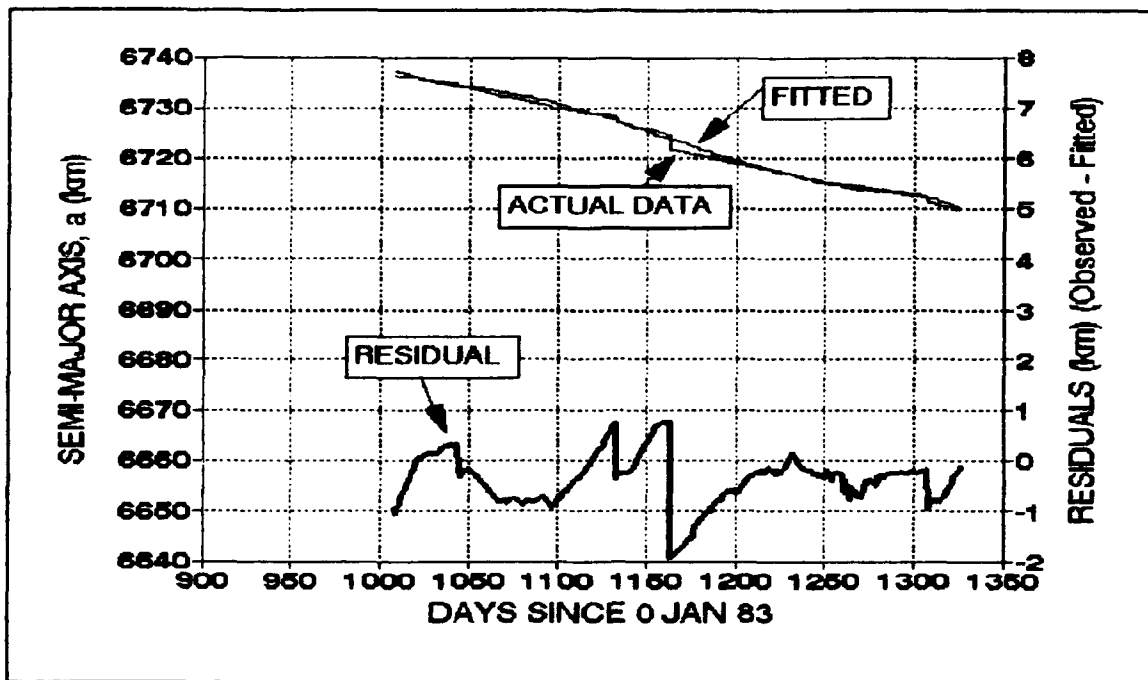


Figure 15. Semi-major Axis (Fitted, Subset 1) for Salyut 7

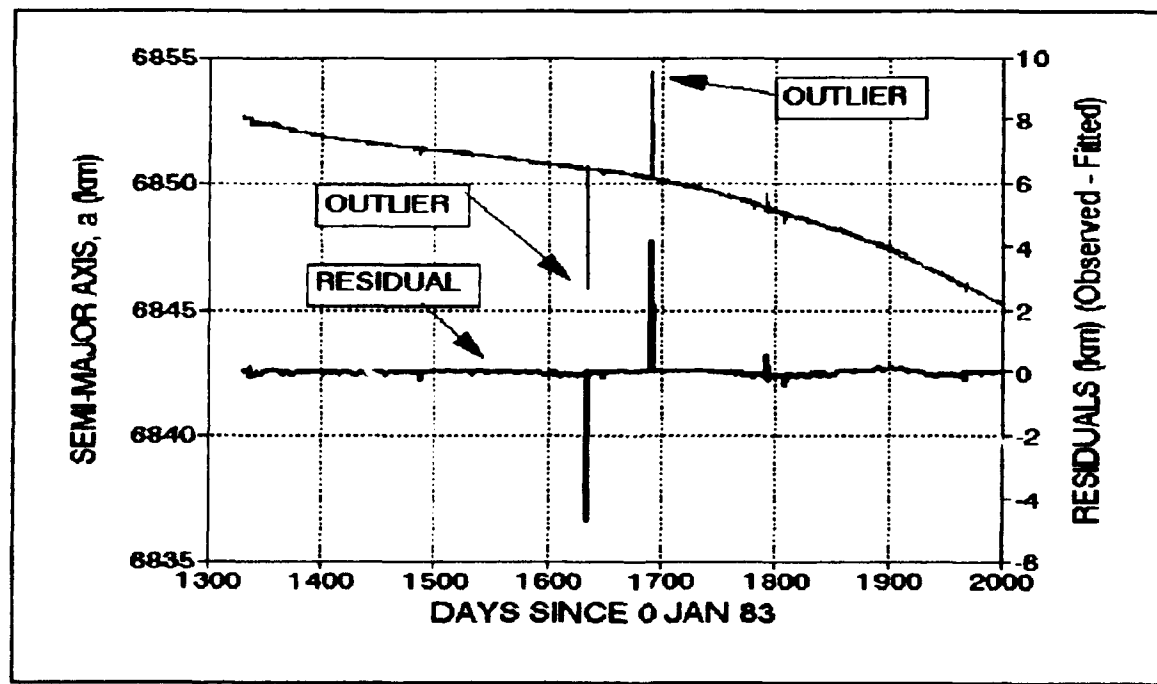


Figure 16. Semi-major Axis (Fitted, Subset 2) for Salyut 7

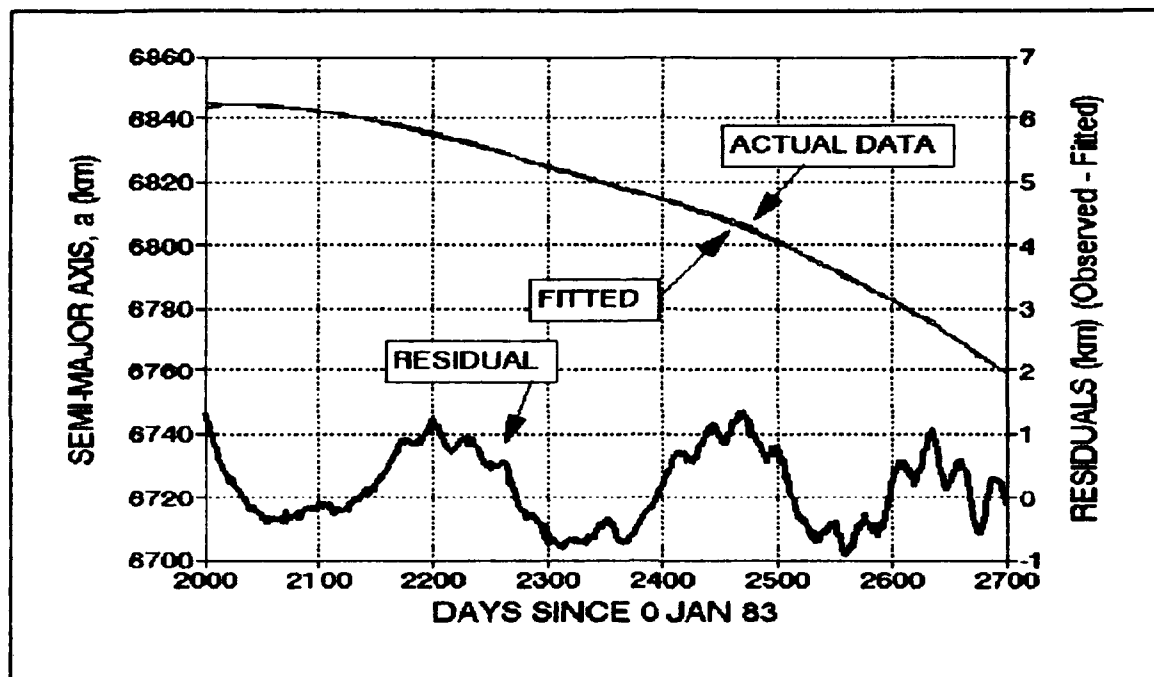


Figure 17. Semi-major Axis (Fitted, Subset 3) for Salyut 7

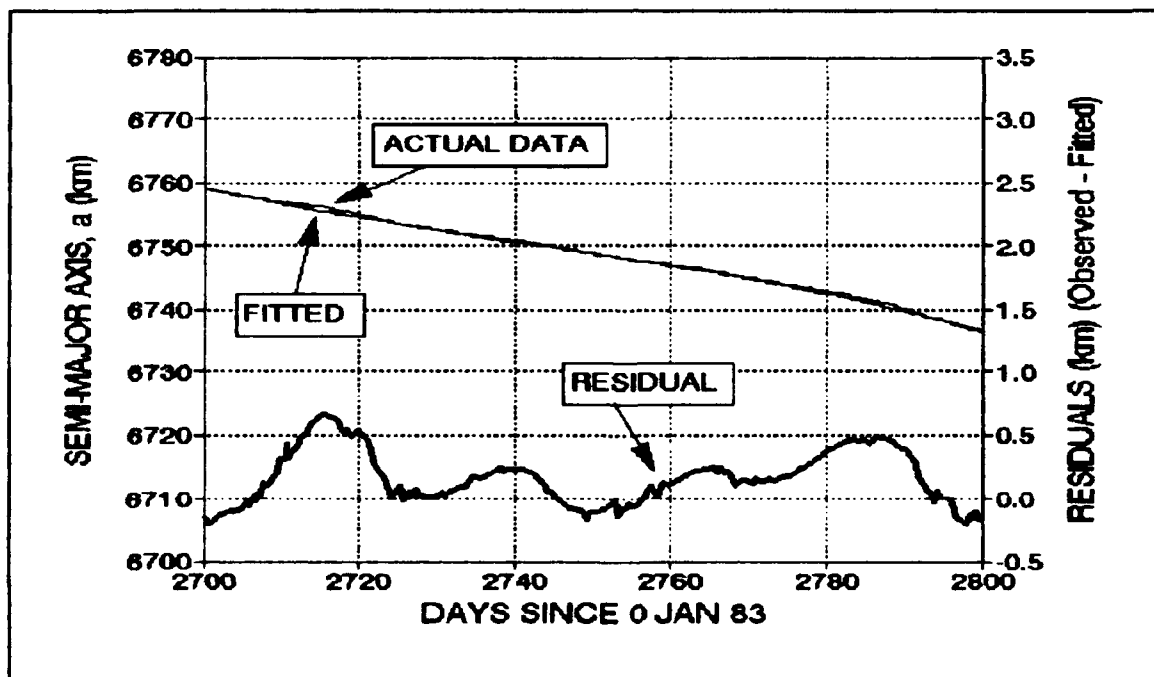


Figure 18. Semi-major Axis (Fitted, Subset 4) for Salyut 7

major axis curve using these curve fitting/interpolation methods based on the original time data.

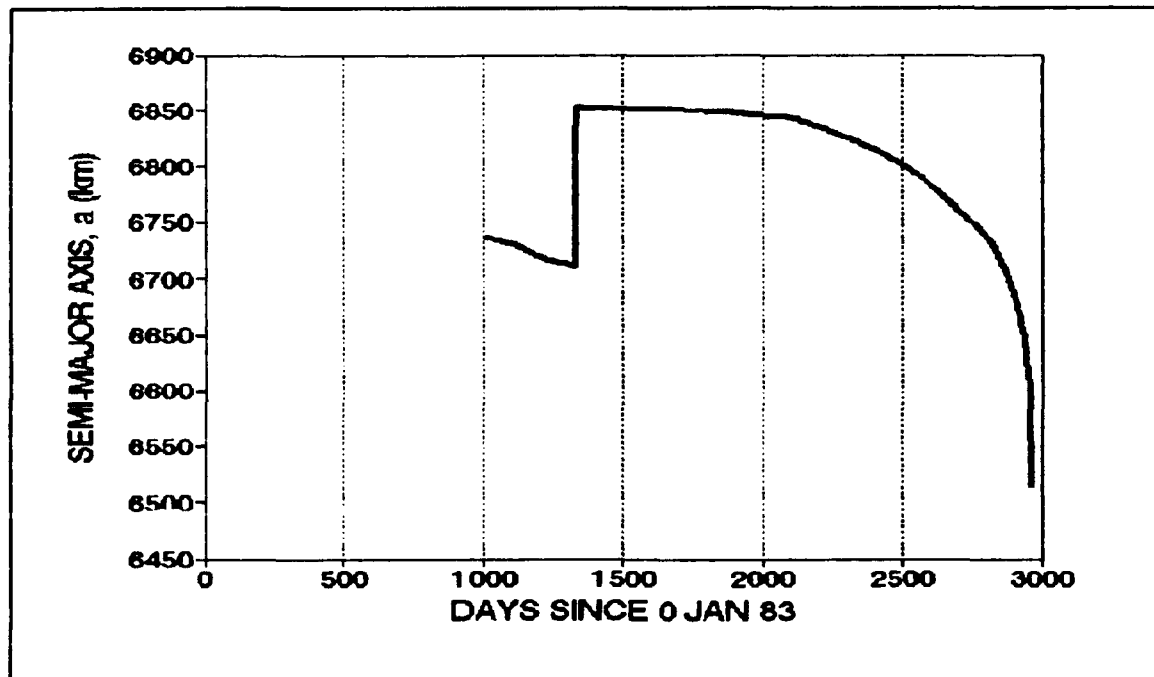


Figure 19. Semi-major Axis (Fitted, Total) for Salyut 7

Finally, semi-major axis curves for LDEF and Salyut 7/Cosmos 1686 were transformed to the standard one-day interval time scale using the polynomial functions just described. No transformation was necessary for those areas of the Salyut 7 curve that were interpolated, as the initial interpolation was done at the one-day intervals. The transformed curves for both systems are plotted simultaneously in Figure 20.

This combined plot of semi-major axis for Salyut 7/Cosmos 1686 and LDEF illustrates some interesting points. First, there is a marked difference in slope in the Subset 1, or pre-boost, portion of the curve

(Days 1008-1326). This dissimilarity is probably due to the difference in atmospheric density that each system would have encountered at any given time during that period. Second, both are at very nearly the same altitude for a considerable period of time after Salyut 7/Cosmos 1686 is boosted to the higher orbit. This reduces the number of variables in the analysis if discrepancies are observed between orbital elements of the two systems during that time period. Finally, it appears that the decay rate of both systems increases around Day 2000. This suggests that atmospheric conditions were adversely affecting both systems.

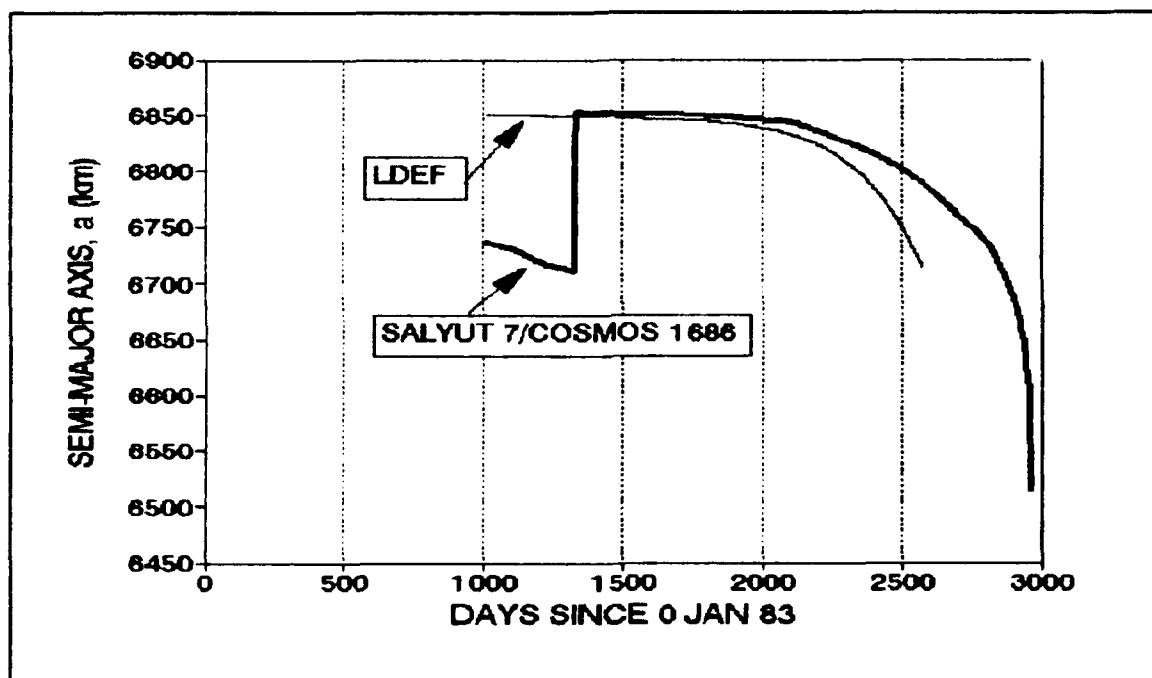


Figure 20. Semi-major Axis for LDEF and Salyut 7/Cosmos 1686

#### Comparing Solar Data with Orbital Data

As mentioned earlier, sunspot number,  $R$ , and 10.7-cm flux,  $F_{10.7}$ , were two indices used in this study to quantify solar activity over

time. Further, these indices were compared directly with the orbital parameters of both LDEF and Salyut 7/Cosmos 1686 in an attempt to determine the extent to which solar activity was a cause of orbital perturbations. First, the time series behavior of each of these indices was studied independently. Second, they were compared with LDEF and Salyut 7/Cosmos 1686 orbital data to determine if there was any evident correlation.

The variation of sunspot number from January 1983 through March 1991 is shown in Figure 21. In addition to the actual observed data, the results of a curve fitting procedure such as that outlined earlier are also shown in the form of a polynomial fitted through the data.

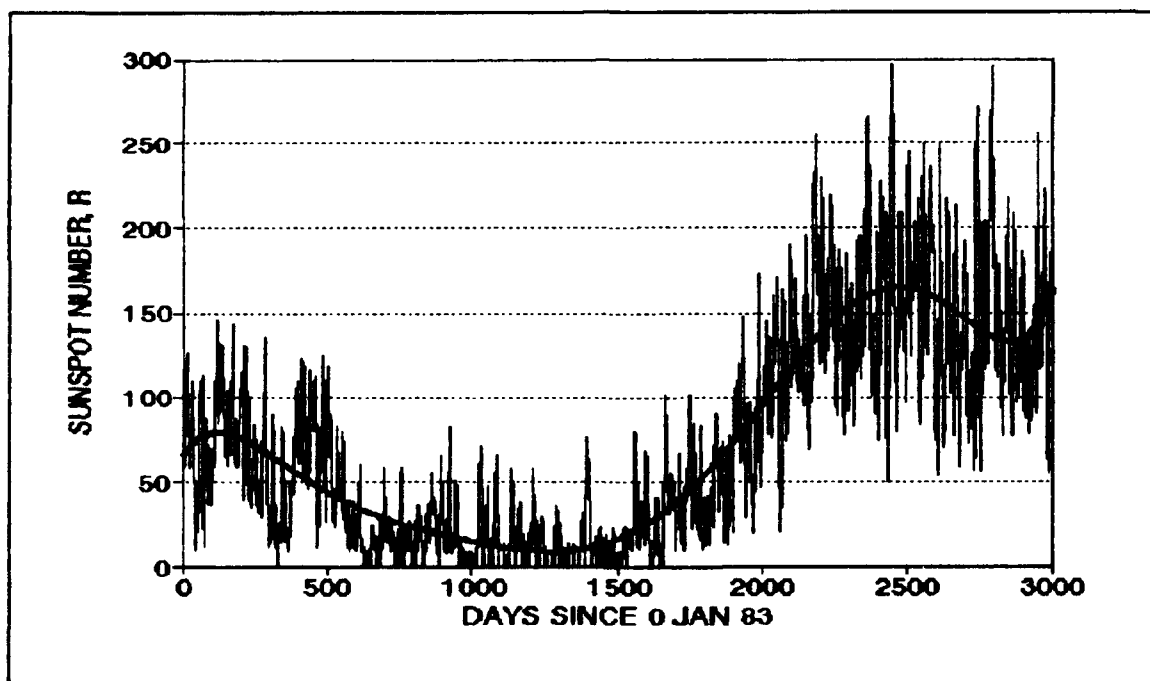


Figure 21. Sunspot Number vs. Time

Overall, Figure 21 illustrates a very noticeable trend. Indeed, it coincides exactly with the 11-year solar cycle as expected. The low point represents the start of a new solar cycle, and is seen to occur around Day 1300. It then shows increasing levels of activity until a high point is reached in the vicinity of Days 2400-2700. This corresponds to a low around July 1986 and a high between July 1989 and March 1990, which reflects activity of the current solar cycle, solar cycle 22 (11:2-18).

Figure 22 illustrates a similar behavior for solar flux, with  $F_{10.7}$  exhibiting a strong upward trend starting at about Day 1300. This is also representative of the current solar cycle, and the resemblance between  $F_{10.7}$  and R is as expected (11:2-18).

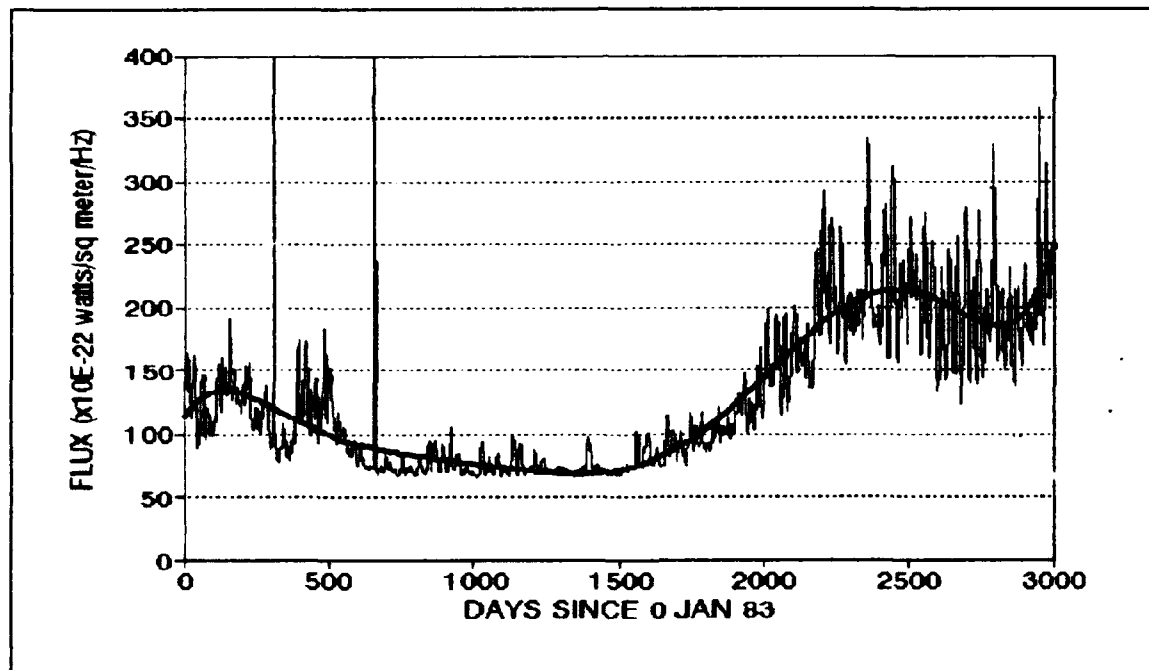


Figure 22. 10.7-cm Solar Radio Flux vs. Time

LDEF. Once the behavior of R and  $F_{10.7}$  had been analyzed separately, each was compared with various orbital parameters for LDEF and Salyut 7/Cosmos 1686. As discussed earlier, these types of comparisons must be done between two data sets at consistent epochs, and the transformation to achieve this consistency can introduce errors. The transformation of semi-major axis curves done earlier was done so that comparisons could be made with solar and geomagnetic data collected at standard daily intervals.

Figure 23 illustrates the relative behavior of LDEF semi-major axis and sunspot number. There appears to be a strong correlation between the increase in R and the increasing decay rate of LDEF, which is logical when considering the effect of solar activity on atmospheric drag. As discussed in Chapters II and III, the force due to atmospheric

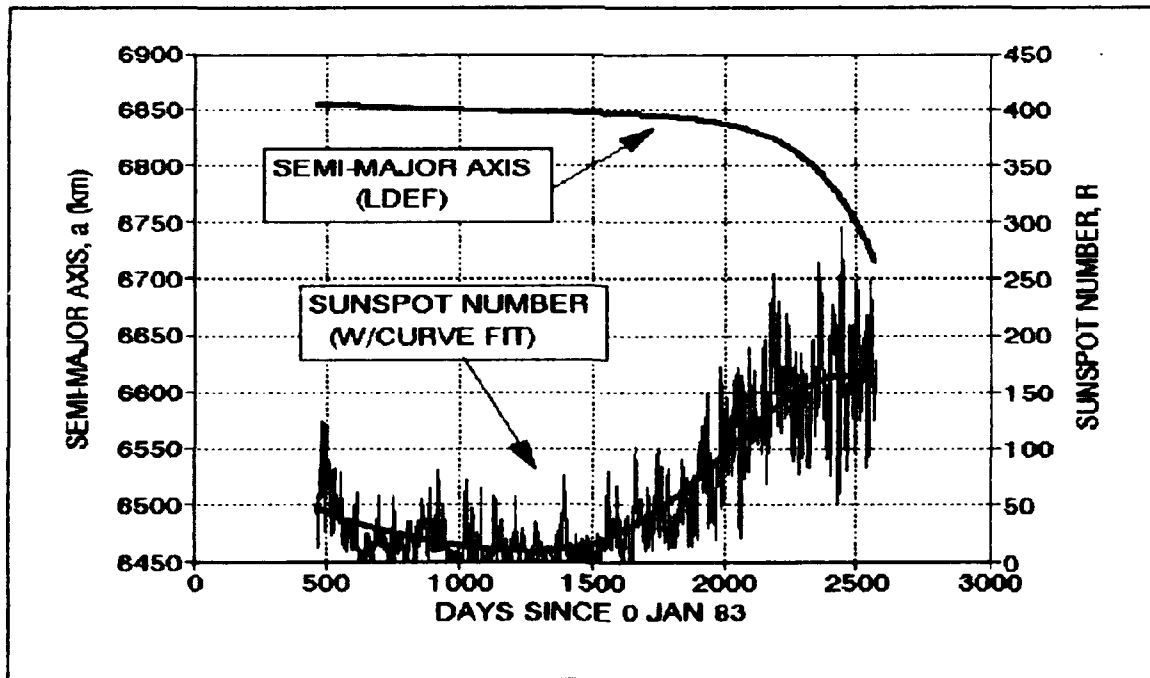


Figure 23. Semi-major Axis and R for LDEF

drag is directly dependent on atmospheric density, which in turn is influenced by solar activity.

Figure 24 shows a similar correlation, as expected, between solar flux and LDEF semi-major axis. Decay rate again appears to be adversely affected by increased solar activity. However, not much else can be concluded from the comparisons to this point.

When first examining the LDEF semi-major axis data, it was pointed out that there were slope changes near Days 1700, 2100, and 2400. It is possible that the increase in solar activity as given by R and  $F_{10.7}$  caused the slope change at day 1700, but slope changes at the other points appear less directly related. Additional comparisons must be made to determine possible causes of slope changes at the other points.

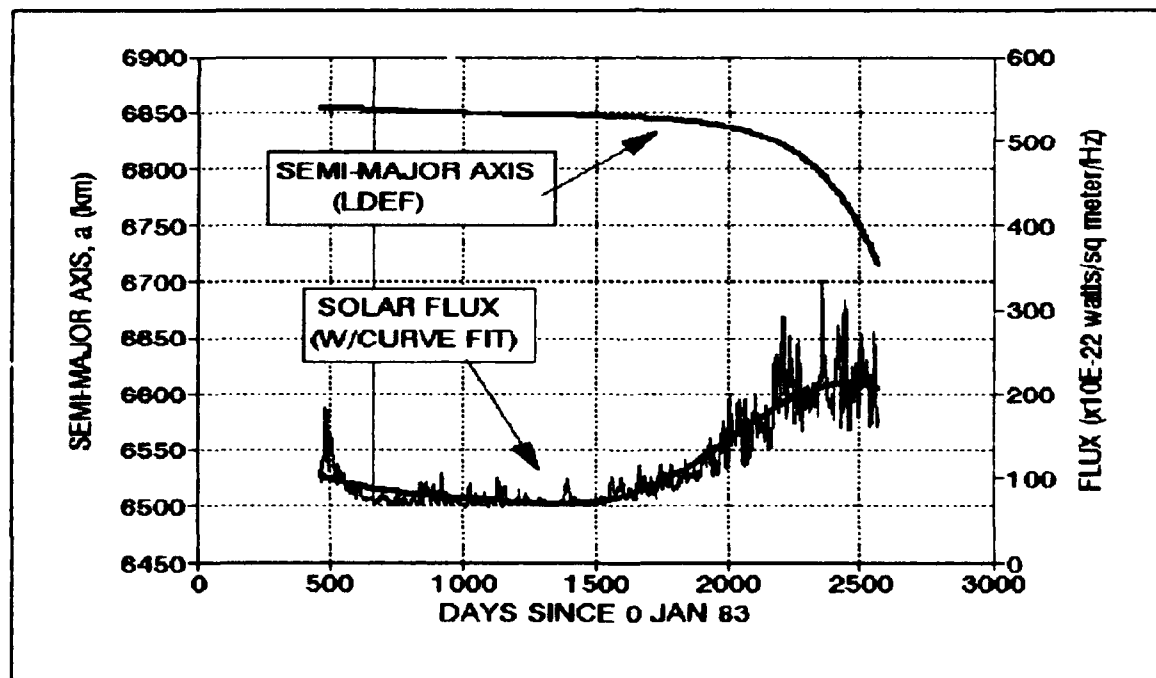


Figure 24. Semi-major Axis and Flux for LDEF

Solar data was also compared to eccentricity and inclination for LDEF, although it had to be done indirectly since the time scales were not consistent. To illustrate, Figures 25 and 26 can be examined simultaneously to get a rough feel for areas of potential correlation.

It could be argued that the increased solar activity toward the end of LDEF's orbit was responsible, at least in part, for the larger fluctuations in both eccentricity and inclination. However, little additional information can be gained from this comparison at this point.

Salyut 7/Cosmos 1686. The comparison of solar data with Salyut 7/Cosmos 1686 was done in much the same way as for LDEF. Again, because semi-major axis was the only orbital parameter converted to a time scale consistent with that of the solar data, it was the only orbital parameter against which solar data was directly compared.

Figure 27 shows a plot of R versus semi-major axis, and the relationship appears to be very similar to that discussed above for LDEF; namely, that decay rate increases with increased solar activity. It is also important to note that solar activity is at a minimum during the period earlier identified as Subset 1 (Days 1008-1326). This would suggest that any significant perturbations noticed during this period would unlikely be due to solar effects, thus allowing an easier examination of other possible causes. Additionally, correlation between sunspot number and slope changes near Days 2100, 2500, and 2800 is not convincing, although there is a significant amount of activity throughout that entire period.

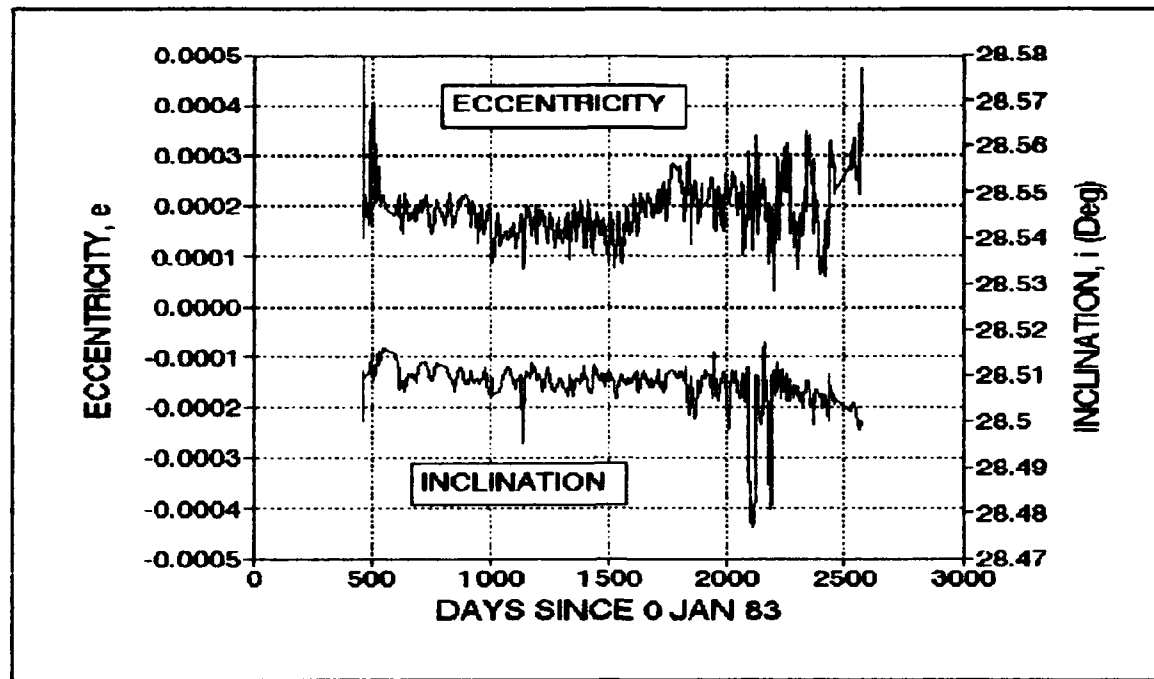


Figure 25. Eccentricity and Inclination for LDEF

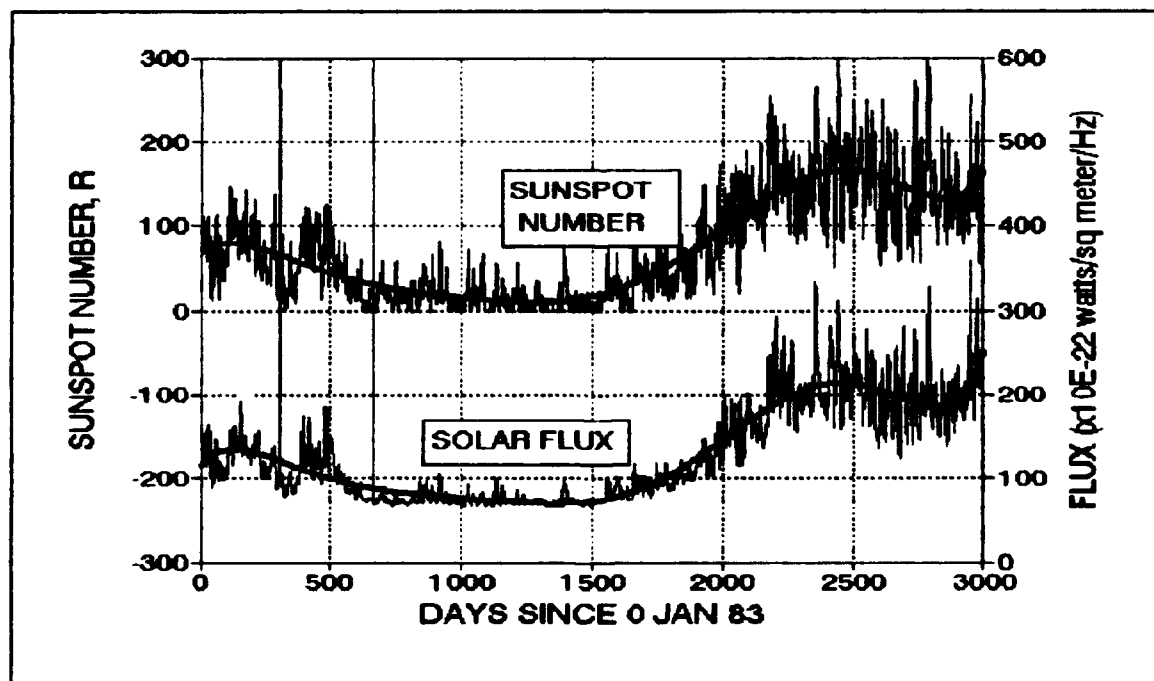


Figure 26. Sunspot Number and Flux

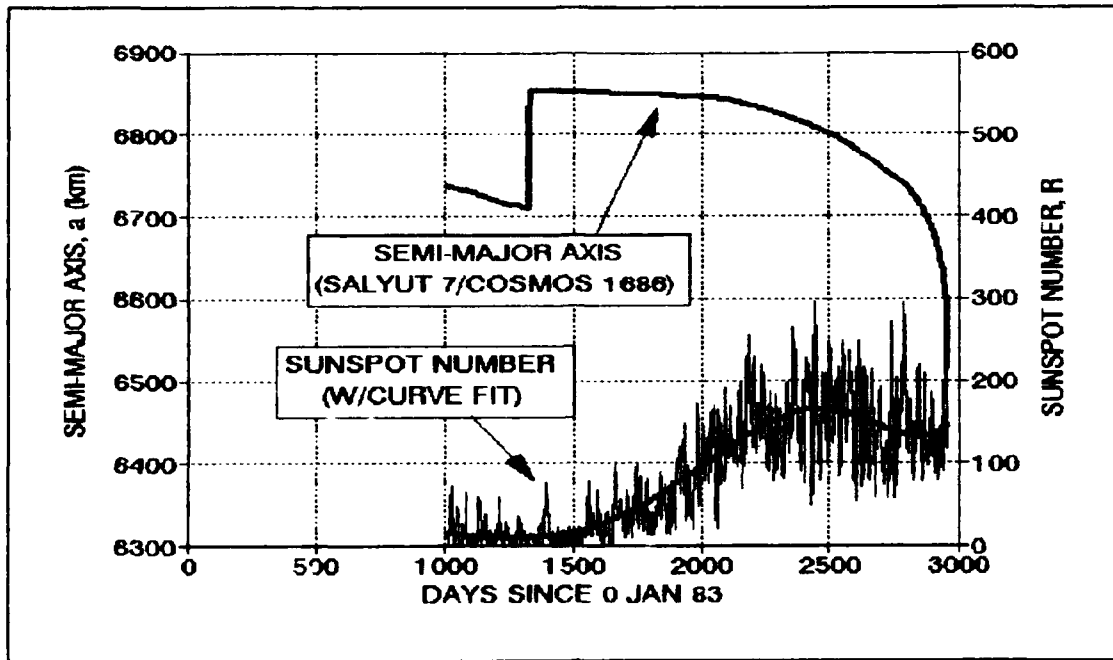


Figure 27. Semi-major Axis and R for Salyut 7/Cosmos 1686

One additional point can be made using Figure 27 by examining the slope of the semi-major axis curve at similar values, but at periods of low and high solar activity, respectively. Semi-major axis during the Subset 1 time period decreases approximately 28 km over the span of 318 days, for an average slope of -0.088 km/day. Looking forward to a point where the semi-major axis is at about the same value later in the orbit (approximately Day 2800), an average slope of -0.560 km/day can be calculated. This is based on a 28 km drop in 50 days, and is more than 6 times the value calculated for the earlier time interval. An obvious conclusion to be drawn is that this further substantiates the claim that increased solar activity had a marked effect on the satellite's decay.

Solar flux and Salyut 7/Cosmos 1686 semi-major axis are plotted simultaneously in Figure 28. The general relationship is basically the

same as for R, thus further substantiating the claim that solar activity directly affected the satellite orbit.

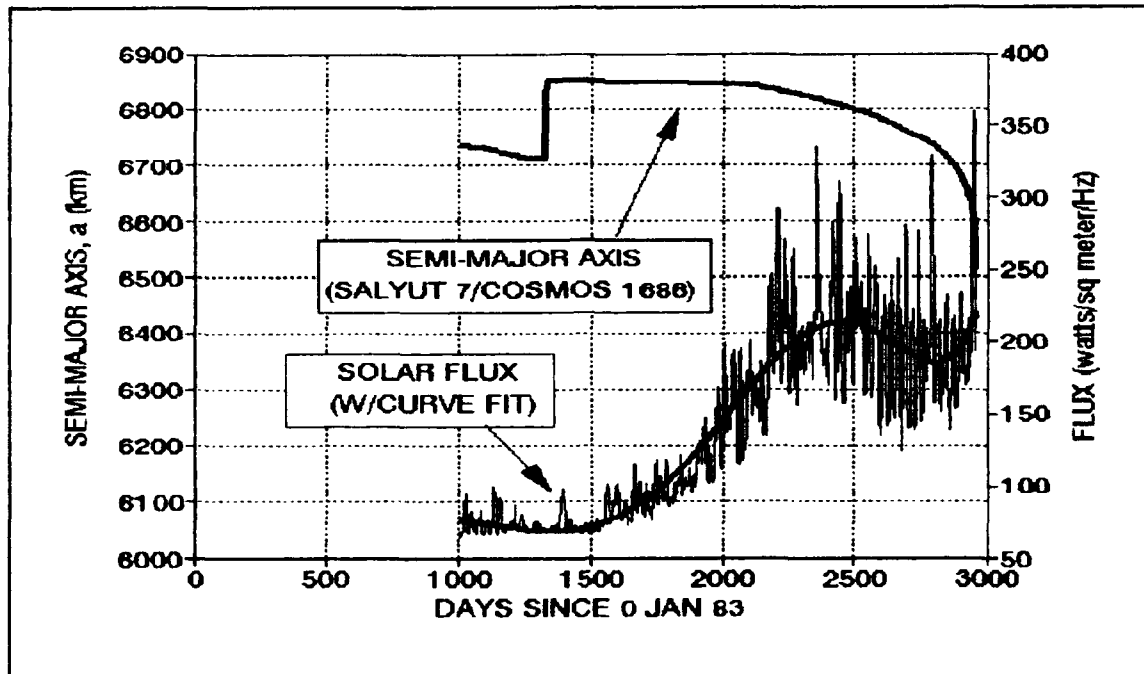


Figure 28. Semi-major Axis and Flux for Salyut 7/Cosmos 1686

Solar data was also compared with eccentricity and inclination for Salyut 7/Cosmos 1686. As for LDEF, this comparison is an imprecise one, but can be done by examining Figures 29 and 30 simultaneously. The breakpoints associated with the maneuvers noted earlier can again be seen in the eccentricity and inclination plots, as can the periodicity in the latter part of the orbit. A slight decrease over time can also be noted in the eccentricity curve, which is an expected result of increased atmospheric drag which is in turn due to increased solar activity.

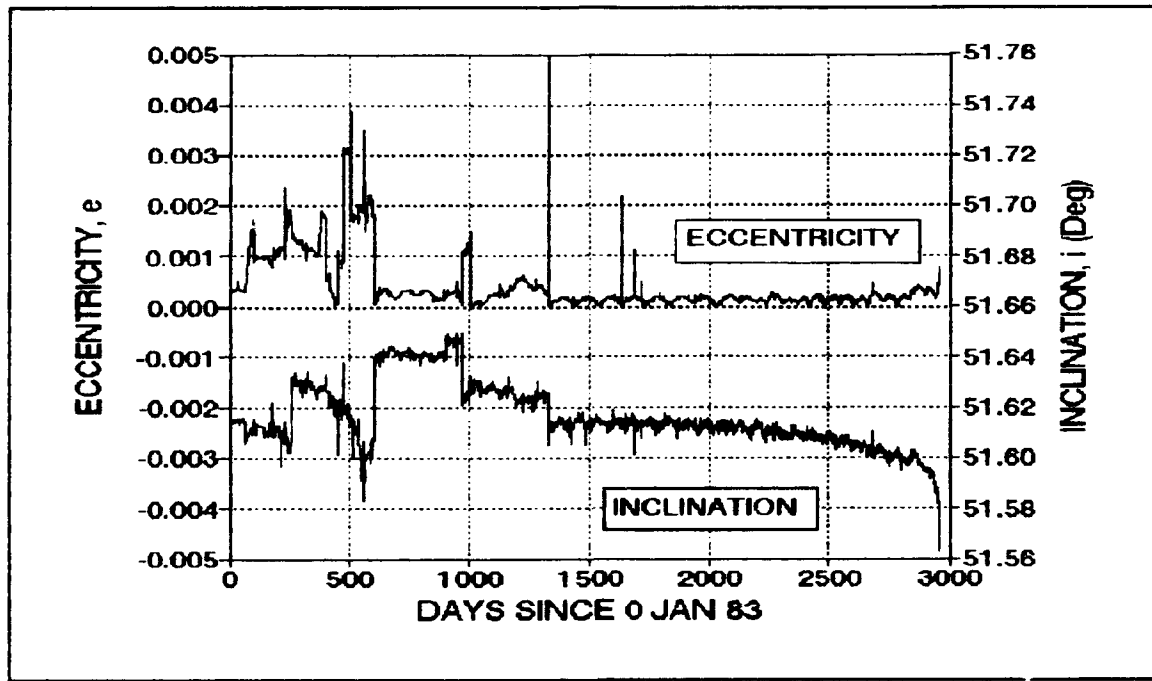


Figure 29. Inclination and Eccentricity for Salyut 7/Cosmos 1686

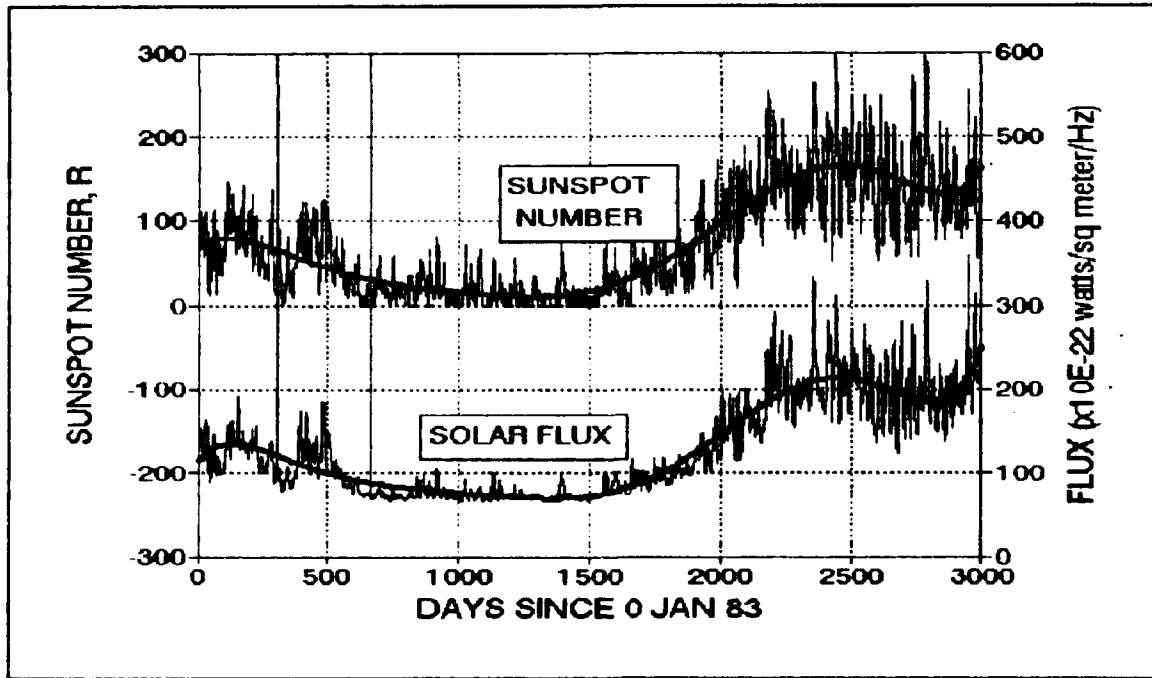


Figure 30. Sunspot Number and Solar Flux

Figure 31 shows a more detailed view of the relationship between solar activity and semi-major axis for Days 1008-1326. This time period was identified earlier as a potential area of interest since it encapsulated all activity between the docking of Cosmos 1686 and the boost to the higher orbit. The first features of Figure 31 worth noting are the slope changes around Days 1220 and 1300. The first slope change is such that the decay rate is decreased, which would suggest either a marked decrease in adverse atmospheric conditions or a maneuver to slow the decay. If ion propulsion was used, this is the type of feature that was expected, since ion thrusters are low thrust and thus more likely to produce gradual changes in the orbital parameters.

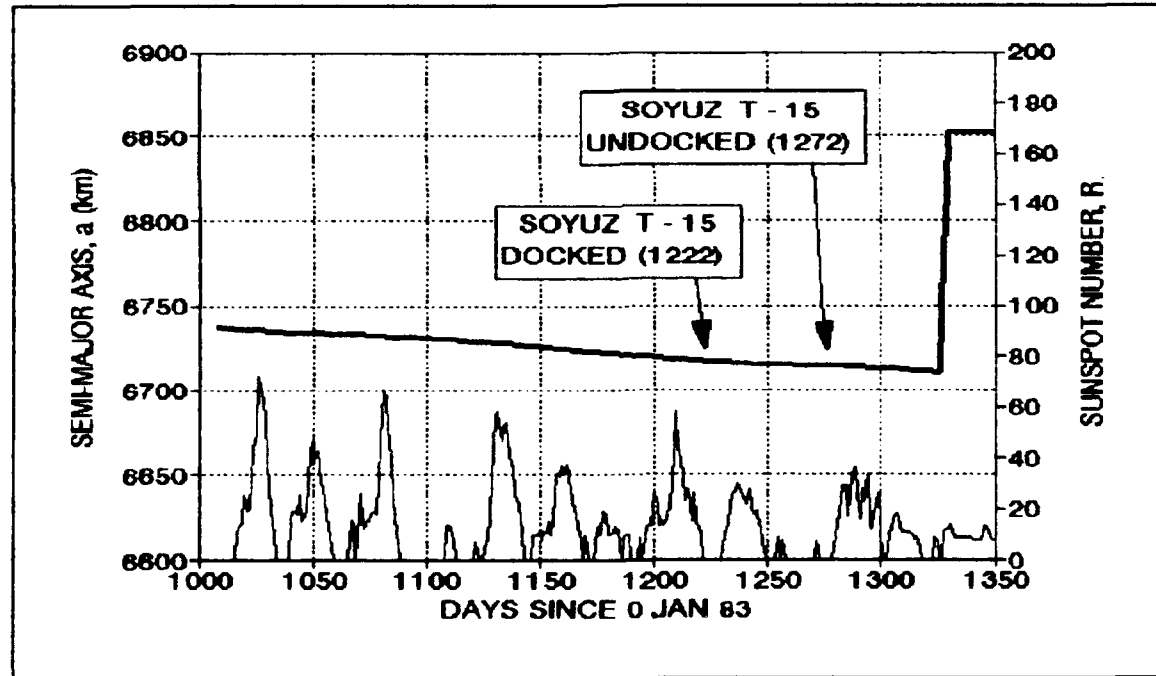


Figure 31. Semi-major Axis and R for Salyut 7/Cosmos 1686 (Pre-Boost)

A look back at Table 4 indicates that these slope changes line up pretty closely with the docking and undocking of the Soyuz T-15 capsule. More precisely, the capsule docked on 6 May 1986 (Day 1222) and undocked on 25 June 1986 (Day 1272). The purpose of the short Soyuz T-15 mission, which was actually a round-trip venture from the Mir space station with two cosmonauts on board, was listed as multi-fold (13:59). First, "experiments and operations had been left undone" from when the previous crew left; second, they wanted to gain experience in inter-orbit transfers; and third, they wanted to retrieve some equipment for use on Mir (13:59). Reference material indicates that the cosmonauts were able to get the station back to operational status and that they carried out a number of experiments and activities while at the station; however, no mention was made regarding the testing or operation of an ion propulsion source during this mission (13:59-63). Nevertheless, the use of ion propulsion during this time period cannot be ruled out, even though the station had plenty of propellant at that point in time that had been brought up by Cosmos 1686.

As an additional note, there were no significant changes in R or  $F_{10.7}$  at the times of the slope changes in this region. This time period also is during a period of low solar activity overall, as noted earlier. Therefore, there is no apparent connection to solar activity.

Figure 32 illustrates the relative behavior of eccentricity and inclination over the same time period. Comparison with Figure 33, which illustrates sunspot number and 10.7-cm solar flux activity, allows an examination of the relationships between e, i, R, and  $F_{10.7}$ . One interesting aspect of these graphs is the steady increase in

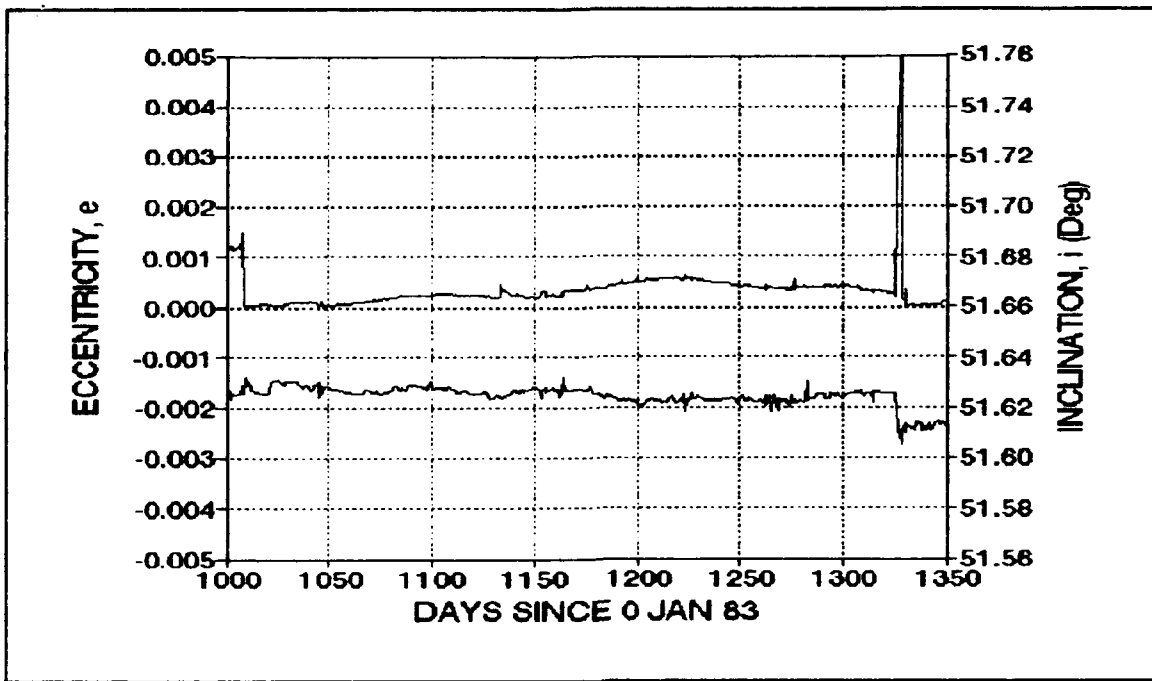


Figure 32.  $i$  and  $e$  for Salyut 7/Cosmos 1686 (Pre-Boost)

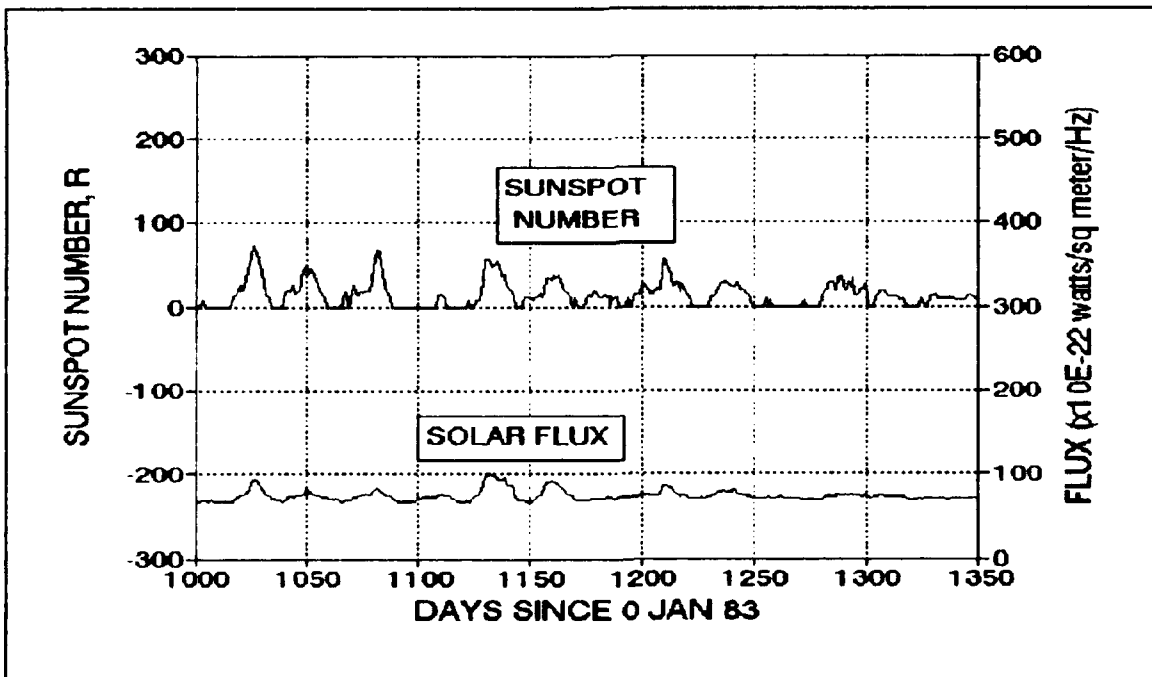


Figure 33.  $R$  and  $F_{10.7}$  (Pre-Boost)

eccentricity up until the point where Soyuz T-15 docked. Theoretically speaking, a secular increase in eccentricity would most likely be due to an application of thrust at a particular point in the orbit. Accordingly, it is possible that an ion propulsion source could have been used in such a way as to increase eccentricity over that time period. However, there does not appear to be a corresponding increase in semi-major axis to suggest an attempt to slow the decay rate.

The inclination over Subset 1 also shows some interesting points. First, it shows an overall decrease for the period, which could be attributed to atmospheric drag. Comparing this portion of the curve with the rest of the data, it is seen that the rate of decrease is larger in this region than for much of the region after the boost. The lower altitude and corresponding higher density and drag support the assertion that air drag is a cause for this difference.

Figure 34 is a plot of argument of perigee,  $w$ , and right ascension of the ascending node,  $\Omega$ , for the same period. It can be compared with the solar data given in Figure 35 to determine possible correlation. Note that the sawtooth appearance of the data is due to its measurement in degrees from 0 to 360. The right ascension of the ascending node shows virtually no fluctuation throughout this time period. The argument of perigee, however, has a couple points of interest. The discontinuity at Day 1008 corresponds to the docking of Cosmos 1686, and the fluctuation around Day 1056 is coincident with the undocking of the Soyuz T-14 capsule. The curve shift around Day 1165, however, is not as easy to explain. There are no maneuvers identified at that time, and there is nothing shown by the solar data that would suggest such a move.

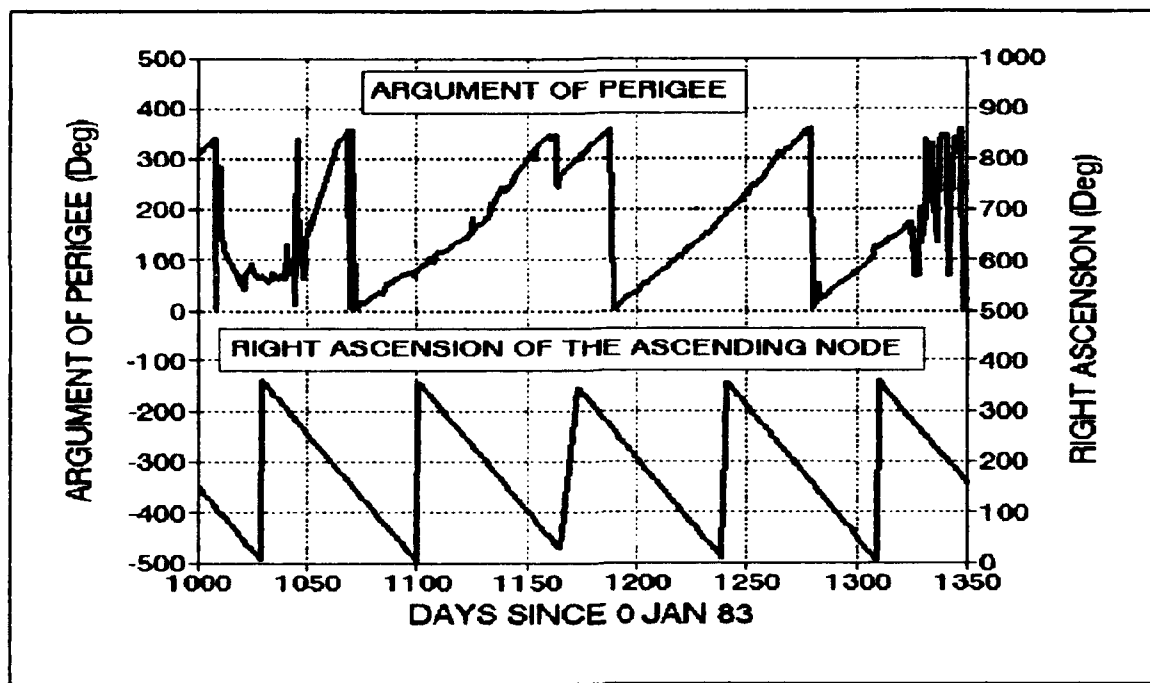


Figure 34.  $w$  and  $\Omega$  for Salyut 7/Cosmos 1686 (Pre-Boost)

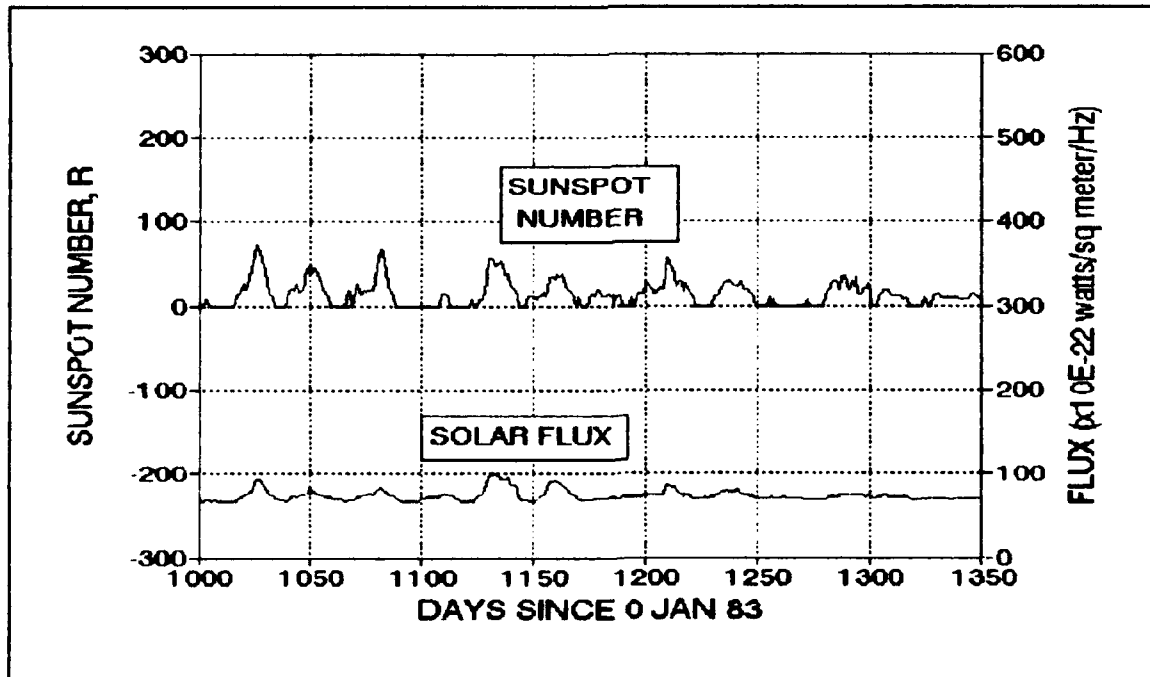


Figure 35.  $R$  and  $F_{10.7}$  (Pre-Boost)

Further, it is not something that an ion thruster would cause due to the fact that the movement appears to occur almost instantaneously. Nevertheless, the most plausible explanation is that the shift is the result of a maneuver, perhaps in preparation for the docking of the Soyuz T-15 crew at Day 1222.

#### Comparing Geomagnetic Data with Orbital Data

The other atmospheric phenomenon considered, in addition to solar activity, is geomagnetic activity. In particular,  $A_p$  and  $K_p$  will be compared to LDEF and Salyut 7/ Cosmos 1686 in the following subsections of this discussion about geomagnetic effects.

First, however, the time series behavior of each of these indices was studied independently. The variation of  $A_p$  from January 1983 through March 1991 is shown in Figure 36. This index does show a lot of fluctuation, but no significant trend is noticeable in any direction such as that seen with the solar data. A polynomial curve fitted through the data does indicate a slight similarity with the solar data, however, as it shows a low point around Day 1500 and a high level of activity near Day 2500.

The variation of  $K_p$  with time is shown in Figure 37. There is significantly more fluctuation in this index than for  $A_p$ , and there is still no obvious trend. As for  $A_p$ , a polynomial fit through the data does show a slight correlation with solar activity. However, because of the large residuals associated with a curve fit through such widely varying data, it is difficult to determine if there is in fact a direct correlation, even though some correlation is expected.

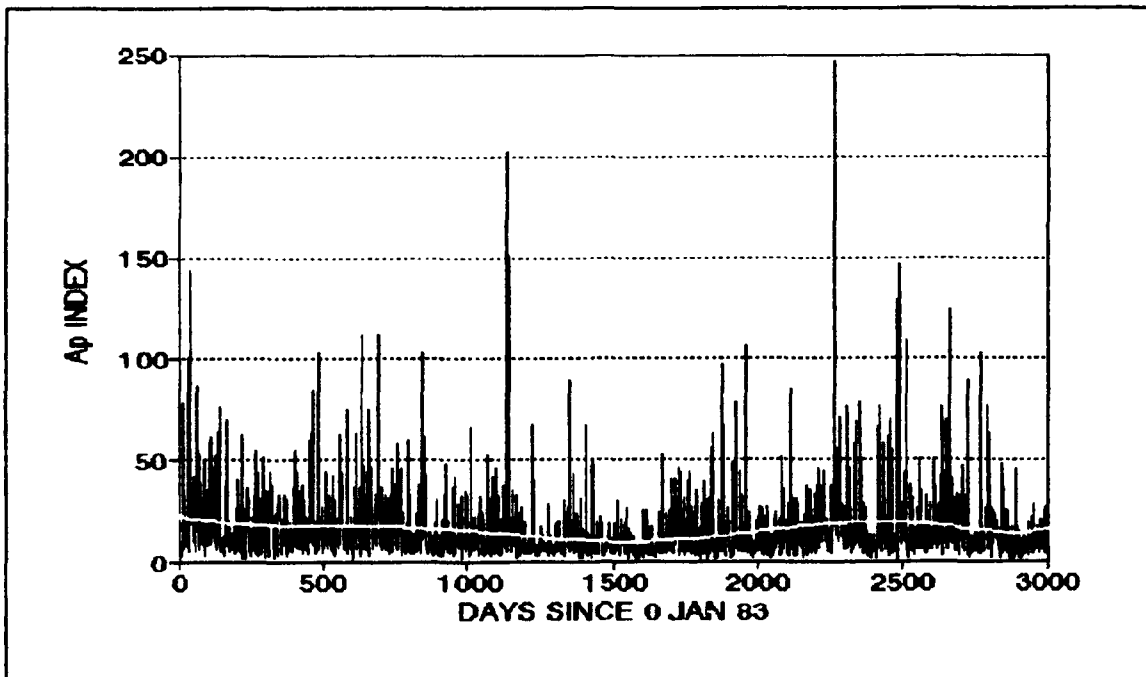


Figure 36.  $A_p$  vs. Time

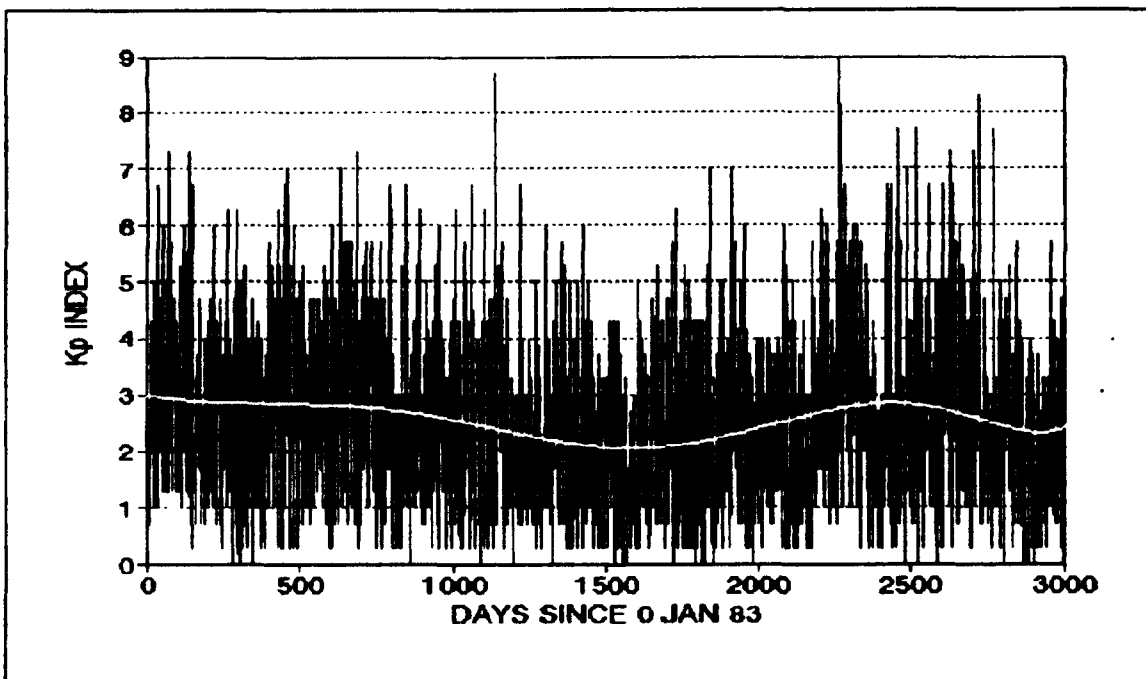


Figure 37.  $K_p$  vs. Time

LDEF.  $A_p$  and  $K_p$  are plotted with LDEF semi-major axis in Figures 38 and 39. These figures do not by themselves support any claim of direct correlation between geomagnetic activity and semi-major axis. While the polynomial curves do indicate a slight increase in activity roughly concurrent with the increase in solar activity, the variance in the data does not allow these curves to be used with much confidence. Further, there appears to be no correlation between geomagnetic activity and semi-major axis slope changes at Days 1700, 2100, and 2400.

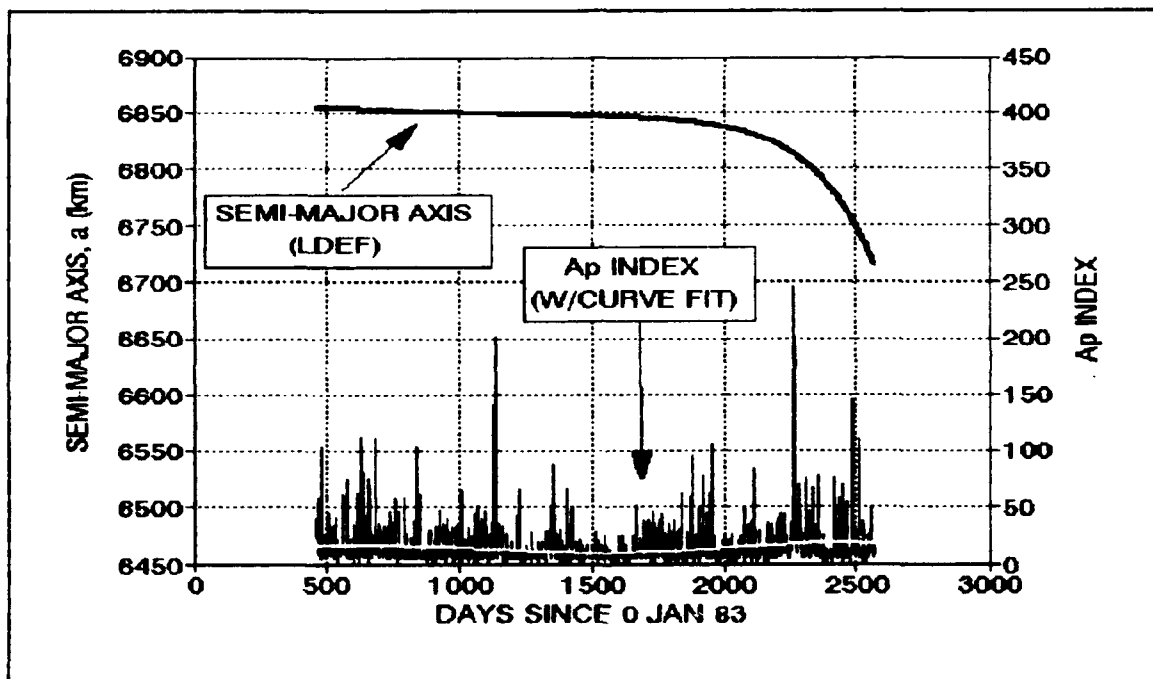


Figure 38. Semi-major Axis and  $A_p$  for LDEF

Comparison with other orbital parameters was also done, but with similar results. These comparisons again have to be done indirectly, since no transformation was done for parameters other than semi-major axis. Figure 40, which is a plot of inclination and eccentricity for

LDEF, can thus be compared with  $A_p$  and  $K_p$  in Figure 41. Because the geomagnetic data has so much variability, it is difficult to determine any correlation visually. However, it would appear that there may be a couple of points which are related. One is between Days 1100 and 1200; it appears to correspond to a significant short-period decrease in both inclination and eccentricity. The effect was short-lived as both returned to their previous values very quickly. Another point of interest lies near Day 2250, as it is near the area of large fluctuation in the inclination data.

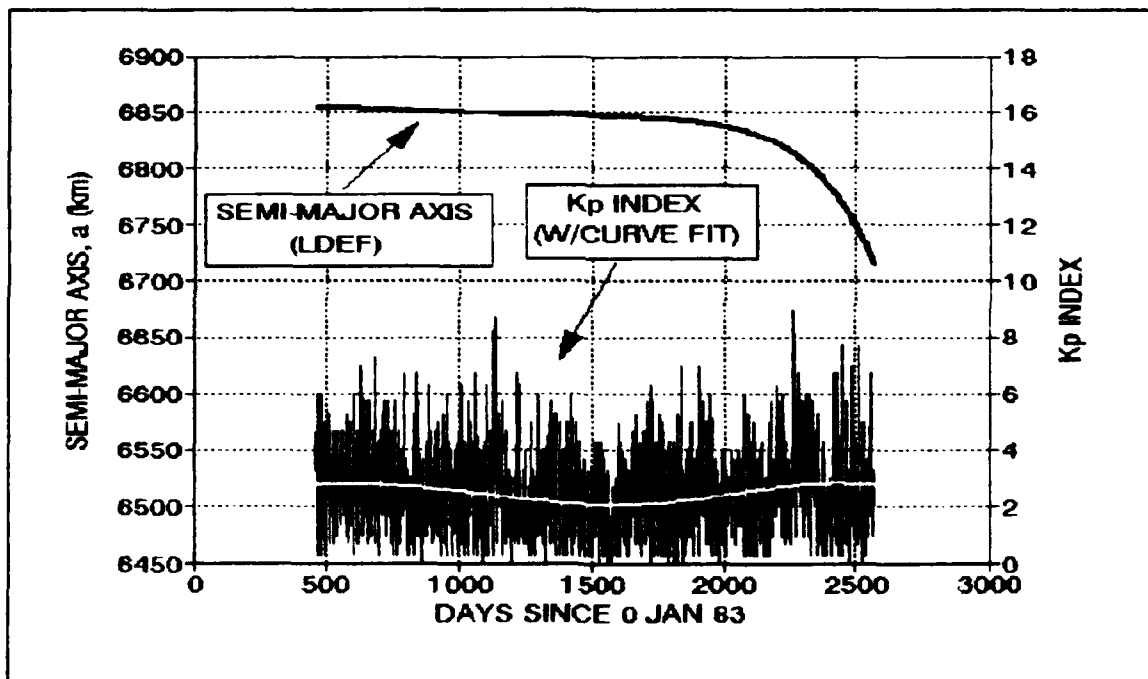


Figure 39. Semi-major Axis and  $K_p$  for LDEF

Salyut 7/Cosmos 1686.  $A_p$  and  $K_p$  are plotted with Salyut 7/Cosmos 1686 semi-major axis in Figures 42 and 43. Based on these figures, there does not appear to be any obvious direct correlation.

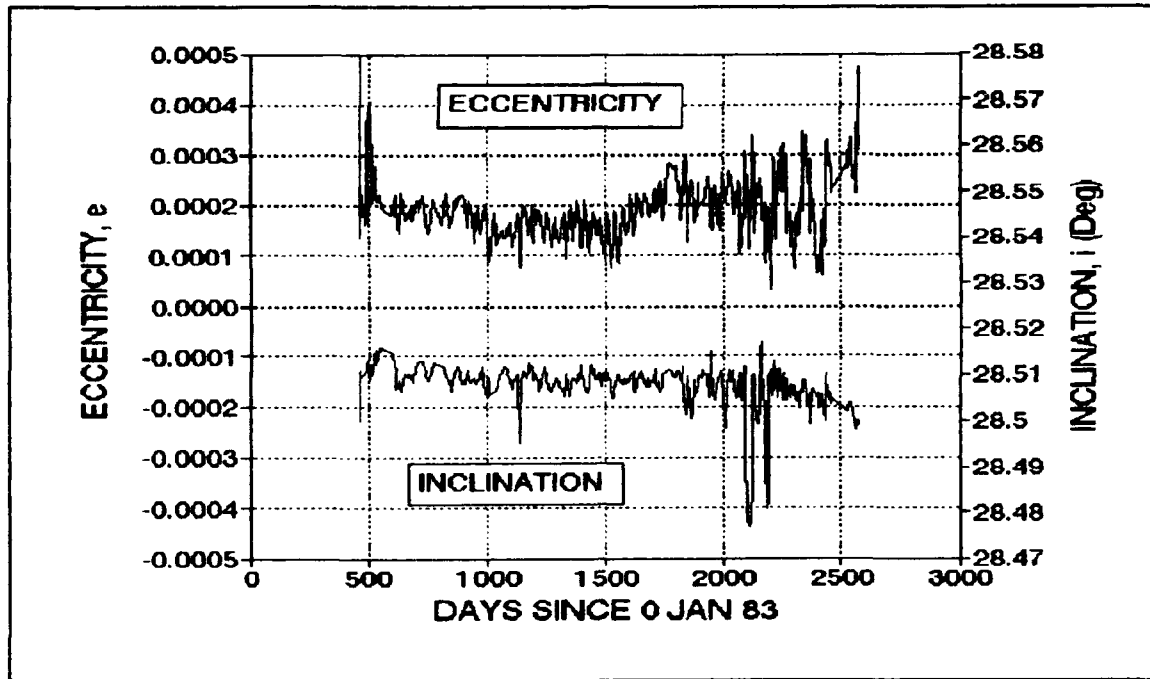


Figure 40. Inclination and Eccentricity for LDEF

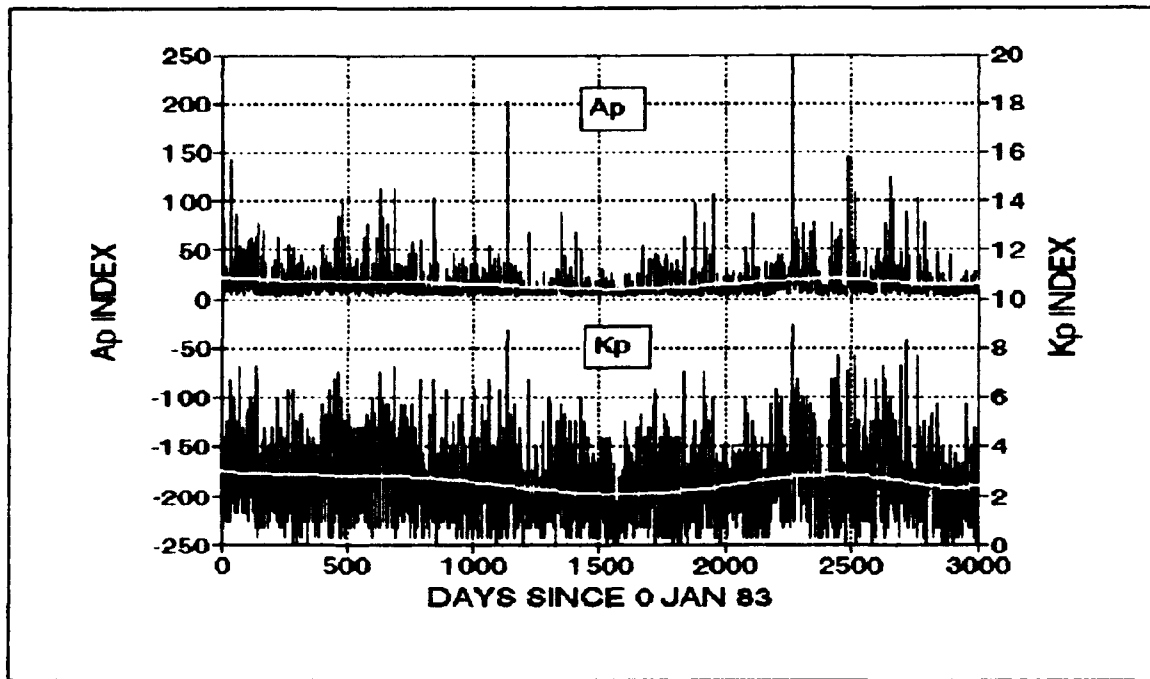


Figure 41.  $A_p$  and  $K_p$

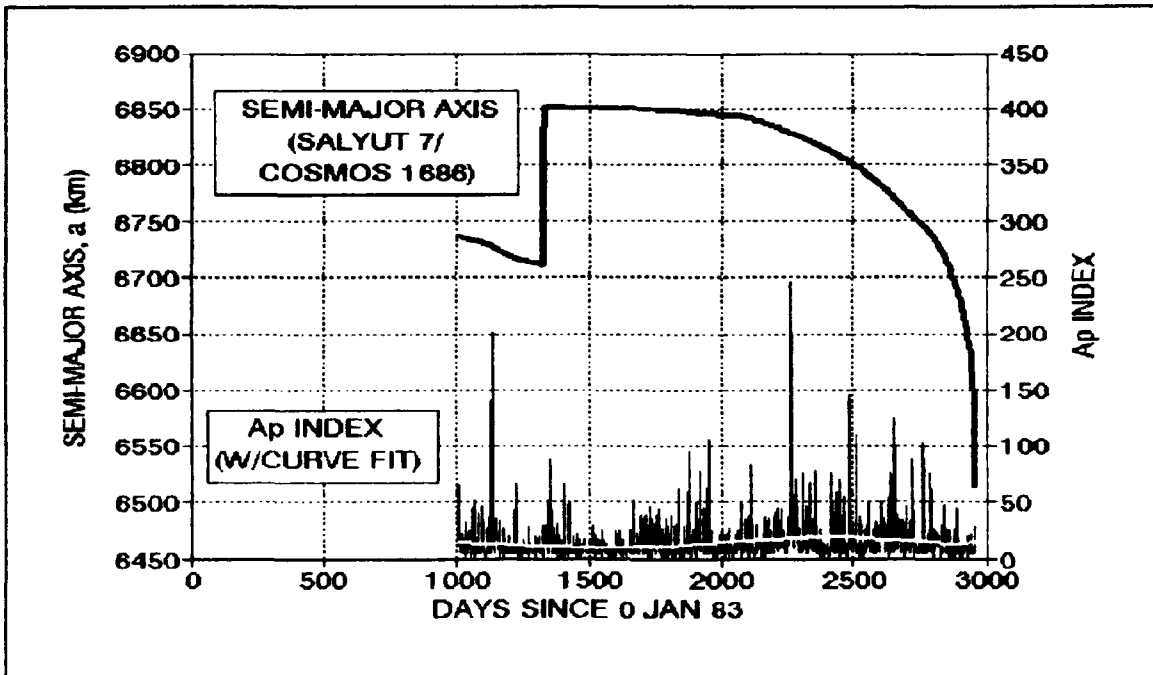


Figure 42. Semi-major Axis and  $A_p$  for Salyut 7/Cosmos 1686

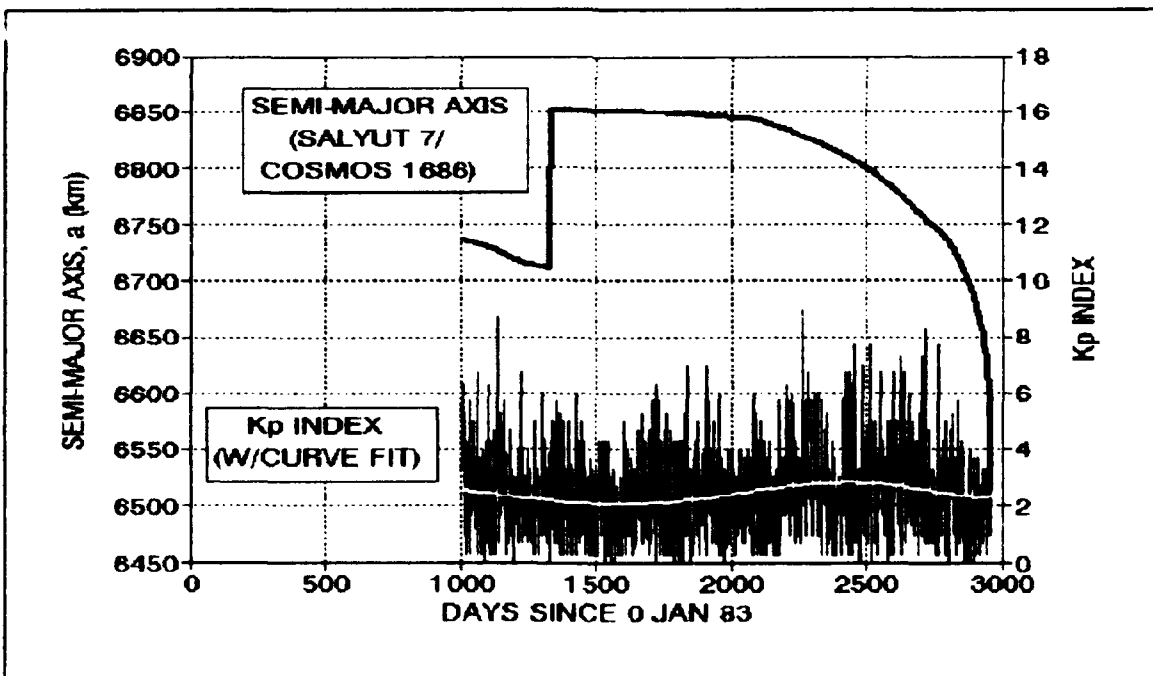


Figure 43. Semi-major Axis and  $K_p$  for Salyut 7/Cosmos 1686

The other orbital parameters were also compared to  $A_p$  and  $K_p$  in an attempt to detect any potential connection between geomagnetic data and orbital behavior. In particular,  $i$ ,  $e$ ,  $w$ , and  $\Omega$  will be plotted for the area of interest between Days 1008 and 1326.

Inclination and eccentricity are plotted together again for Salyut 7/Cosmos 1686 and presented in Figure 44. A combined plot of  $A_p$  and  $K_p$  is presented with it (Figure 45) to enable a visual comparison. There does not appear to be any obvious correlation in this case.

Argument of perigee and right ascension are presented with  $A_p$  and  $K_p$  in Figures 46 and 47. As before, there is nothing to gain from the analysis of right ascension of the ascending node since there is no variation in the data. Examination of argument of perigee reveals little else, although it is worth mentioning the change in slope around Day 1130. It appears that this may be connected to the sharp rise in  $A_p$  at that point. This is possible, but there was also a small maneuver performed on Day 1133 which could account for part or all of the change.

#### Atmospheric Density Model

Analysis of the direct effects of atmospheric density on the various orbital parameters of the two satellites was desirable given the known theoretical influence of density on atmospheric drag. For example, the classic exponential density profile given by Equation (3) shows that drag is directly proportional to atmospheric density.

The density model used for this research is attributed to L.G. Jacchia, as outlined in the 1985 Handbook of Geophysics and the Space Environment. The model takes into account geomagnetic activity via  $K_p$

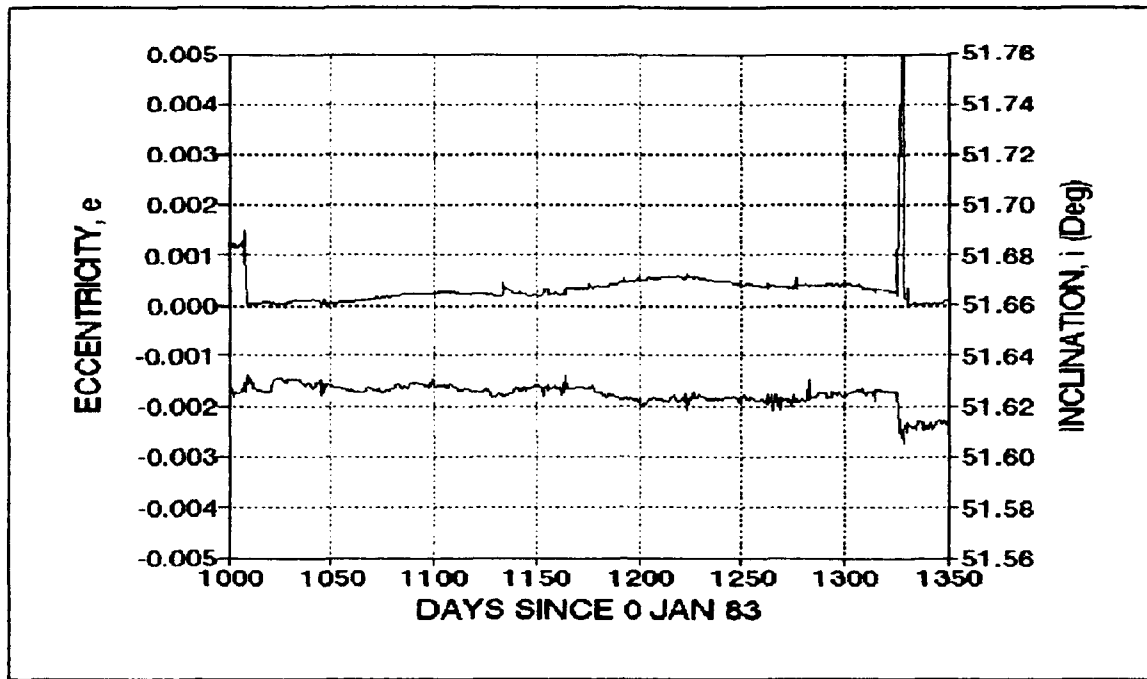


Figure 44.  $i$  and  $e$  for Salyut 7/Cosmos 1686 (Pre-Boost)

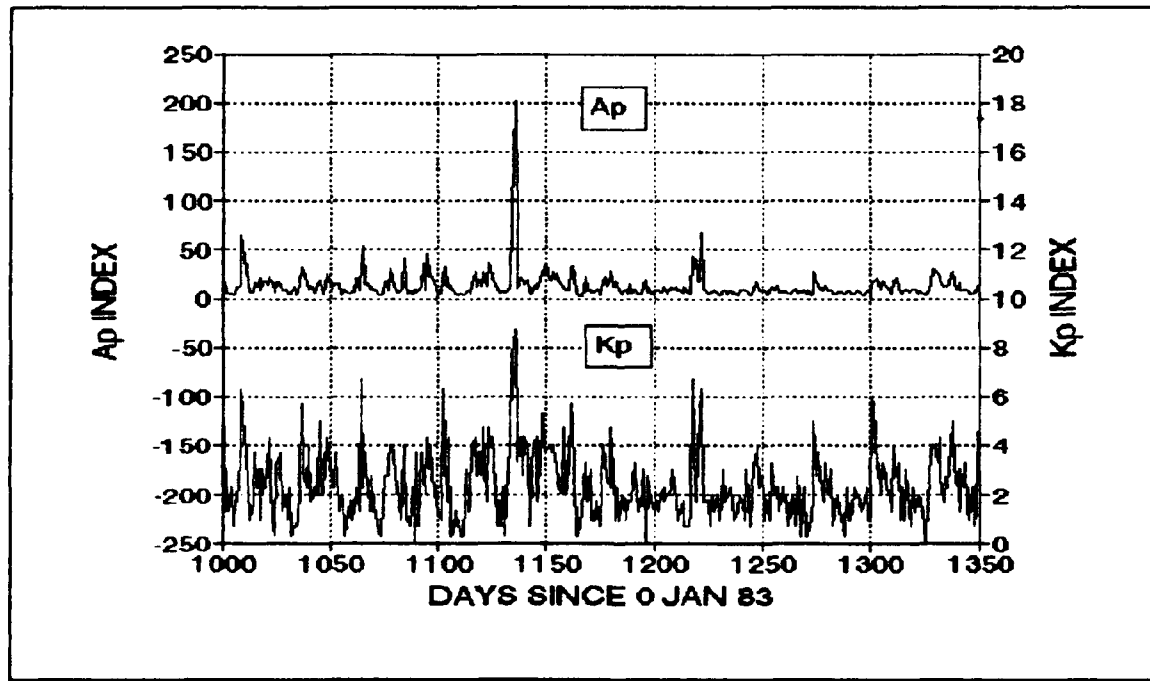


Figure 45.  $A_p$  and  $K_p$  (Pre-Boost)

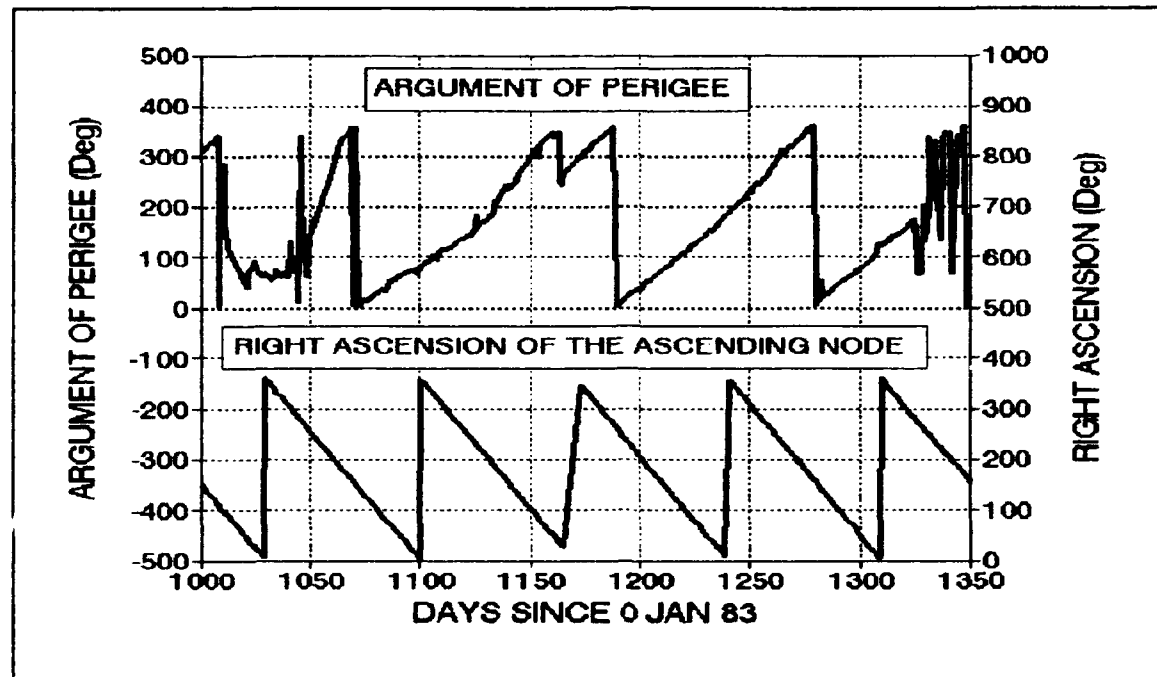


Figure 46.  $\omega$  and  $\Omega$  for Salyut 7/Cosmos 1686 (Pre-Boost)

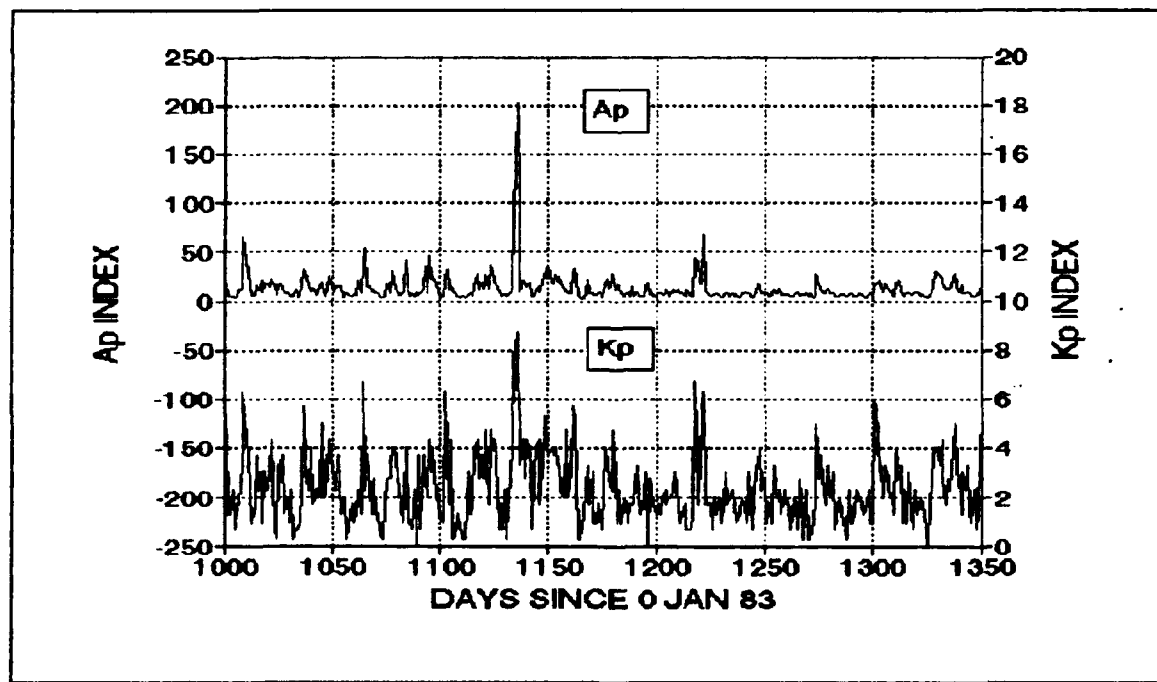


Figure 47.  $A_p$  and  $K_p$  (Pre-Boost)

and solar activity via  $F_{10.7}$ , as well as various other types of variations (11:14-36). It is based on exospheric temperature, which as discussed in Chapter II is consistent with typical atmospheric modeling in that it is based on temperature. The basis for the model is a simple function of  $F_{10.7}$  (11:14-28,14-38):

$$T_c = 379 + 3.24F'_{10.7} + 1.3(F_{10.7} - F'_{10.7}) \quad (5)$$

where

$T_c$  = minimum exospheric temperature for  $K_p = 0$

$F_{10.7}$  = 10.7-cm solar radio flux

$F'_{10.7}$  = mean reference value of  $F_{10.7} = 145$

Equation (5) assumes that  $F_{10.7}$  is in units of  $10^{-22}$  watts/m<sup>2</sup>/Hz; the value given for  $F'_{10.7}$  is also in the same units.

To account for  $K_p > 0$ , the model includes a change in exospheric temperature as a function of  $K_p$ , the result of which is a model dependent on both solar flux and the geomagnetic index  $K_p$  (11:14-38).

This equation is given as:

$$\delta T_c = 28K_p + 0.08\exp(K_p) \quad (6)$$

where

$\delta T_c$  = the change in exospheric temperature

Equations (5) and (6) can be combined to give a representative exospheric temperature for any given values of  $F_{10.7}$  and  $K_p$ . Exospheric temperature is then used to enter a table which gives density values as a function of altitude (11:14-38 - 14-42). This model, then, is

actually a function of three factors: solar flux, geomagnetic activity, and altitude.

The density profile for Salyut 7/Cosmos 1686 is shown in Figure 48. This multi-year view does not reveal much detail, other than the expected increase in atmospheric density as the satellite altitude decreases. Examination of the altitude-density relationship over shorter periods of time, however, will enable a more in-depth analysis as to whether or not there are any areas correlated with density.

Figure 49 illustrates the density experienced by Salyut 7/Cosmos 1686 through the Subset 1 period defined as Days 1008 through 1326. There are slight increases in density around Days 1050

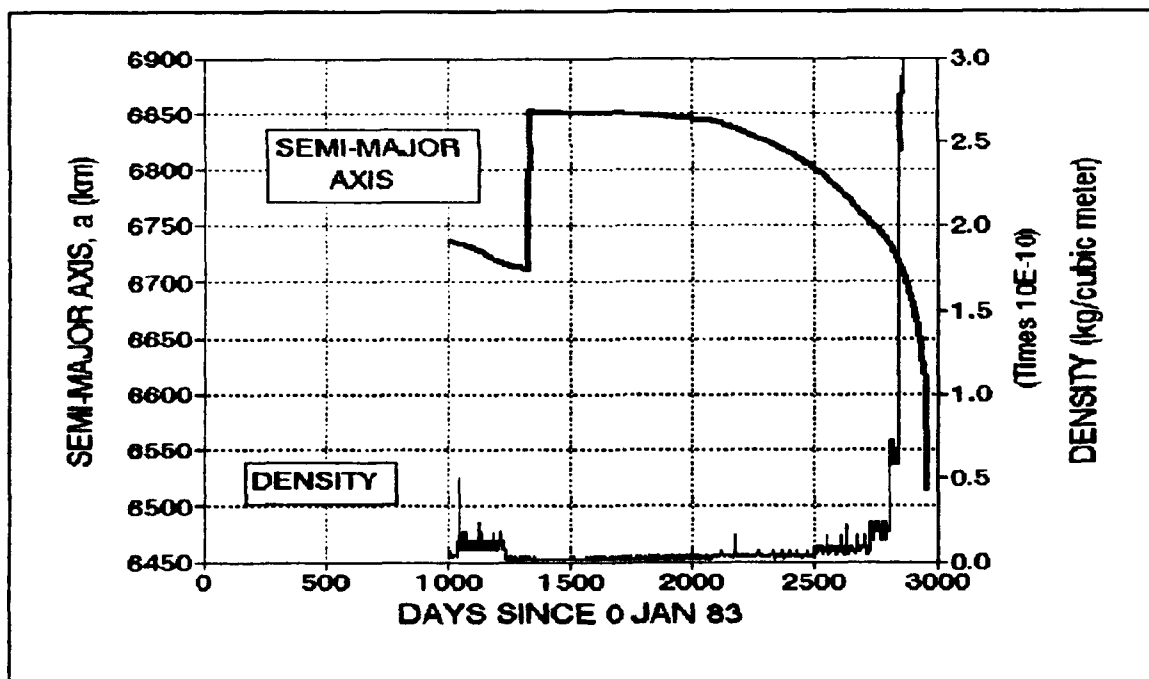


Figure 48. a and Density for Salyut 7/Cosmos 1686

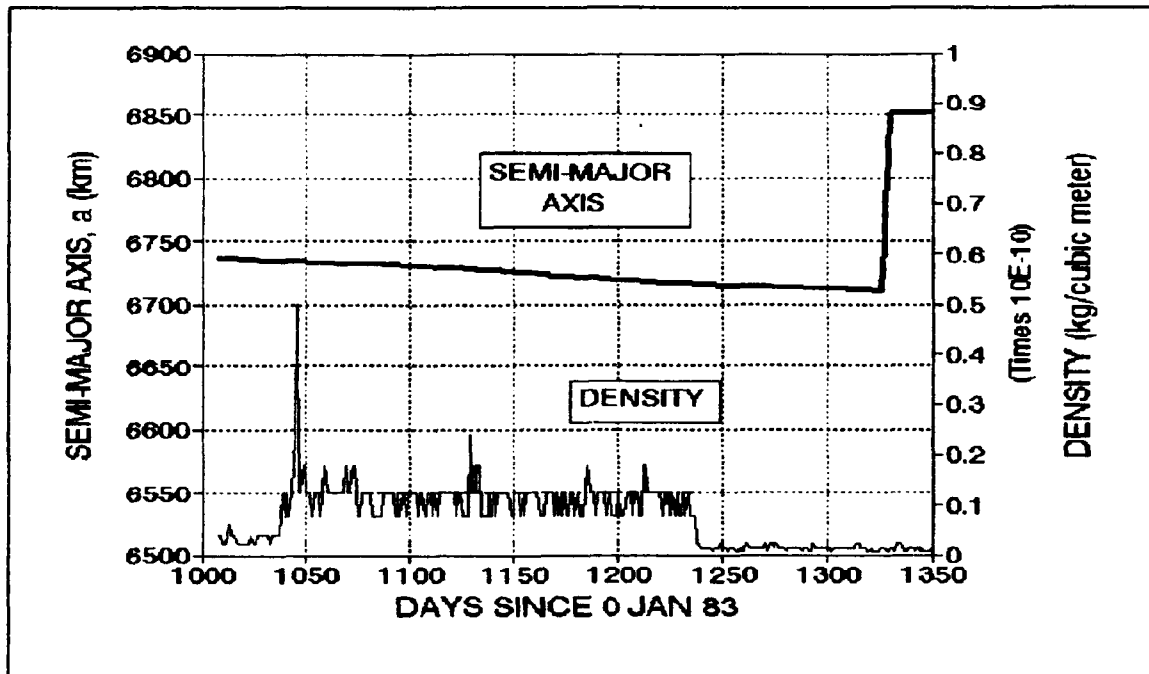


Figure 49.  $a$  and Density for Salyut 7/Cosmos 1686 (Pre-Boost)

and 1125, which are probably due to the altitude decrease, since there were no sustained increases in either solar or geomagnetic data at those points. Because of the nature of the table used to determine density values, these types of step responses are inevitable. In this case, the combination of exospheric temperature and altitude combined at Day 1125 to force the model into another regime within the density tables.

The other significant change in density occurs near Day 1325. This obviously corresponds to the large boost to a higher orbit and thus to a lower density. Another interesting point is the density spike near Day 1220, which is very near the time Soyuz T-15 docked with the Salyut 7/Cosmos 1686 complex. Had the cosmonaut crew not been there to put the station back in operation, this density increase could have adversely affected the decay rate at that point (if it affected it at

all). Instead, the slope of the curve increased at that point, which tends to substantiate the claim that they were able to get the station back into operation.

Determining Possible Use of Ion Propulsion.

Based on the analysis presented in this chapter, it is clear that a determination as to the absolute existence of an ion propulsion unit would be a difficult task. The large amounts of data were looked at in several different ways to gain insight into how various factors were or were not able to explain the behavior of the various orbital parameters.

The time period between Days 1008 and 1326 appeared to be the most likely region where an auxiliary ion propulsion unit would be tested, with Day 1008 being the docking of Cosmos 1686 and Day 1326 being the beginning of the boost to an orbit too high for further manned operation. Additionally, the station was still not able to respond to ground controllers, so attempts to test an ion propulsion device on an unmanned system would not appear feasible.

If an ion propulsion unit were aboard Cosmos 1686, it is possible that the Soyuz T-15 crew could have experimented with it to assist in stationkeeping during their 50-day stay there. It was not known whether or not the Salyut 7/Cosmos 1686 complex had any additional power generation equipment on board which could have supported continuous operation of an ion propulsion unit, although it was revealed that one purpose of Cosmos 1686 was to augment the power generation capability of Salyut 7 (13:169). Nevertheless, some limited operation may have been possible using existing battery power. Recall that the XIPS system

claimed it could operate 1 hour/day on the existing battery power of an Intelsat satellite. Because the normal propulsion capability was available, though, it was not possible to separate out response due to ion propulsion.

## V. Conclusions and Recommendations

### Summary of Results

This project's initial purpose was to analyze orbital data for the Salyut 7/Cosmos 1686 complex to determine the extent to which solar and geomagnetic data could explain anomalies of the orbital elements. Where they could not, a determination as to the possible use of ion propulsion was to be made. As seen in the analysis, there were many variables that made it very difficult to perform a simple cause-effect analysis at each phase of the research.

Solar and geomagnetic data could explain some of the disturbances, but because data was not given at consistent time intervals, many of the comparisons had to be done visually in the absence of some method to convert the data to a consistent time scale without losing the integrity of the data. This greatly limited the extent to which detailed comparisons could be done, and the result was an analysis where general trends were the only thing that could really be distinguished accurately.

These general trends did for the most part consistently match the expected behavior per the perturbation theory outlined in Chapter II. This helped confirm throughout the research that judgments regarding possible causes were somewhat consistent.

Given the limitations just described, presence of an ion propulsion source could not be confirmed. While it is conceivable that an ion propulsion source was used during the Soyuz T-15 crew's stay,

this analysis did not enable a judgment to be made one way or the other with any certainty. Further, it is possible that an ion propulsion source was used at some other time and its operation masked by other variables; however, that is not likely.

#### Potential Applications

While this research project had its limitations, it does provide some insight into how a determination such as the one sought here might be made. An obvious area for further research involves the problem of getting different element sets converted to a standard time scale. While a simple curve fitting procedure may work for a smooth curve, it was seen in this project that most data is far from smooth. If such a conversion could be done for any two sets of data, then the door is opened for a much more precise analysis by way of time series analysis techniques. This is the only way judgments and predictions can be made with any consistency and accuracy.

Had the data more clearly indicated the use of ion propulsion, possible operational characteristics of such a unit could have been computed. In the absence of other perturbing factors, a given change in the orbital parameters over a certain time period could be used to determine the propulsive parameters necessary to achieve such a change. These parameters could then be compared with the capabilities of various ion propulsion systems to determine if an ion system could have effected the changes.

APPENDIX

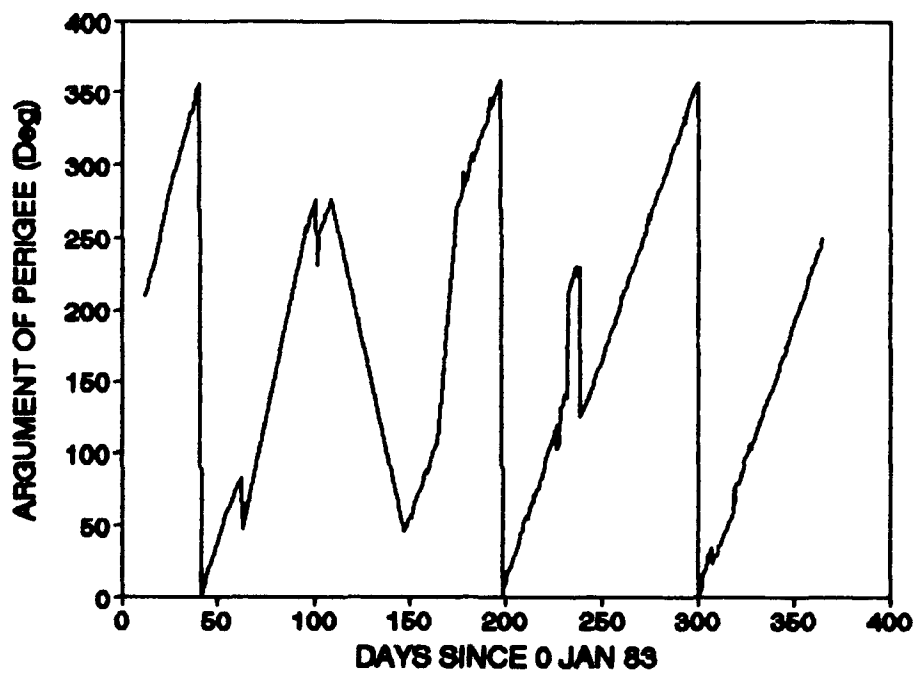


Figure 50. Argument of Perigee for Salyut 7, 1983

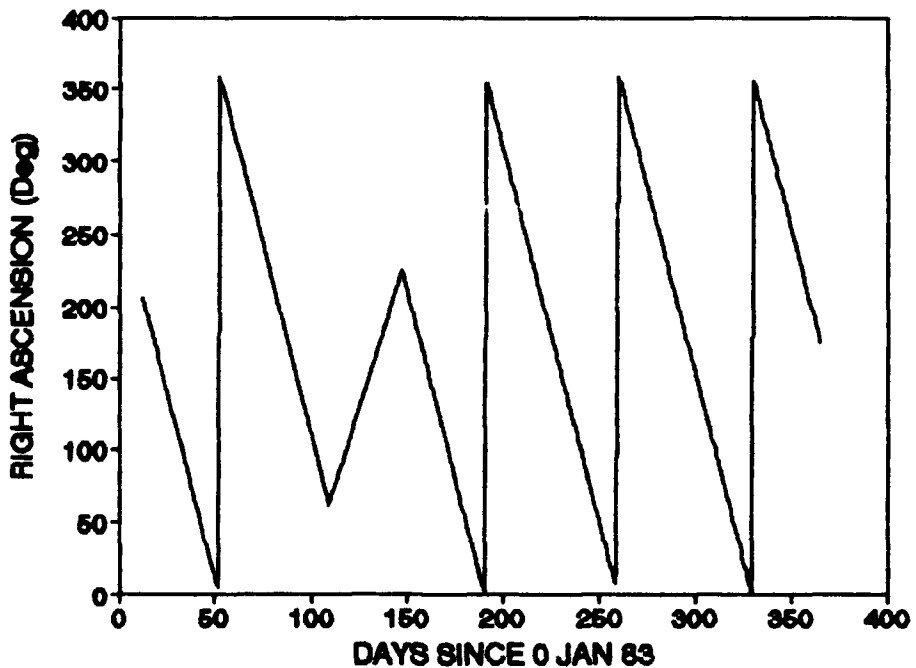


Figure 51. Right Ascension of the Ascending Node for Salyut 7, 1983

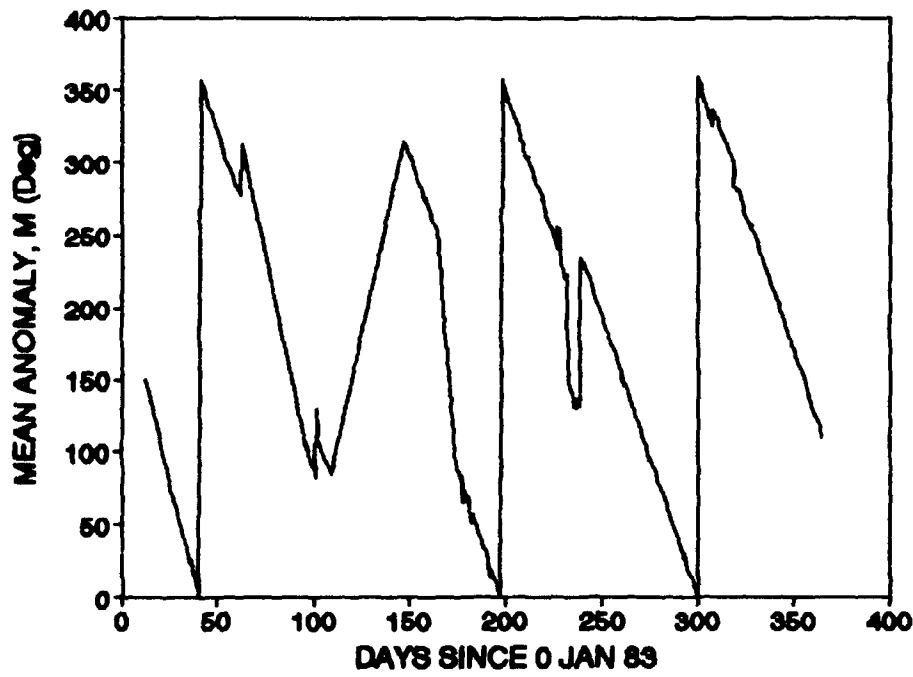


Figure 52. Mean Anomaly for Salyut 7, 1983

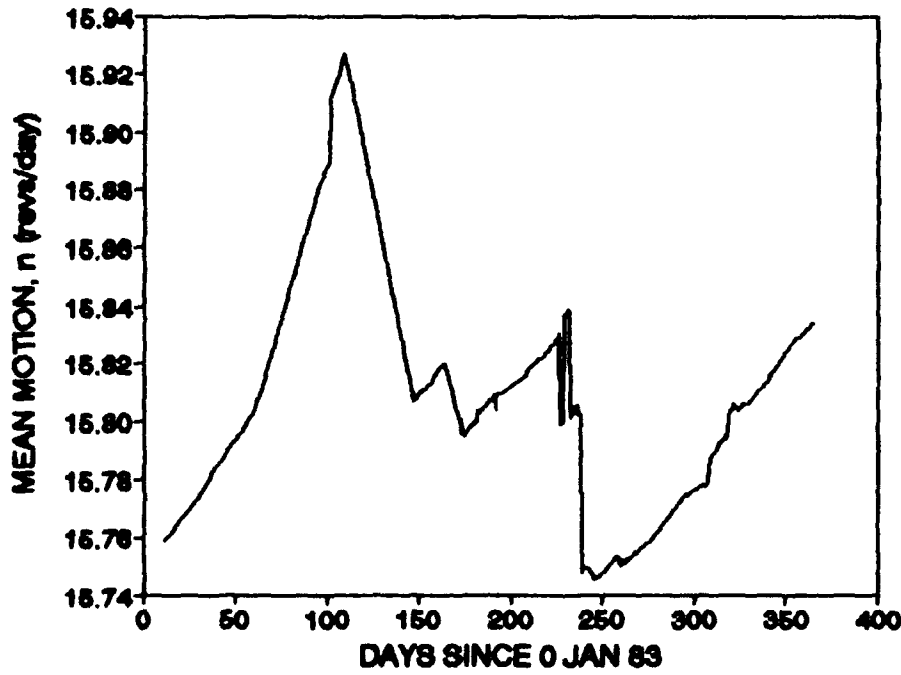


Figure 53. Mean Motion for Salyut 7, 1983

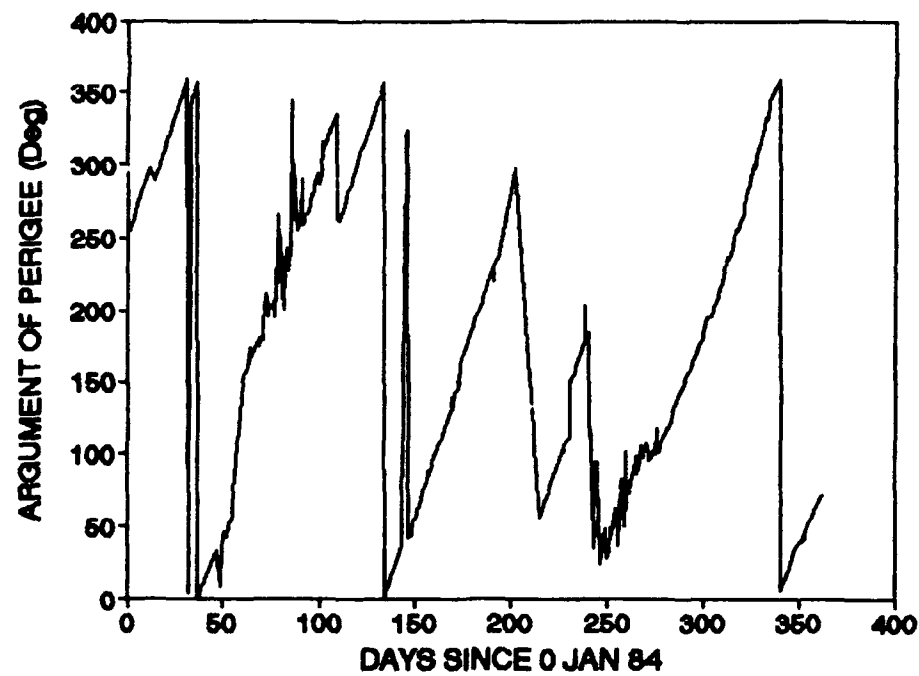


Figure 54. Argument of Perigee for Salyut 7, 1984

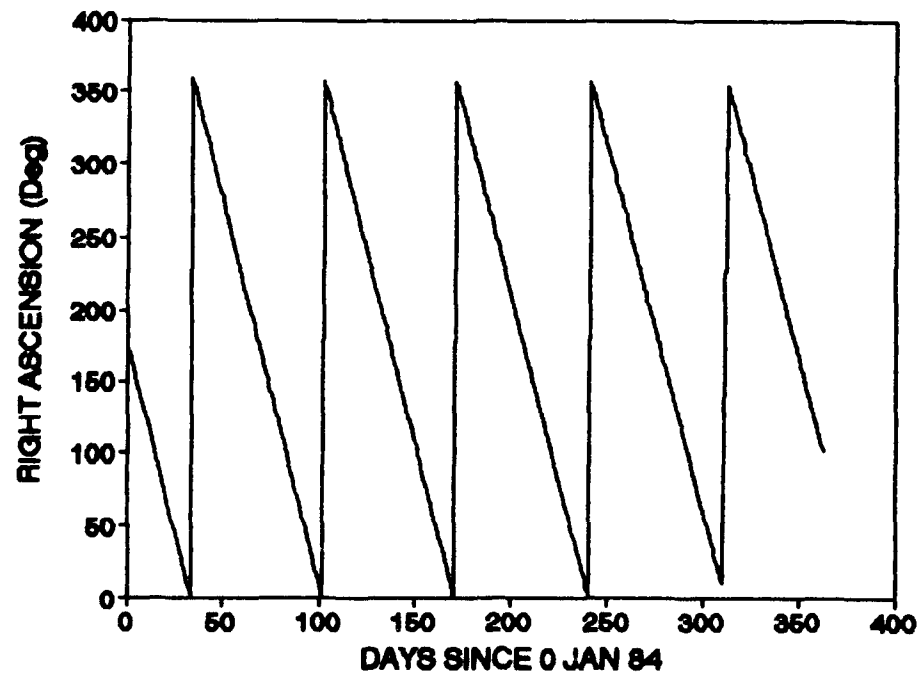


Figure 55. Right Ascension of the Ascending Node for Salyut 7, 1984

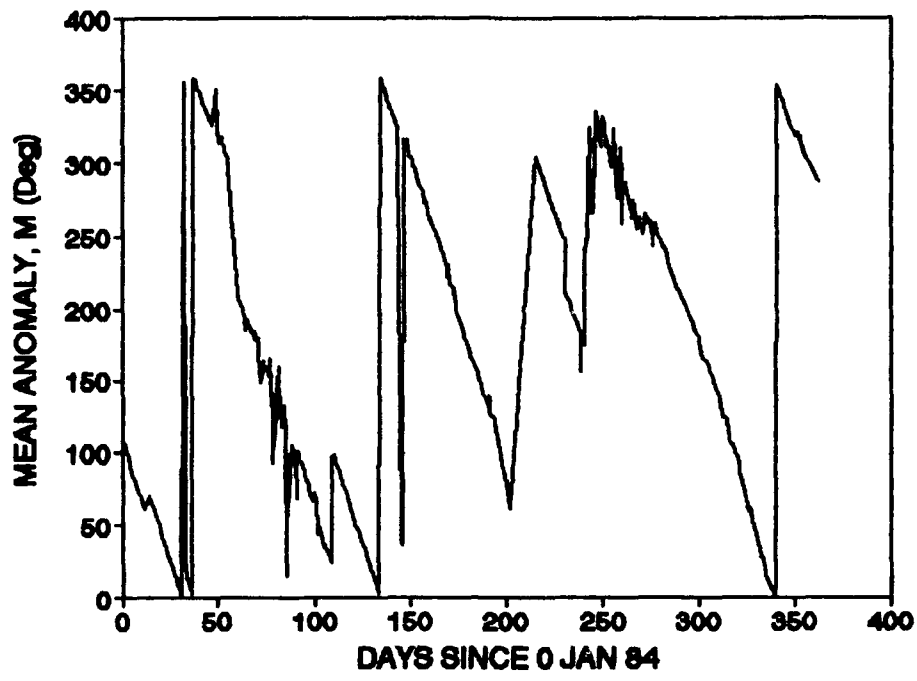


Figure 56. Mean Anomaly for Salyut 7, 1984

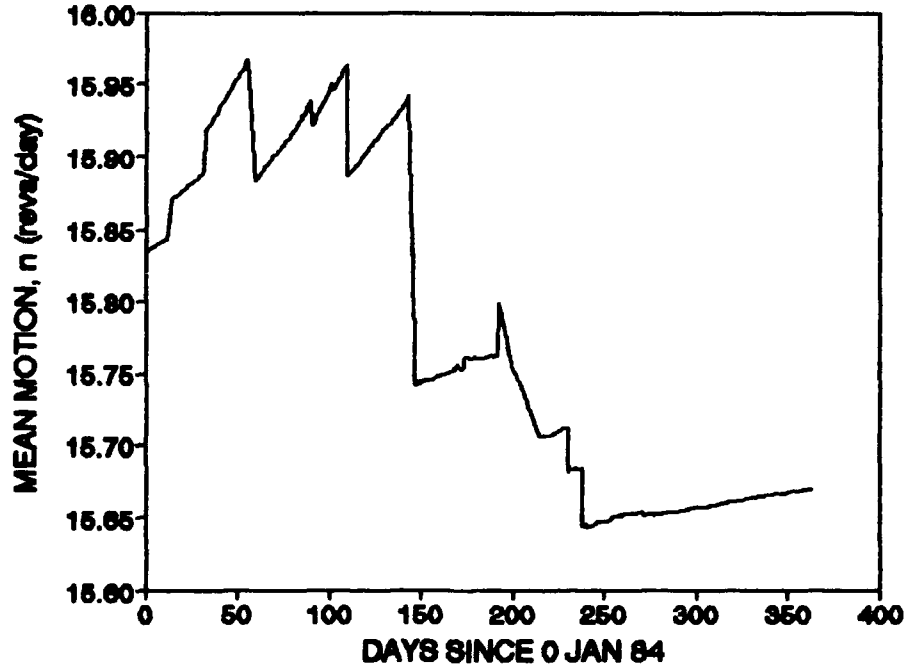


Figure 57. Mean Motion for Salyut 7, 1984

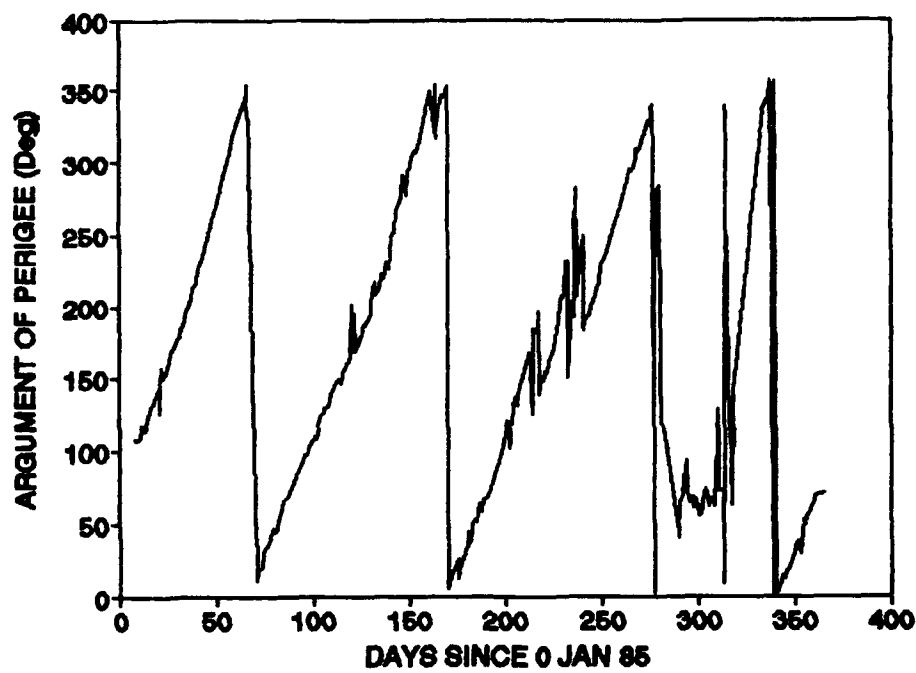


Figure 58. Argument of Perigee for Salyut 7, 1985

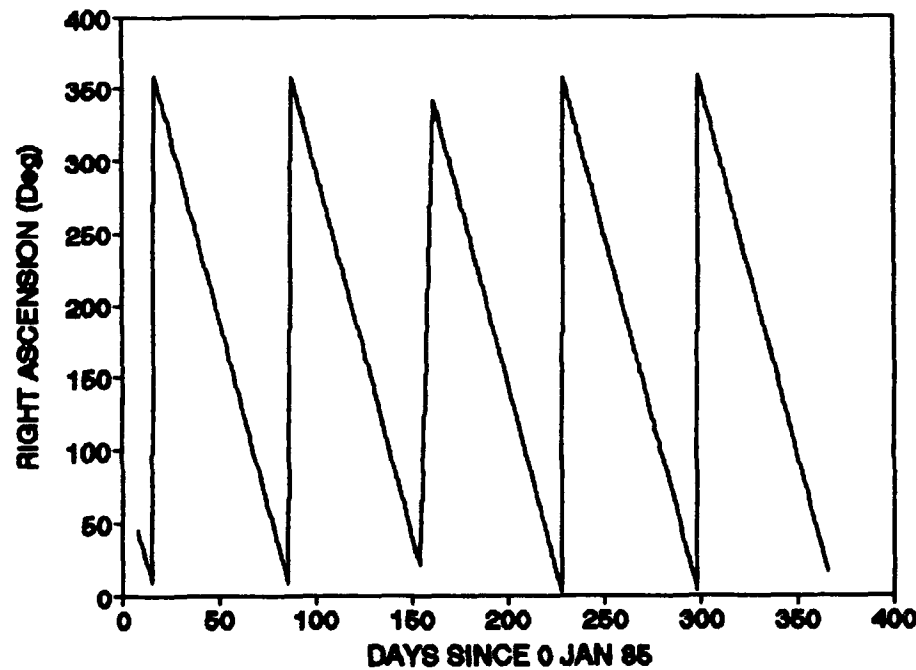


Figure 59. Right Ascension of the Ascending Node for Salyut 7, 1985

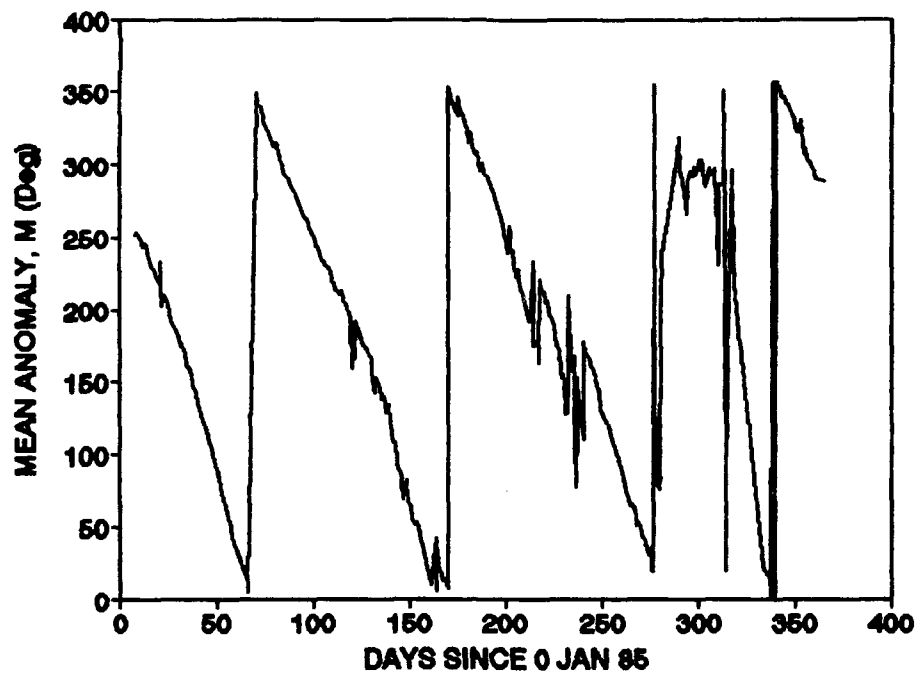


Figure 60. Mean Anomaly for Salyut 7, 1985

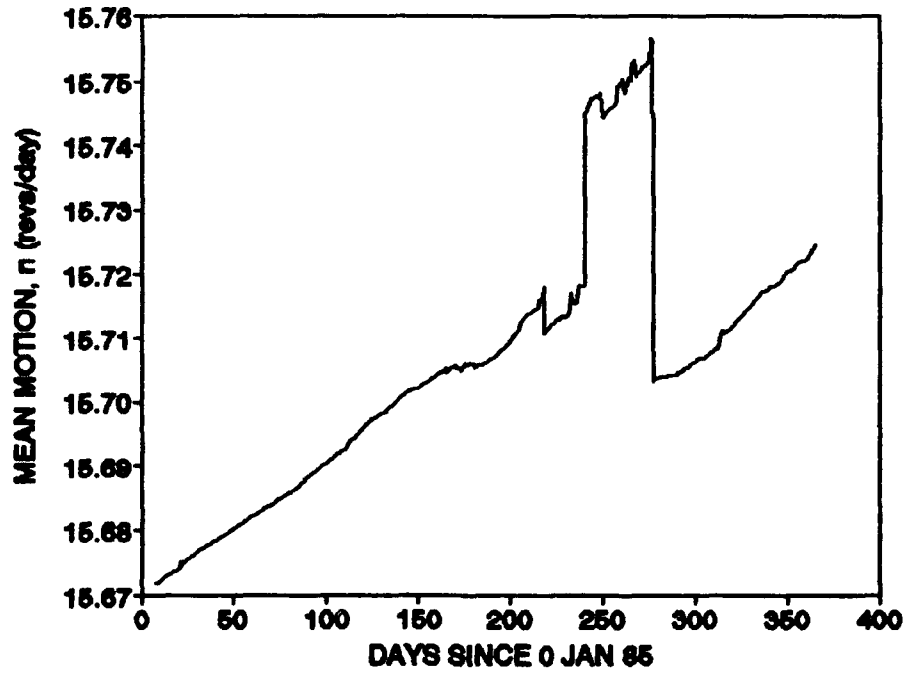


Figure 61. Mean Motion for Salyut 7, 1985

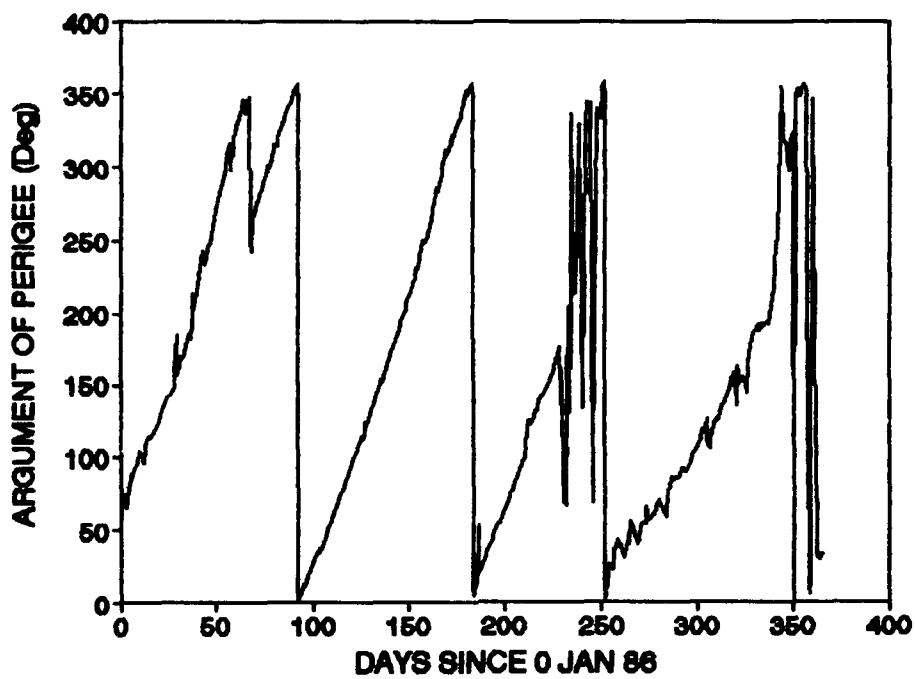


Figure 62. Argument of Perigee for Salyut 7, 1986

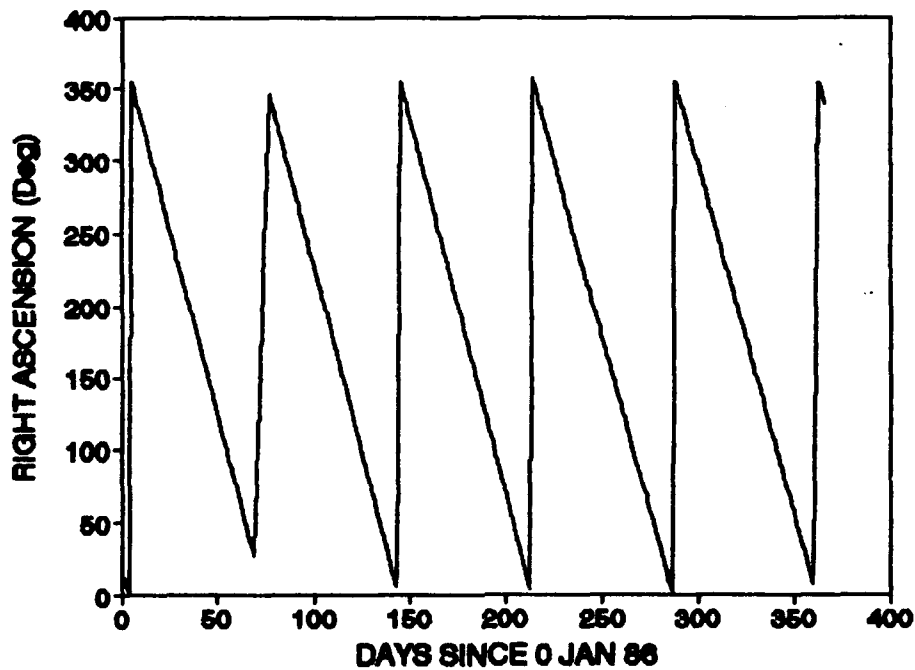


Figure 63. Right Ascension of the Ascending Node for Salyut 7, 1986

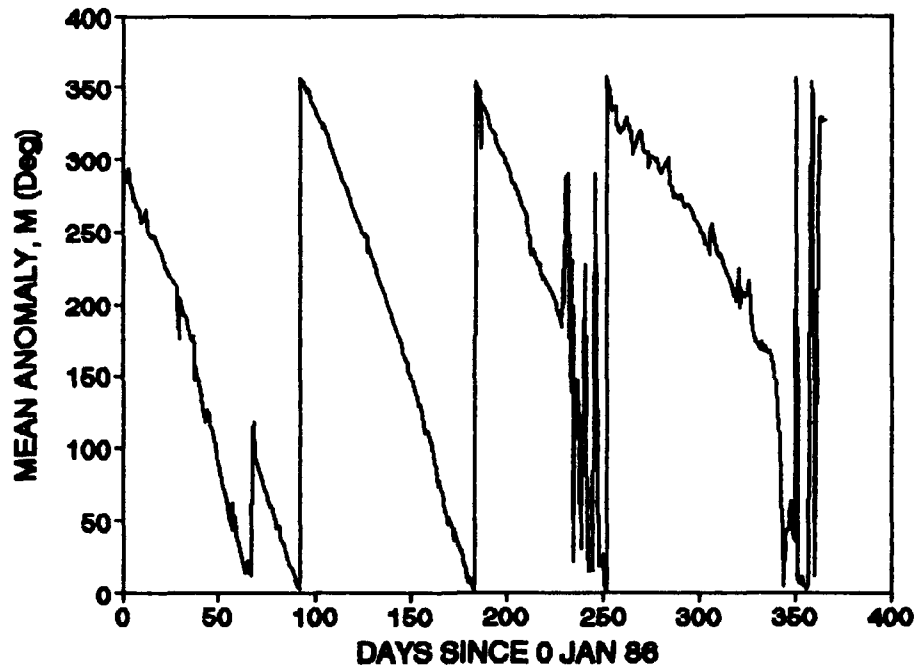


Figure 64. Mean Anomaly for Salyut 7, 1986

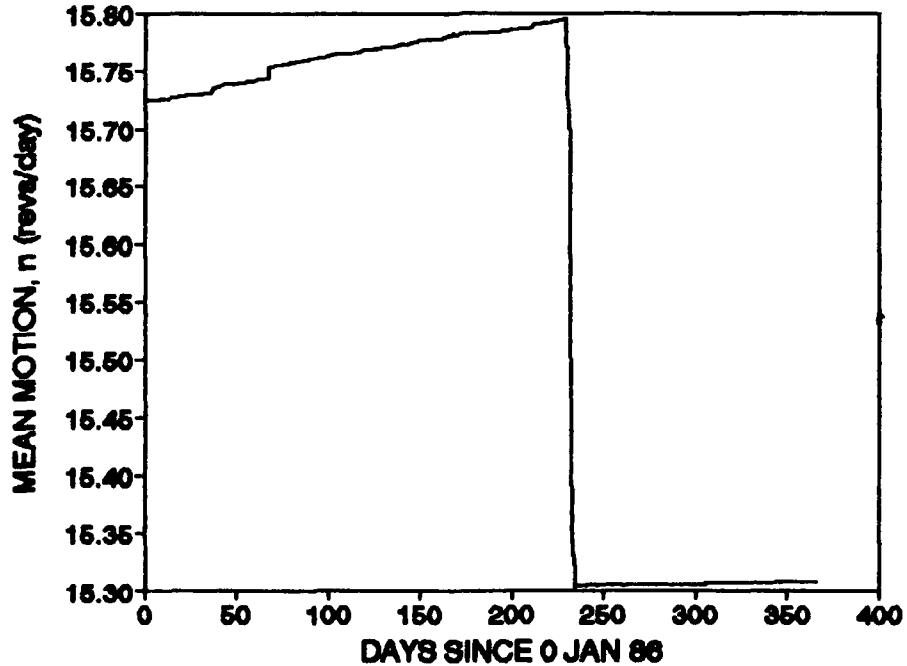


Figure 65. Mean Motion for Salyut 7, 1986

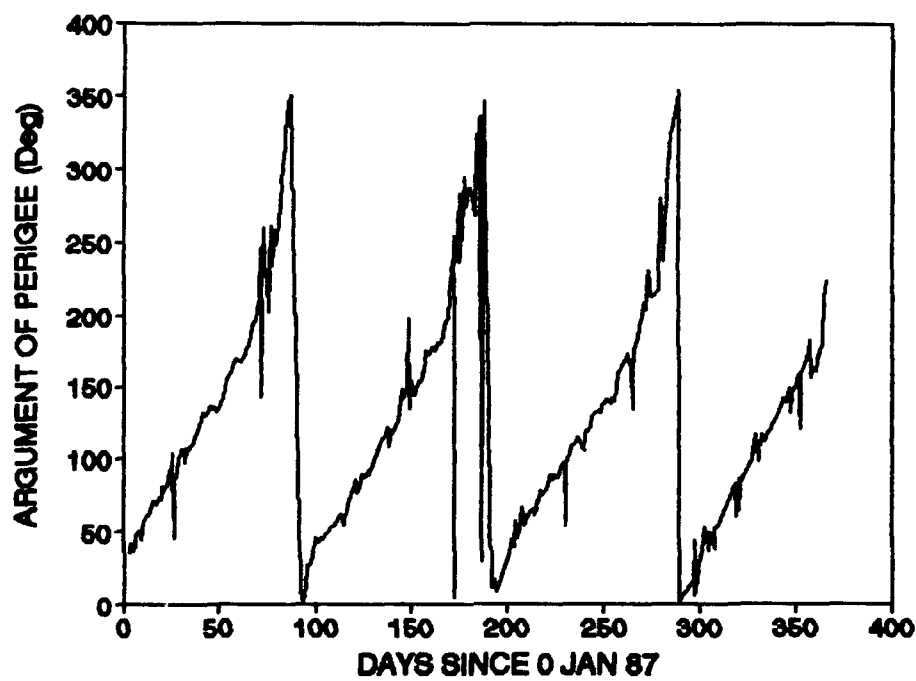


Figure 66. Argument of Perigee for Salyut 7, 1987

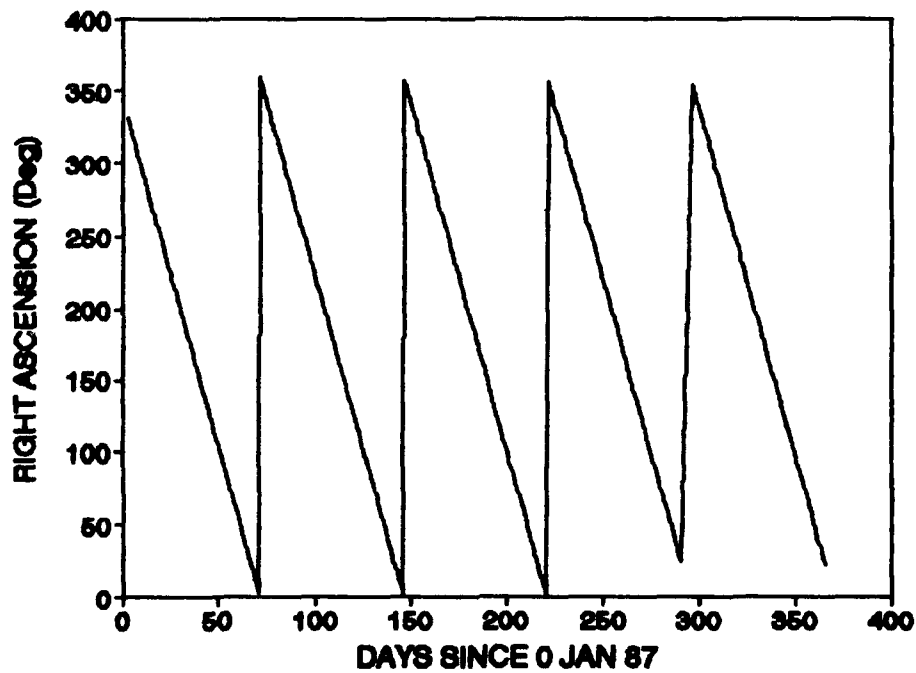


Figure 67. Right Ascension of the Ascending Node for Salyut 7, 1987

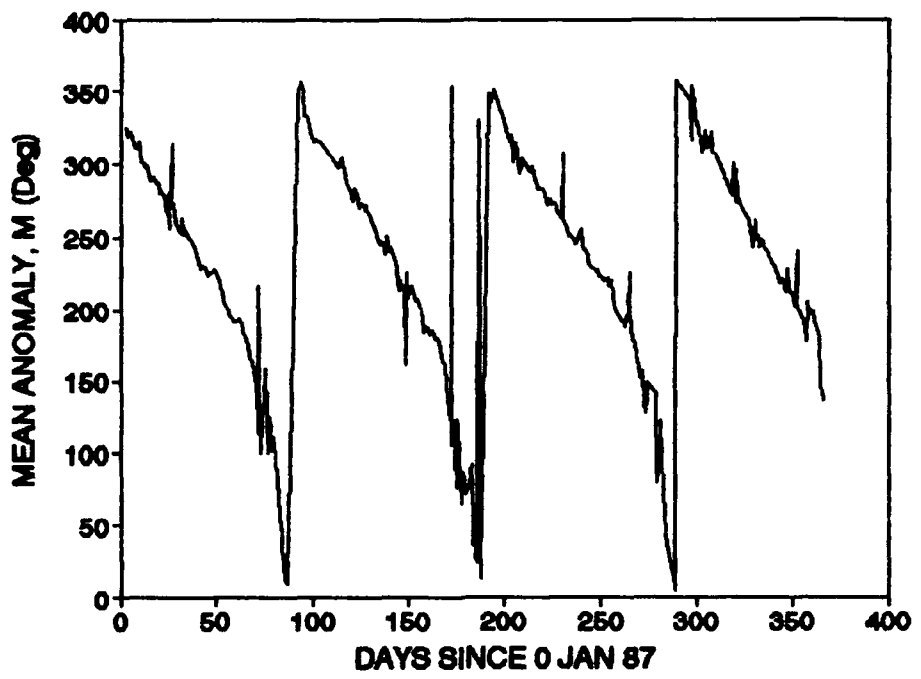


Figure 68. Mean Anomaly for Salyut 7, 1987

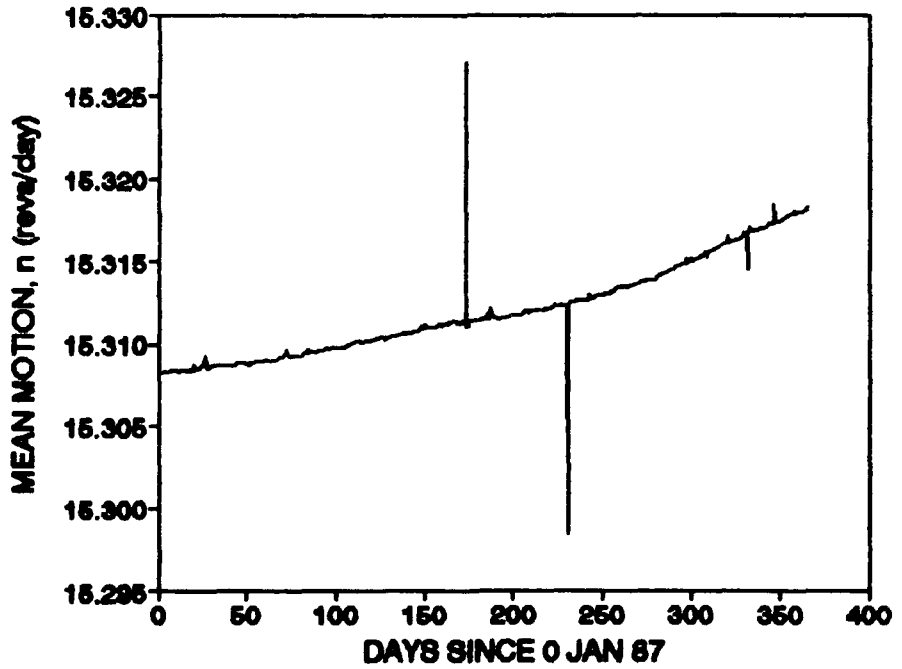


Figure 69. Mean Motion for Salyut 7, 1987

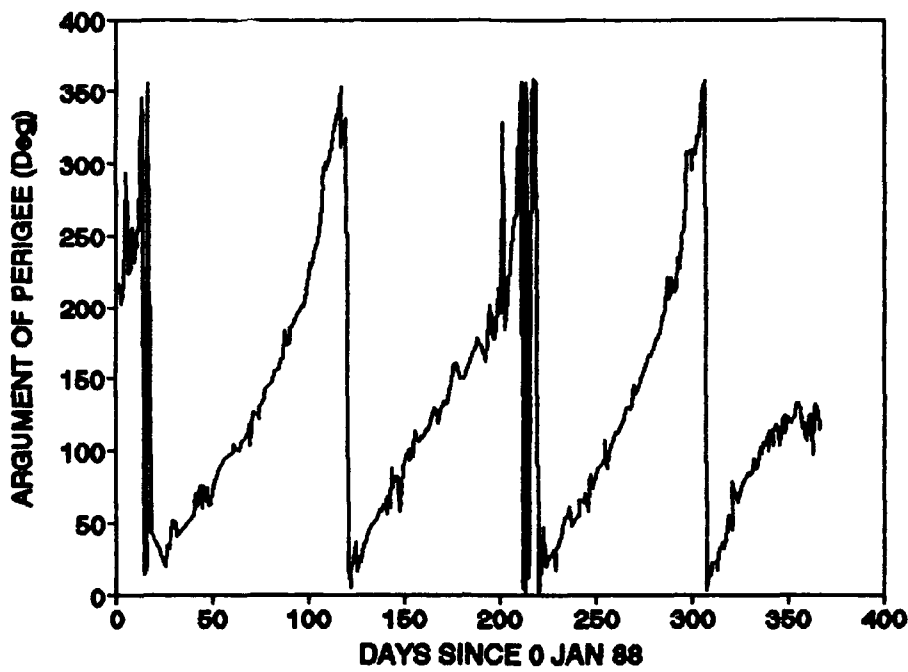


Figure 70. Argument of Perigee for Salyut 7, 1988

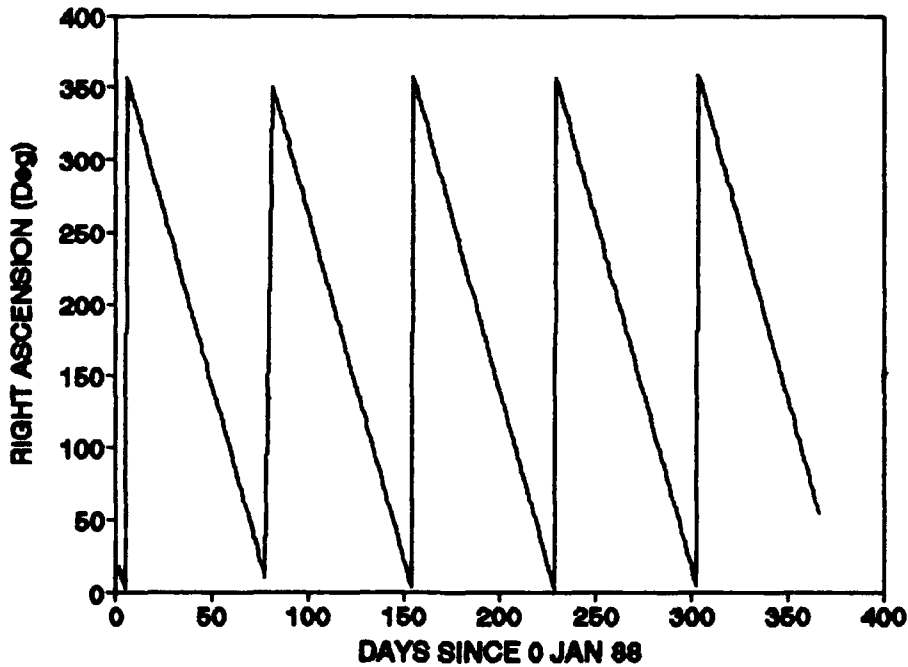


Figure 71. Right Ascension of the Ascending Node for Salyut 7, 1988

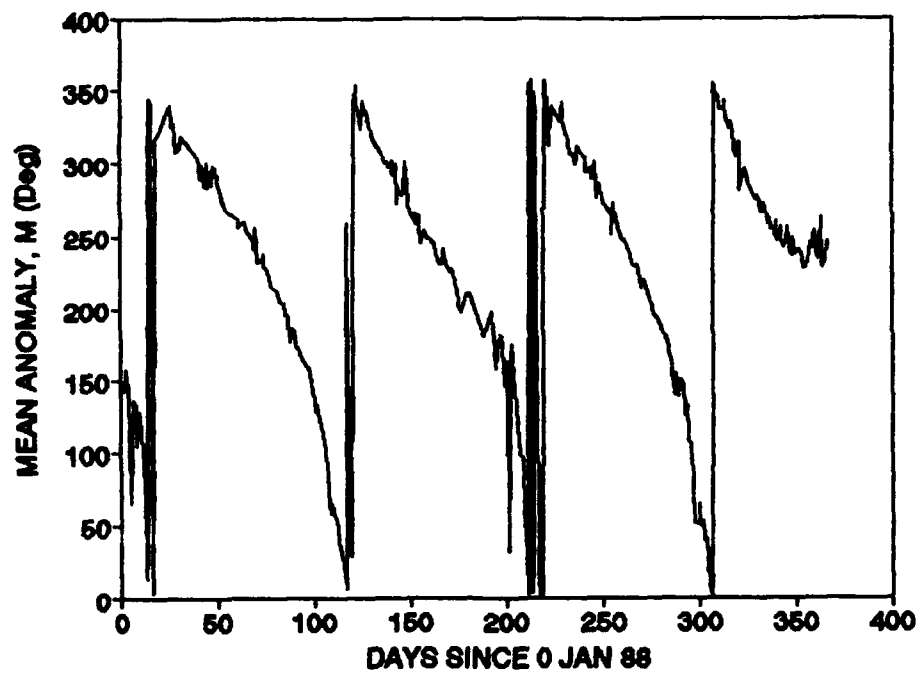


Figure 72. Mean Anomaly for Salyut 7, 1988

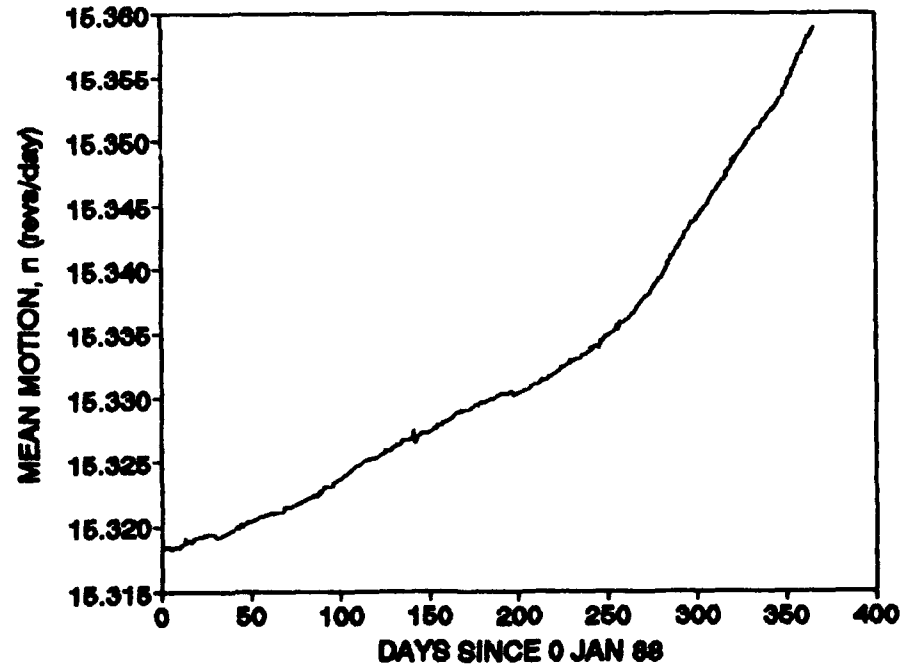


Figure 73. Mean Motion for Salyut 7, 1988

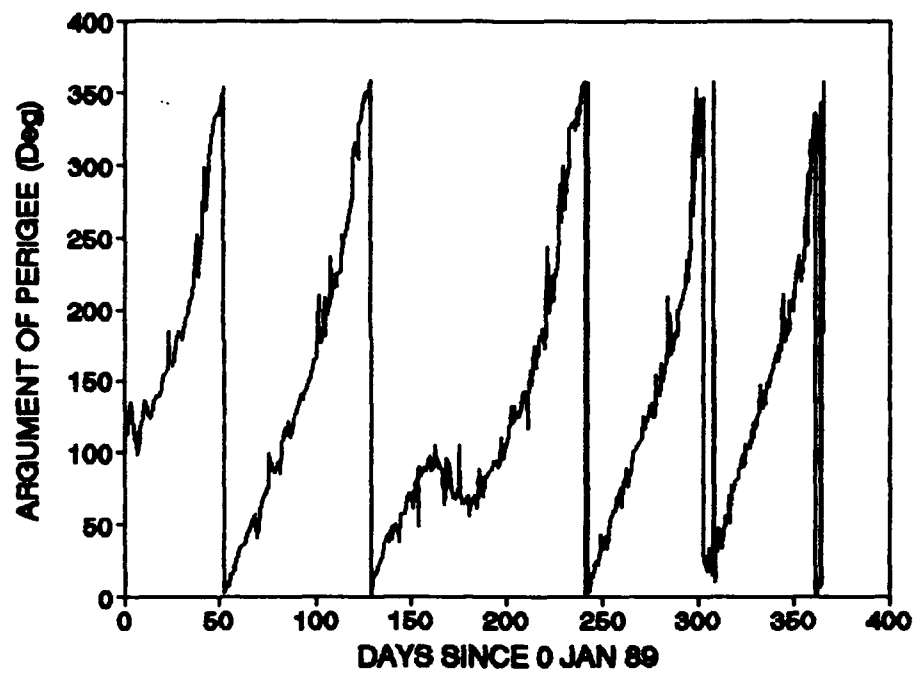


Figure 74. Argument of Perigee for Salyut 7, 1989

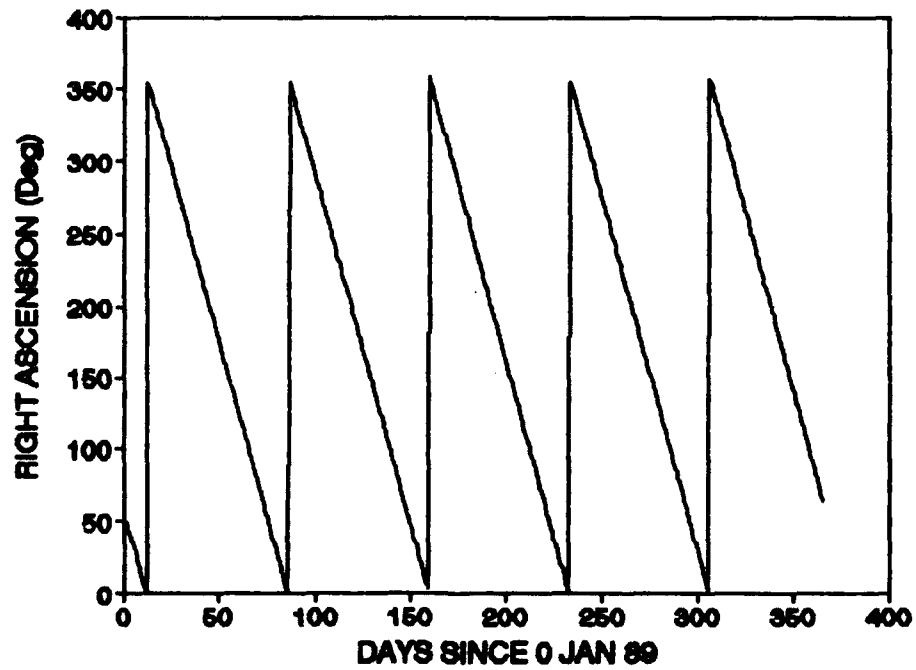


Figure 75. Right Ascension of the Ascending Node for Salyut 7, 1989

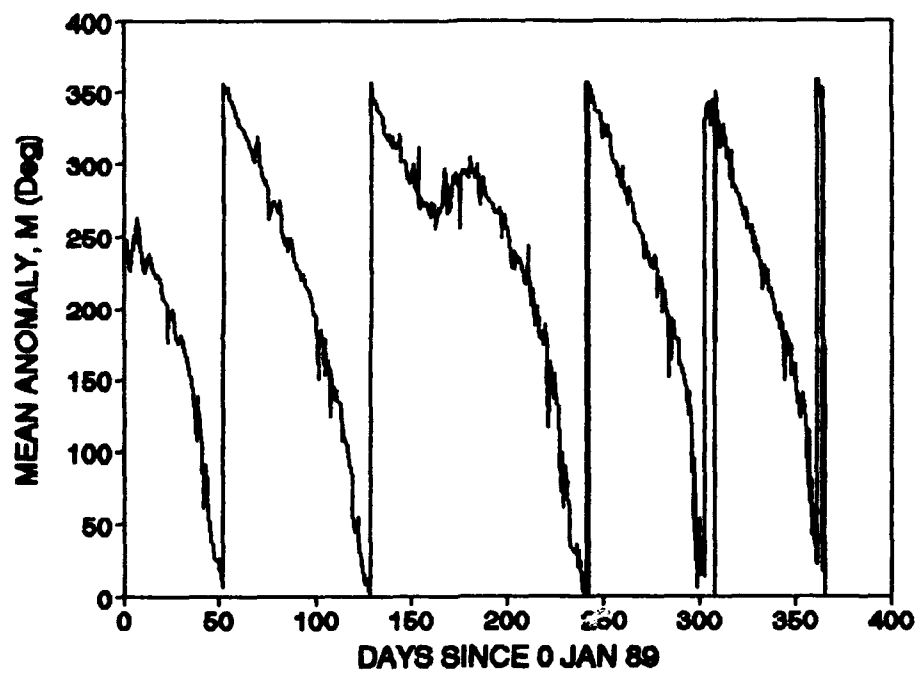


Figure 76. Mean Anomaly for Salyut 7, 1989

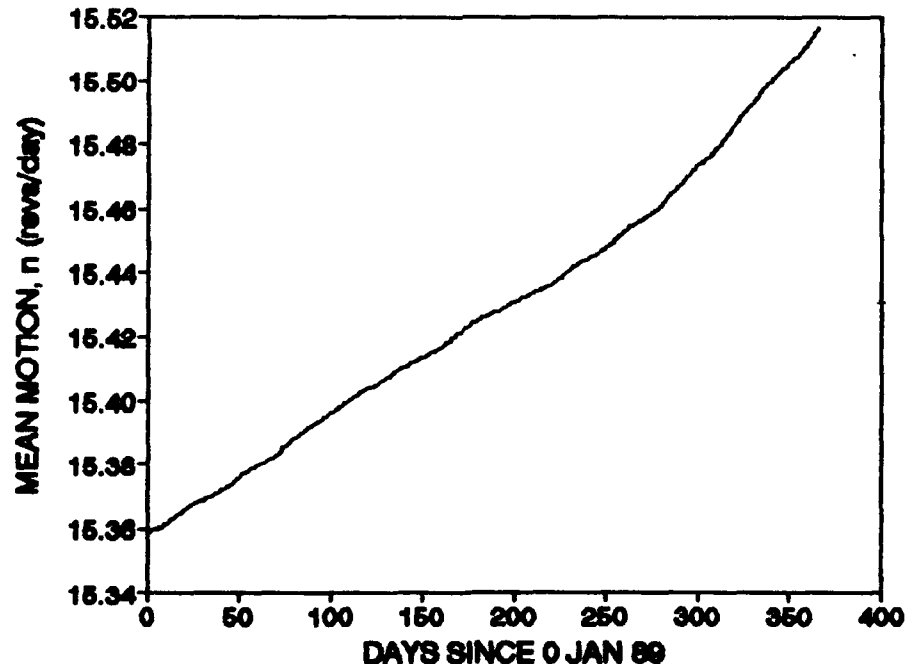


Figure 77. Mean Motion for Salyut 7, 1989

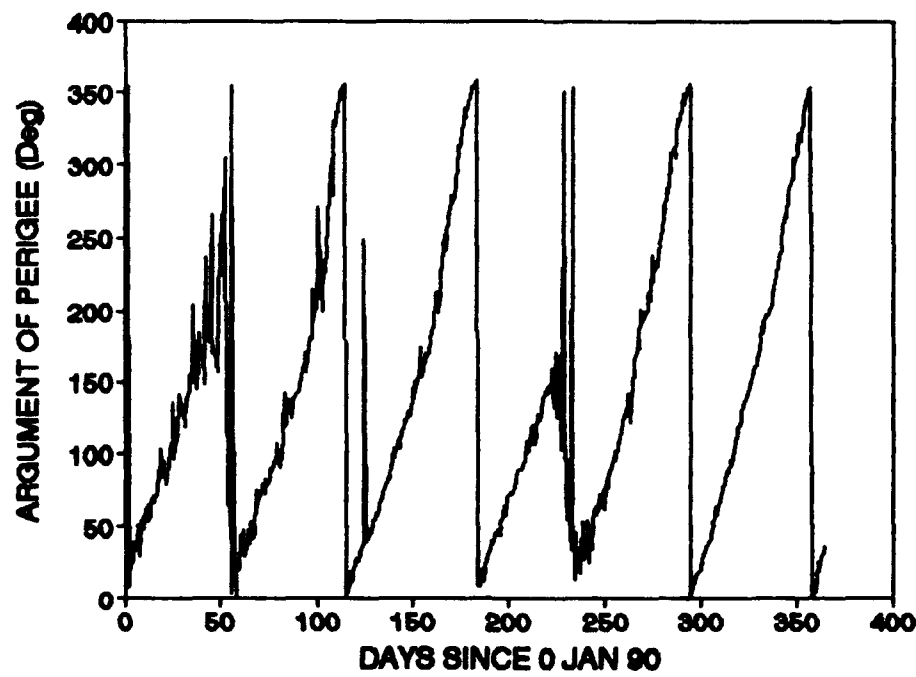


Figure 78. Argument of Perigee for Salyut 7, 1990

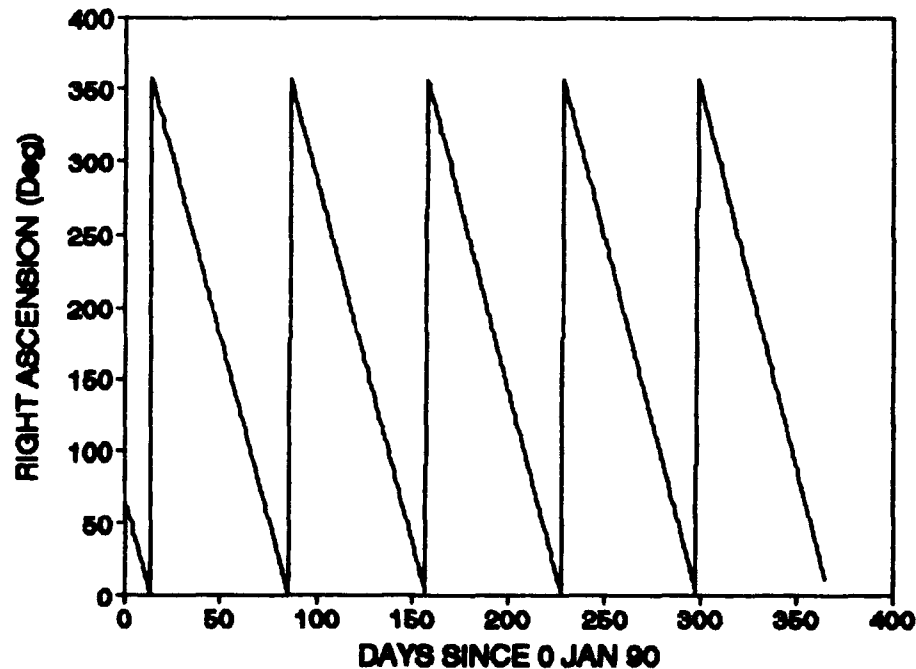


Figure 79. Right Ascension of the Ascending Node for Salyut 7, 1990

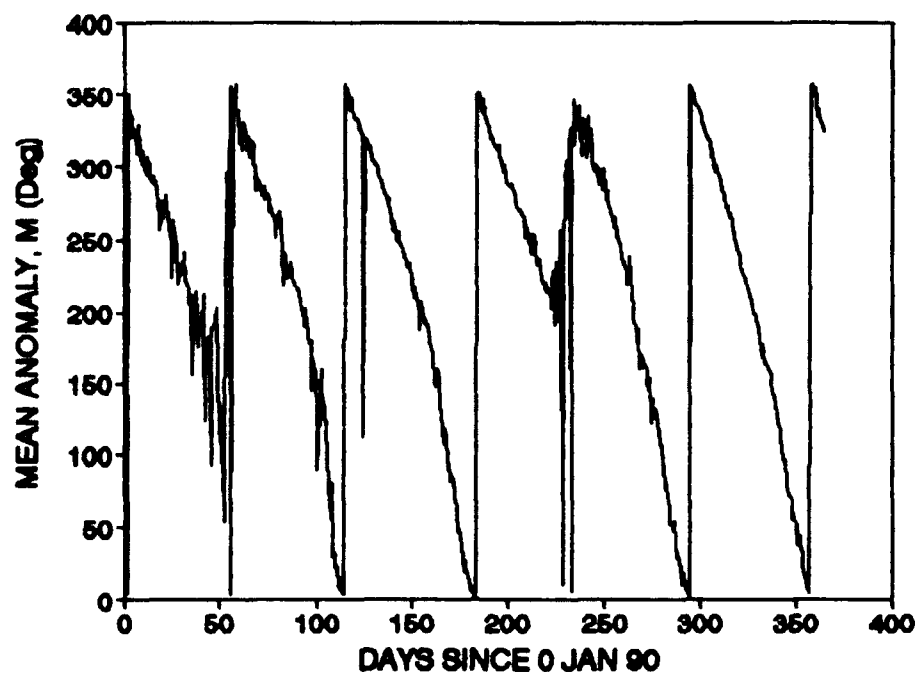


Figure 80. Mean Anomaly for Salyut 7, 1990

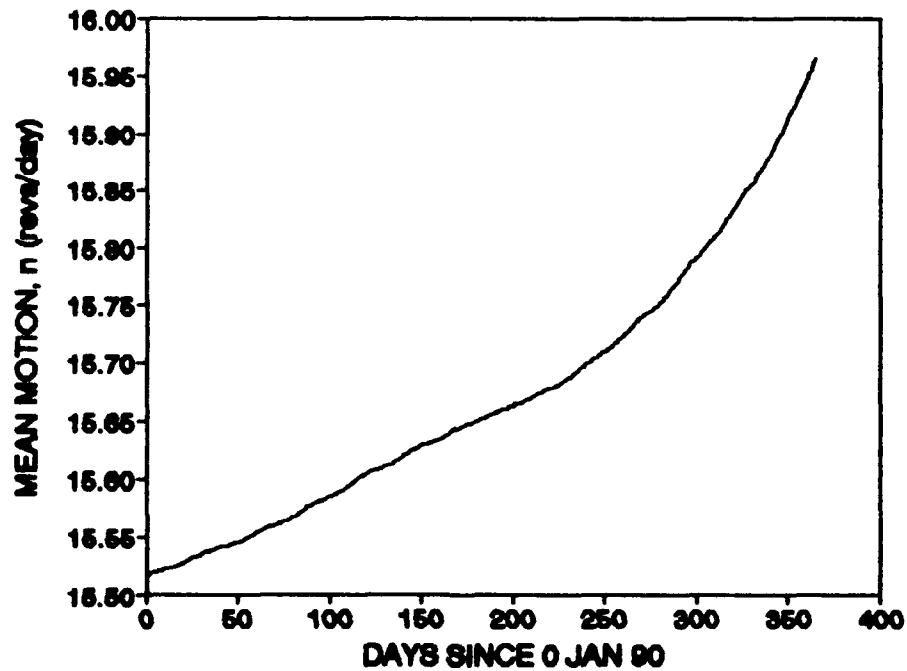


Figure 81. Mean Motion for Salyut 7, 1990

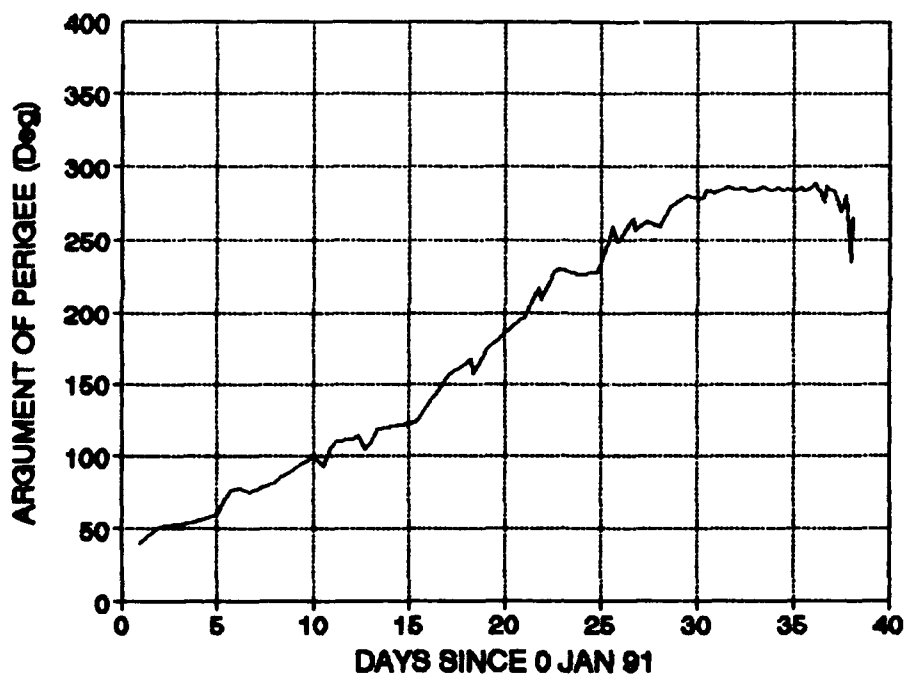


Figure 82. Argument of Perigee for Salyut 7, 1991



Figure 83. Right Ascension of the Ascending Node for Salyut 7, 1991

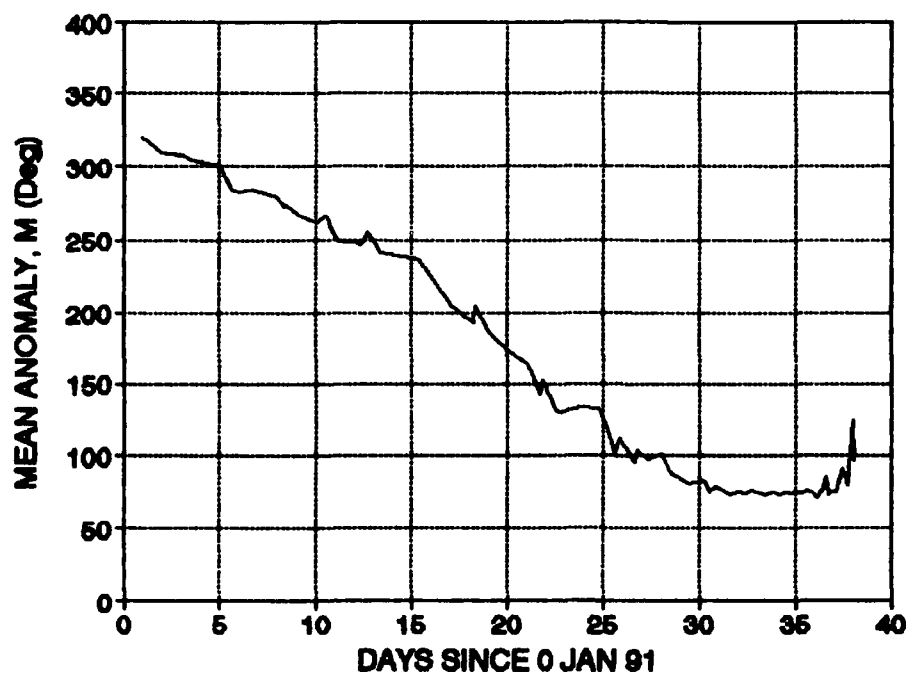


Figure 84. Mean Anomaly for Salyut 7, 1990

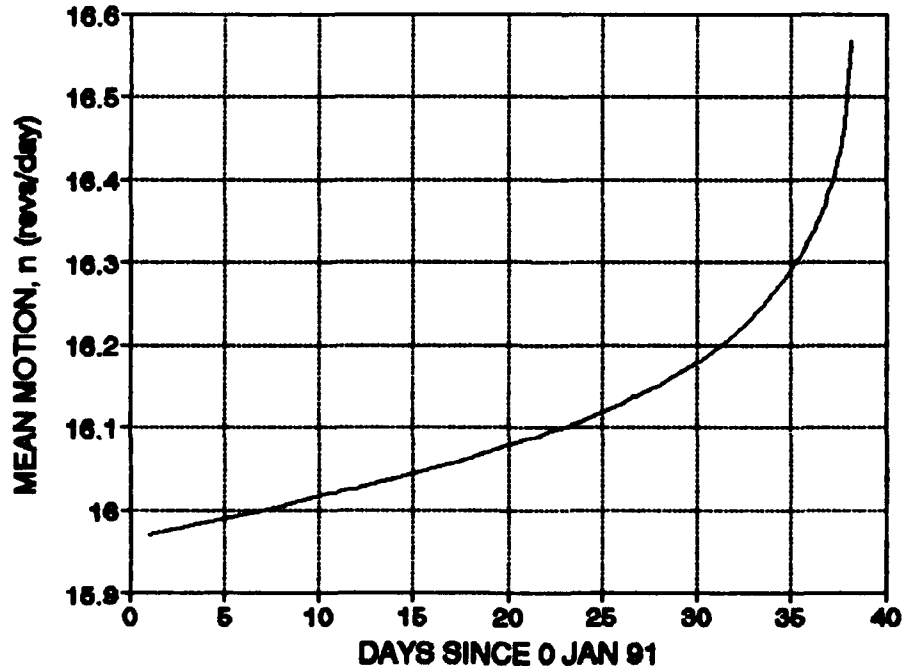


Figure 85. Mean Motion for Salyut 7, 1990

### Bibliography

1. Bassner, H.F. and others. "Radio Frequency Ion Propulsion Application to Commercial Satellites," *AIAA/ASME/SAE/ASEE 25th Joint Propulsion Conference*, AIAA Paper 89-2276: 1-8 (10-12 July 1989).
2. Battin, Richard H. "An Introduction to the Mathematics and Methods of Astrodynamics," *AIAA Education Series*, J.S. Przemieniecki, Series Editor-in-Chief. New York: AIAA, 1987.
3. Beattie, J. R. and others. "Xenon Ion Propulsion Subsystem," *Journal of Power and Propulsion*, Vol. 5, No. 4: 438-444 (July-August 1989).
4. Beattie, J. R. and others. "Status of Xenon Ion Propulsion Technology," *Journal of Power and Propulsion*, Vol. 6, No. 2: 145-150 (March-April 1990).
5. Champion, K. S. W. "Properties of the Mesosphere and Thermosphere and Comparison with CIRA 72," *Advanced Space Research*, Vol. 3, No. 1: 45-53 (1983).
6. Clark, Phillip S. "Soviet Space Activity, 1985-1986," *Journal of the British Interplanetary Society*, 40: 203-221 (May 1987).
7. Cody, Ronald P. and Jeffrey K. Smith. *Applied Statistics and the SAS Programming Language* (Second Edition). New York: Elsevier Science Publishing Co., Inc., 1987.
8. *Electric Propulsion and its Applications to Space Missions*, Progress in Astronautics and Aeronautics, Volume 79, edited by Robert C. Finke. New York: AIAA, 1979.
9. Fearn, D. G. and P. Smith. "The Application of Ion Propulsion to Intelsat VII Class Spacecraft," *AIAA/ASME/SAE/ASEE 25th Joint Propulsion Conference*, AIAA Paper 89-2275: 1-8 (10-12 July 1989).
10. Hall, R. "The Soviet Cosmonaut Team, 1978-1987," *Journal of the British Interplanetary Society*, 41: 111-116 (March 1988).
11. *Handbook of Geophysics and the Space Environment* (Fourth Edition), Adolph S. Jursa, Scientific Editor, Air Force Geophysics Laboratory. Washington: Government Printing Office, 1985.

12. Hill, Philip G. and Carl R. Peterson. *Mechanics and Thermodynamics of Propulsion*. Reading, Massachusetts: Addison-Wesley Publishing Company, 1970.
13. Jane's Spaceflight Directory (Second Edition), edited by Reginald Turnill. New York: Janes's Publishing Inc., 1986.
14. Johnson, Nicholas L. *The Soviet Year in Space 1986*. Colorado Springs: Teledyne Brown Engineering, 1987.
15. King-Hele, Desmond. *Theory of Satellite Orbits in an Atmosphere*. Washington: Butterworth, Inc., 1964.
16. Kolcum, Edward H. "Investigators Note Effects of Space During Removal of LDEF Trays," *Aviation Week & Space Technology*, 133: 23-24 (26 February 1990)
17. McCleary, Richard and Richard A. Hay, Jr. *Applied Time Series Analysis for the Social Sciences*. Beverly Hills: SAGE Publications, Inc., 1980.
18. Planeaux, Jim, Capt. Class handout distributed in MENG 632, Nonchemical Propulsion. School of Engineering, Air Force Institute of Technology (AU), Wright-Patterson AFB OH, May 1991.
19. Roy, A. E. *Orbital Motion*. Bristol, Great Britain: Adam Hilger Ltd., 1982.
20. Sponable, Jess M. and Jay P. Penn. "Electric Propulsion for Orbit Transfer: A Case Study," *Journal of Power and Propulsion*, Vol. 5, No. 4: 445-451 (July-August 1989).
21. Tipler, Paul A. *Physics*. New York: Worth Publishers, Inc., 1976.
22. USAFETAC. "USAFETAC Project 910809, SESS Data for Satellite Orbits." USAFETAC/DNE Letter with 2 Attachments, 15 August 1991.
23. Wiesel, William E. "Spaceflight Dynamics," *McGraw-Hill Series in Aeronautical and Aerospace Engineering*. New York: McGraw-Hill Book Company, 1989.